RD.
539.7
G 326
V4, No.3

POWER REACTOR TECHNOLOGY

A Quarterly Technical Progress Review

Prepared for U. S. ATOMIC ENERGY COMMISSION by GENERAL NUCLEAR ENGINEERING CORP.

ILLINOIS STATE LIBRARY
OCT 13 1961

June 1961

● VOLUME 4

● NUMBER 3

TECHNICAL PROGRESS REVIEWS

To meet the needs of industry for concise summaries of current atomic developments, the Atomic Energy Commission is publishing this series, Technical Progress Reviews. Issued quarterly, each of the reviews digests and evaluates the latest findings in a specific area of nuclear technology and science.

The four journals published in this series are:

Nuclear Safety, W. B. Cottrell, editor, R. A. Charpie, advisory editor, and associates, Oak Ridge National Laboratory

Power Reactor Technology, Walter H. Zinn and associates, General Nuclear Engineering Corporation

Reactor Core Materials (covering solid material developments), R. W. Dayton, E. M. Simons, and associates, Battelle Memorial Institute

Reactor Fuel Processing, Stephen Lawroski and associates, Chemical Engineering Division, Argonne National Laboratory

Each journal may be purchased ($2.00 per year for subscription and individual issues $0.55) from the Superintendent of Documents, U. S. Government Printing Office, Washington 25, D. C. See back cover for remittance instructions and foreign postage requirements.

The views expressed in this publication do not necessarily represent those of the United States Atomic Energy Commission, its divisions or offices, or of any Commission advisory committee or contractor.

Availability of Reports Cited in This Review

Unclassified AEC reports are available for inspection at AEC depository libraries and are sold by the Office of Technical Services, Department of Commerce, Washington 25, D. C. Some of the reports cited are not available owing to their preliminary nature; however, the information contained in them will eventually be made available in formal progress or topical reports.

Unclassified reports issued by other Government agencies or private organizations should be requested from the originator.

Unclassified British and Canadian reports may be inspected at AEC depository libraries. British reports are sold by the British Information Service, 45 Rockefeller Plaza, New York, N. Y.; Canadian reports (AECL series) are sold by the Scientific Document Distribution Office, Atomic Energy of Canada, Ltd., Chalk River, Ontario, Canada.

Classified U. S. and foreign reports identified in this journal as Classified may be purchased by properly cleared Access Permit Holders from the Office of Technical Information Extension, U. S. Atomic Energy Commission, P. O. Box 1001, Oak Ridge, Tenn. Such reports may be inspected at classified AEC depository libraries.

POWER REACTOR TECHNOLOGY

A REVIEW OF RECENT DEVELOPMENTS

Prepared for U. S. ATOMIC ENERGY COMMISSION
by GENERAL NUCLEAR ENGINEERING CORP.

● JUNE 1961

● VOLUME 4

● NUMBER 3

foreword

This quarterly review of reactor development has been prepared at the request of the Office of Technical Information of the U. S. Atomic Energy Commission. Its purpose is to assist interested organizations in the task of keeping abreast of new results in reactor technology for civilian application.

Power Reactor Technology contains reviews of selected recently published reports that are judged noteworthy, in the fields of power-reactor research and development, power-reactor applications, design practice, and operating experience. It is not meant to be a comprehensive abstract of all material published during the quarter, nor is it meant to be a treatise on any part of the subject. However, related articles are often treated together to yield reviews having some breadth of scope, and from time to time background material is added to place recent developments in perspective.

The intention is to cover the various areas of reactor development from the general viewpoint of the reactor designer rather than from the more detailed points of view of specialists in the individual areas. To whatever extent the coverage of *Power Reactor Technology* may occasionally overlap the fields of the other Technical Progress Reviews, the overlaps will be motivated by this objective of viewing current progress through the eyes of the reactor designer.

A degree of critical appraisal and some interpretation of results are often necessary to define the significance of reported work. Any such appraisals or interpretations represent only the opinions of the reviewers and the editor of *Power Reactor Technology*, who are General Nuclear Engineering Corporation personnel. Readers are urged to consult the original references in order to obtain all the background of the work reported and to obtain the interpretation of the results given by the original authors.

W. H. ZINN, President
J. R. DIETRICH, Vice President and Editor
General Nuclear Engineering Corporation

P.D
539.7
G 316
V. 4, No 3

contents

Issued quarterly by the U. S. Atomic Energy Commission. Use of funds for printing this publication approved by the Director of the Bureau of the Budget on November 1, 1960.

Section I

REACTOR APPLICATIONS

Chemonuclear Reactors

The possible application of nuclear reactors to the direct production of useful chemical products is discussed at some length in the February 1961 issue of *Nucleonics*. The series of articles discusses the general principles and problems of this application[1,2] and describes work that has been done at Argonne National Laboratory (ANL) and at Battelle Memorial Institute (BMI) on the synthesis of ethylene glycol from methanol.[3] An earlier Brookhaven study of the synthesis of oxides of nitrogen has been reported in reference 4. A recent article[5] in *Chemical Engineering Progress* describes the work that is under way at Aerojet-General Nucleonics on the chemonuclear production of hydrazine (N_2H_4) from ammonia. Hydrazine is a promising liquid rocket fuel, which is relatively expensive to produce by conventional means, and therefore appears to be one of the more attractive possibilities for chemonuclear processes.

Although the use of gamma rays to promote certain chemical reactions is well known and has reached the practical stage for certain favorable cases, the large-scale use of the fission reaction to promote chemical reactions requires that the 84 per cent of the fission energy that appears as kinetic energy of fission fragments be utilized. In the usual nuclear reactor, almost all this energy is absorbed in the fuel elements, as indeed it must be if radioactive fission fragments are to be kept out of the circulating coolant. In the chemonuclear reactor the fission fragments must be allowed to enter the process fluid, which may or may not serve also as the coolant, in order to deposit their kinetic energy there, and the problems of operating the reactor with fission products in the circulating fluid, and of decontaminating the chemical product, must be accepted. The fuel must be incorporated in a finely divided form to allow easy escape of the fission recoil fragments. Small suspended particles of UO_2, either unbonded or glass-bonded, and either spherical, fiberlike, or slablike in shape, have been suggested. The smaller the particle size, the greater the efficiency of energy deposition in the process stream. The particle size must be large enough, however, to avoid particle agglomeration and to allow efficient dispersal of fuel and easy separation from the process stream. Fuel particle sizes in the 1- to 5-μ range appear optimum for the hydrazine reactor. Production facilities involve problems of fuel separation and dispersal, shielding, remote operation, and product separation and decontamination.

The first-phase experimental study presently under way on hydrazine production is concentrated on determining the yield. This will be accomplished by exposure of a small capsule reaction vessel (loaded with fissile material suspended in liquid NH_3) to a measured neutron flux in a nuclear reactor. The hydrazine yield will be determined in terms of the G value (the number of hydrazine molecules produced per 100 ev of fission-fragment energy deposited in the ammonia). Preliminary economic evaluation indicates that a G value as low as 0.5 would justify further study. However, any realistic prediction for hydrazine is difficult. The overall reactions expected are

$$2NH_3 \rightarrow N_2H_4 + H_2$$

$$2NH_3 \rightarrow N_2 + 3H_2$$

The ratio of the rates of these two reactions is currently a matter of conjecture.

Reference 5 presents a description of the reaction capsule and of the methods and prob-

lems involved in analyses of experimental yields and in determination of energy-deposition efficiency.

The reference[5] states that direct experimental evidence of the fissiochemical production of hydrazine has already been obtained in some relatively simple experiments carried out in a 5-watt AGN-201M reactor. Here the flux was extremely low, and the measured G values (in the 1.0 to 1.9 range) are subject to a relatively high uncertainty. The future irradiations are to be made in a much higher neutron flux.

Reactor–Fuel Cell Combination

Experimental work and theoretical considerations relative to ionic-hydride fuel cells are reported in reference 6. The possibility is considered of using a nuclear reactor as the heat source, or regenerator, in the closed system consisting of the fuel cell and the fuel regenerator. The metal electrode of the hydride fuel cell consists of an alkali metal (such as lithium, sodium, or rubidium) in direct contact with the electrolyte. The electrolyte should be a salt or liquid metal, compatible with the metal electrode, in which some of the alkali metal is present in ionic form. Alkali-metal halides have been satisfactory electrolytes. The hydrogen electrode consists of a metal with a high surface area for contacting the H_2 effectively with the electrolyte. Stainless-steel mesh and porous plate have proven satisfactory. In the case of lithium, the reactions are

$$2Li^0 \rightarrow 2Li^+ + 2e \text{ at the metal electrode}$$

$$H_2 + 2e \rightarrow 2H^- \text{ at the hydrogen electrode}$$

$$2Li + H_2 \rightarrow 2LiH \text{ net fuel-cell reaction}$$

The electrons flow through the electrical load in the external circuit while the ions migrate through the electrolyte. The LiH formed by the cell reaction is carried in solution by the electrolyte to the regenerator wherein the LiH is thermally decomposed (calculated decomposition temperature of 850°C at 1 atm pressure). The H_2 evolves from the system, permitting separation, and the lithium metal and the H_2 are then recycled to the fuel cell.

The efficiency of the fuel cell, i.e., the ratio of the electrical energy produced to the free energy of the cell reactants, can be quite high, and is expected, for the LiH cell[6] to be in the range 80 to 90 per cent. When the cell is used with a regenerator, however, no net chemical change (other than losses) occurs in the system, and the system comprising the cell and regenerator is a self-contained thermodynamic system that must be subject, in the usual way, to the second law of thermodynamics. The upper limit of the thermodynamic efficiency of the system is therefore the Carnot efficiency

$$\eta = \frac{T_h - T_c}{T_h}$$

where T_c is the operating temperature in the fuel cell, and T_h is the temperature in the regenerator. The thermal efficiency for the LiH system is expected[6] to be in the range 35 to 50 per cent. It does not seem probable that this system will better the efficiency of the conventional power-conversion systems.

The temperature of the cell has an important effect on its operation; the net result of an increase in cell temperature is a decrease in open-circuit voltage and an increase in current capability of the cell. In cases where peak power must be withdrawn from minimum-sized cells, the cells would operate at near half voltage, and cell efficiencies would drop to about 50 per cent.

The reference[6] describes a small regenerative system which was operated with an electrolyte consisting of the eutectic mixture of the chlorides of lithium, rubidium, cesium, and sodium. With this laboratory-scale system, open-circuit voltages of 0.5 volt at 1000°F have been observed, and current densities of 65 amp/sq ft at 0.1 volt have been measured; higher current densities (230 amp/sq ft at equilibrium) have been observed in other cells.

High heat-transfer capabilities are expected in the hydride regenerator as a result of the violent agitation of the liquid by the H_2 gas evolved in the dissociation process (similar to that of boiling). Vapor blanketing of the heat-transfer surface (burnout) would be the limitation; the peak heat flux for boiling liquids, as correlated from experimental data by Rohsenow and Griffith,[7] suggests a burnout heat flux for LiH at 1650°F of 11.6×10^6 Btu/(hr)(sq ft) (compared to 0.4×10^6 for water).

Two general methods of integrating the fuel cell and nuclear reactor are considered:[6] (1) external regeneration in which a pumped heat-transfer fluid conveys heat from reactor to re-

generator and (2) internal regeneration in which the hydride dissociation process occurs within the reactor proper. With internal regeneration, some dissociation from nuclear radiation would also occur. The reference[6] estimates that the external system would have to operate some 100°F hotter than the internal system and would require about four times the flow rate.

References

1. Chemonuclear Reactors—Where Do They Stand ?, *Nucleonics*, 19(2): 47 (February 1961).
2. Thin Unclad Fuel Needed for Chemonuclear Reactors, *Nucleonics*, 19(2): 48 (February 1961).
3. A. K. Wiebe et al., Fission Fragments Initiate Ethylene Glycol Synthesis, *Nucleonics*, 19(2): 50 (February 1961).
4. G. Lellouche and M. Steinberg, Industrial Chemical Production by Chemo-Nuclear Processes with Special Reference to the Production of Fixed Nitrogen, USAEC Report BNL-574, Brookhaven National Laboratory, September 1959.
5. C. P. Fritsch et al., Hydrazine Production by Nuclear Reaction, *Chem. Eng. Progr.*, 57(3): 37–41 (March 1961).
6. T. A. Ciarlariello and R. C. Werner, Fuel Cells Based on Nuclear Reactors, *Chem. Eng. Progr.*, 57(3): 42–45 (March 1961).
7. W. M. Rohsenow and D. Griffith, Correlation of Maximum Heat-Flux Data for Boiling of Saturated Liquids, *Chem. Eng. Progr. Symposium Ser. No. 18*, 52: 47–49 (1959).

Section II

REACTOR PHYSICS: CRITICAL AND EXPONENTIAL EXPERIMENTS

A critical-assembly program[1] was conducted at the Battelle Critical-Assembly Laboratory, for Advanced Technology Laboratories (a division of American-Standard), as part of a program to evaluate the technical and economic feasibility of the Variable-Moderator Reactor (VMR) concept. The VMR system is a boiling light-water reactor controlled by varying the active core height through changes in the height of the moderator surrounding the fuel elements. The concept was reviewed briefly in the December 1960 issue of *Power Reactor Technology*, Vol. 4, No. 1, pages 77 and 78. The core of the critical assembly consisted of 37 hexagonal, stainless-steel, fuel-element cans, each containing 61 fuel pins. The fuel pins were 0.485-in.-OD aluminum tubing filled with 1.8 per cent enriched UO_2 pellets 0.415 in. in diameter. Fuel pins and elements were arranged in triangular lattices. Core configurations that were combinations of 0.633- and 0.703-in. pin pitches and 5.54-, 5.95-, and 6.34-in. element pitches were investigated. Light water served as the moderator, whereas water, furfural, furfuryl alcohol, and air were used within the fuel elements as coolant-simulating materials. The purpose of the critical-assembly program was to provide data on VMR type reactor lattices to aid in verifying the assumptions and techniques used in the physics analysis. Criticality, reactivity worths of joint and separate changes in moderator and coolant liquid levels, macroscopic flux and power distributions, and the temperature coefficient of reactivity were measured for several core configurations. Also, measurements were made to determine the disadvantage factor, cadmium ratios, fast-fission parameters for U^{238} and U^{235}, and effective neutron temperatures, as functions of core configuration.

Reference 2 describes the measurements made by Atomics International with the SNAP Critical Assembly (SCA) to substantiate and augment nuclear calculations on minimum-weight reactor systems. The SCA is a pseudo-spherical nuclear reactor with a fixed hydrogen moderator, U^{235} fuel, and a beryllium and graphite reflector. The core is made up of segments of cold-pressed zirconium hydride containing 8 wt.% UO_2 powder enriched to 93.17 per cent U^{235}. Reactivity measurements consisted of determinations of critical mass for four different configurations and determination of the variation of critical mass with graphite reflector thickness. Because of the extremely high leakage from SNAP reactors, the relative ability of various materials to reflect neutrons back to the system was measured. The temperature coefficient of reactivity, and reactivity coefficients for various samples of materials, were measured. Subcritical reactivity calibrations were made by employing both subcritical multiplication and rod drop techniques. Activation measurements determined the spatial distribution of power and the spatial distributions of neutrons in various energy ranges. The ratio of prompt-neutron lifetime to effective delayed-neutron fraction was measured in one configuration by both the noise analysis and the Rossi-alpha methods.

A summary of the single-rod fast-fission factors measured during the past five years and a description of the methods used to measure them is presented in reference 3. The fast-fission factor has been measured for 1 per cent enriched uranium rods with diameters of 0.25, 0.387, 0.600, and 0.750 in. and for natural-uranium rods with diameters of 1.100, 1.345, 1.938, 2.898, and 3.636 in., all surrounded by graphite. The slow-neutron flux was measured

in the 1.938-, 2.898-, and 3.636-in.-diameter natural-uranium rods and the surrounding graphite moderator. The distributions of total, slow, and fast fissions across the 2.898- and 3.636-in.-diameter natural-uranium rods were also measured.

The results of additional critical experiments being performed under the Multiregion Reactor Lattice Studies Program at the Westinghouse Reactor Evaluation Center are reported in reference 4. Measurements were carried out in uniformly loaded lattices using stainless-steel-clad UO_2 rods of 3.7 per cent enrichment, in a cylindrical configuration. The volume ratio of water to equivalent uranium metal was 2.5 to 1. The peripheral fuel-rod worth was measured by the period method. The U^{238} cadmium ratios for radiative capture in the fuel at several radial positions were obtained. Three-region critical experiments were performed on a cylindrical core having a volume ratio of 2.5 to 1 for water to uranium metal and having fuel enrichments of 1.6 per cent in the center region, 2.7 per cent in the middle region, and 3.7 per cent in the outer region. Measurements of critical height, peripheral fuel-rod worth, fission activity, and cadmium ratios were made for various core sizes. The buckling and reflector savings obtained from the measurements made on a 2.7 per cent rectangular core are compared with the values obtained for the cylindrical 2.7 and 3.7 per cent cores.

Neutron multiplication measurements[5] were made by the Dow Chemical Company on bare cylindrical assemblies containing layers of plutonium metal disks, Plexiglas disks, and boron carbide impregnated Epolene-n disks. The assembly diameters used were 12.5 and 18.0 in. An attempt was made to convert the extrapolated critical dimensions to equivalent sphere radii, infinite cylinder diameters, and infinite slab thicknesses. Neutron multiplication measurements were also made on a 42-in.-diameter cylindrical stainless-steel tank filled with aqueous, enriched solutions of $UO_2(NO_3)_2$ and $1\frac{1}{2}$-in. Pyrex Raschig rings. Reference 6 contains a compilation of critical extrapolations of subcritical neutron multiplication measurements made on assemblies of plutonium metal tamped with Plexiglas. Some recent data on a 20- by 20-in. slab of metal, tamped on its top and bottom with Plexiglas, are also presented. A simple empirical equation was found which fits the data and which predicts the infinite slab and cylinder dimensions.

A summary of the critical approach and exponential measurements made at Hanford Laboratories with 3.063 per cent enriched uranium rods in light water is presented in reference 7. The scope of these measurements was reviewed in the December 1960 issue of *Power Reactor Technology*, Vol. 4, No. 1. A series of exponential measurements[8,9] has also been completed with 0.925-in.-diameter natural-uranium fuel elements in light water. Buckling measurements were made for three lattice spacings (1.40, 1.50, and 1.60 in.) with fuel elements encased in thin-walled Lucite tubes and loaded into hexagonal lattice frameworks. The purpose of these measurements was to obtain further data on the critical mass of natural uranium in light water and to obtain buckling values for the interpretation of planned experiments involving a 3 per cent enriched uranium lattice reflected by a natural-uranium tamper.

Material buckling measurements[10] have been completed in exponential piles for a series of graphite–uranium metal lattices. Measurements were made with tube-in-tube natural-uranium fuel elements (2.5-in. OD), for most lattice spacings with tube-and-rod and I & E fuel elements, and for one lattice with a second tube-and-rod fuel element having a smaller size solid rod. Bucklings were measured for both air and water coolant. The series of measurements on the second tube-and-rod fuel element was curtailed because the results were close to the results obtained from the I & E fuel elements.

The results of correlating the computed critical mass with the measured critical mass when determining shape-perturbation effects have been revised in reference 11. The experimental investigations were reported in reference 12 and reviewed in the December issue of *Power Reactor Technology*, Vol. 4, No. 1.

A series of critical approach and exponential measurements[13] were begun at Hanford for determining criticality parameters of 2.00 per cent enriched uranium rods in light water. The data will be used for evaluating nuclear safety in support of processing enriched uranium from power-reactor fuels. The critical approach measurements have been completed for the 0.925-in.-diameter rods having lengths of 16 and 32 in.; exponential measurements were made with the 32-in. fuel-rod length only. The

fuel rods were encased in thin-walled Lucite tubes and inserted into a hexagonal lattice in a water-reflected lattice assembly. Buckling and critical mass data were obtained for five lattice spacings ranging from 1.5 to 1.95 in.

Reference 14 gives the results of a series of Hanford measurements for determining the amount of neutron absorber needed to make a heterogeneous system of 1.007 per cent enriched uranium rods safe. The information can be used for determining the amount of poison needed in dissolver batches as a secondary safety control against criticality. The lattice, of 0.925-in.-diameter aluminum-clad rods, and the poisoned moderator were enclosed in a stainless-steel tank which separated the light-water reflector from the poisoned moderator. Buckling values were obtained for three lattice spacings (1.40, 1.50, and 1.60 in.) and four poison concentrations per lattice.

Neutron multiplication and exponential experiments[15] were conducted in the Thermal Test Reactor (TTR) room at Hanford with plutonium-aluminum alloy rods in light water. The purpose of the experiments was to provide critical mass data needed for plutonium-aluminum alloy fuel elements in support of the Plutonium Recycle Program. The data would be used in the preparation of nuclear safety specifications concerning the handling and storage of this kind of fissile material. The critical mass data would also provide desirable check points for correlating critical mass calculations with experiments for heterogeneous plutonium systems. The plutonium-aluminum alloy rods were 0.506 in. in diameter and 24 in. in length, were clad in Zircaloy-2, and contained 5 wt.% plutonium. Critical masses were determined for hydrogen-to-plutonium atomic ratios from about 300 to 900, and bucklings were measured for ratios from about 200 to 2400.

A series of experiments[16] has been completed in the Physical Constants Test Reactor (PCTR) at Hanford in support of the Experimental Gas-Cooled Reactor (EGCR) program. Measurements of the infinite multiplication and thermal utilization factors were made for 2.6 per cent enriched UO_2 fuel elements clad in stainless steel. The effect of using beryllium spiders and end caps in place of the stainless-steel spiders and end caps was determined by using graphite to mock up the beryllium and by comparing copper-foil flux traverses for the two constructions. Previous measurements[17] of the radial and angular power distributions made on the EGCR lattice with 1.8 per cent enriched UO_2 fuel elements were repeated with the 2.6 per cent enriched fuel elements. Reference 18 describes the measurement made in the PCTR of the worth of a boron carbide control rod in a 4×4 array of EGCR lattice cells 21.875 in. long.

The EGCR will contain several experimental loops that will be used for such purposes as component testing.[19] The stainless-steel loops decrease the reactivity of the reactor through parasitic absorption, but the net reactivity effect of the loop and its loading may be either positive or negative, depending on the exact loading. To obtain quantitative experimental information about this effect, two measurements were made in the PCTR. The infinite multiplication and thermal utilization factors were measured for a 3×3 array of EGCR cells fueled with 1.8 per cent UO_2, with the center fuel assembly replaced by an empty type 304 stainless-steel tube of 4.468-in. OD. The measurements were then repeated with an EGCR seven-rod cluster fueled with 2.6 per cent UO_2 inserted into the same stainless-steel tube in the 3×3 array.

The status of a second series of experiments performed in the PCTR, for the study of the space-energy distribution of neutrons in moderating media of graphite with nonuniform physical temperatures, is reported in reference 20. The main purposes of this work are (1) to determine rethermalization cross sections of graphite as functions of the temperature of the media in which the neutrons are being moderated and (2) to test the validity of the two-Maxwellian group model by comparison of calculated and measured activation traverses with a non-$1/v$ detector such as lutetium. Secondary objectives of the work are to establish analytical methods which treat the entire PCTR (rather than the experimental region alone) and which can evaluate simultaneously the different rethermalization cross sections of dissimilar media or of a homogeneous medium with two temperature regions. The relaxation lengths for rethermalization were estimated from the activation data taken in radial traverses and are presented for several graphite temperatures for both plane and cylindrical geometries. The experimental activation data and descriptions of the experiments, methods of analysis, and results obtained thus far are also included in this

reference. Some of the earlier work on rethermalization was reviewed in the June 1960 issue of *Power Reactor Technology*, Vol. 3, No. 3, pages 1 to 3.

Some measurements[21] have been made at Oak Ridge National Laboratory (ORNL) on a flux-trap critical assembly, using an enriched solution of $UO_2(NO_3)_2$ dissolved in mixtures of D_2O and H_2O. This assembly was a preliminary mockup of the proposed High Flux Isotope Reactor (HFIR), and the data were intended to aid in the establishment of design parameters for the HFIR. The critical-assembly vessel consisted essentially of four coaxial aluminum cylinders, having nominal outside diameters of 6, 16, 32, and 44 in. and forming a set of four coaxial containers. The center region contained H_2O, region 2 contained the fuel solution, region 3 contained D_2O, and region 4 contained H_2O. The experiments were divided into four groups on the basis of fuel concentrations in region 2 and of boron poison concentration in the D_2O of region 3. The measurements included the critical parameters of the assembly with various amounts of neutron absorber in the D_2O reflector, the relative flux distributions under various conditions of reflector poison and fissile solution concentration, the ratio of the absolute thermal-neutron flux in the center of the assembly to the power in the fissile solution, the reactivity effect of reduction of the hydrogen density in the center region of the assembly, and the reflector savings.

A program of critical experiments[22–24] with homogeneous hydrogen-moderated assemblies of 2 per cent U^{235}-enriched uranium tetrafluoride (UF_4) and paraffin ($C_{25}H_{52}$) is in progress at ORNL to establish the bases for nuclear safety specifications and to provide general reactor analysis information. The minimum critical masses and minimum critical volumes have been established for bare and reflected cylinders and parallelepipeds for hydrogen-to-U^{235} atomic ratios of 195, 294, 404, and 501. In two additional experiments, assemblies with effective hydrogen-to-U^{235} atomic ratios of 245 and 400 were investigated. The assemblies were reflected by an effectively infinite thickness of paraffin or Plexiglas.

Several criticality experiments[25] have been performed at ORNL with assemblies of unclad ThO_2-UO_2 pellets, randomly stacked in aluminum or steel cylinders and moderated and reflected by water. The results were to be used as guides in the design of dissolver equipment for processing of spent fuel in the form of small, metal-clad pellets of thoria and urania. Sensitivity to the degree of moderation was determined for the critical dimensions.

The critical parameters of slabs of 93.4 wt.% U^{235}-enriched uranium metal have been measured[26] with the ORNL Critical Experiments Facility in a series of neutron multiplication experiments. Critical thicknesses and critical masses were determined for reflected and unreflected slabs of various areal dimensions. The effect of Plexiglas as a neutron reflector was determined by varying the reflector thickness for each areal dimension measurement, and a few measurements with beryllium and graphite reflectors were made.

A series of critical experiments[27] with the fuel elements of the Puerto Rico Nuclear Center research reactor has been completed in the Pool Critical Assembly of the Bulk Shielding Facility at ORNL. The purpose of the experiments was to verify the computations on which the design fuel-plate loading was based. The amount of excess reactivity to be expected from three clean, cold loadings was determined.

The ORNL determination of the thermal value for η of U^{233} and U^{235}, based on the direct comparison of the critical parameters of unreflected homogeneous aqueous solutions of the uranyl nitrates of U^{233} and U^{235}, is reported in reference 28.

The final corrected results of the manganese-bath measurements[29] for η of U^{233} and U^{235} have also been published. A detailed description of the experiment, including a complete listing and discussion of the corrections applied to the experimental data, is given in reference 30.

Flexible critical experiments[31,32] were conducted on the SM-2—the second reactor in the Army's Stationary Medium Power Plant series—at the Alco Products Criticality Facility in Schenectady, N. Y. The critical experiments consisted of a series of parametric studies designed to define some critical characteristics of stainless steel–UO_2 matrix fuel plates and to verify the analytically determined uranium and boron burnable poison loadings for the SM-2 core. Both the SM-1 and the SM-2 core arrays consist of 38 stationary fuel elements plus seven control-rod assemblies arranged in a 7×7 lattice with the four corner positions omitted. The parametric studies determined the initial criticality of the core and

gave calibration curves for estimating the excess reactivity for the fully fueled SM-2 core. Several SM-2 mockups, cold, clean, and midlife, were assembled. The measurements made on the cold, clean SM-2 core mockup included comparison of control-rod arrays, rod bank calibrations, critical control-rod configurations, and reactivity worth of a stainless steel–water laminated reflector. The core material coefficients and temperature coefficients of reactivity, as well as reflector effects, the effects of rotating elements, and the effect of substituting stationary elements for control rods, were measured on the final mockup. The final experiments were performed on mockups of the SM-2 midlife and initial core compositions, for the purpose of investigating the power-producing and control characteristics of the reactor. The midlife experiments consisted of measurements of the criticality, flow divider effects, reflector effects, critical rod configuration, and flux measurements.

Detailed experimental mockups[32] of the SM-1 core were assembled to study the reliability of the experimental and assembly techniques and to provide an estimate of the actual SM-1 loading. In the course of the experiments, heterogeneity factors were obtained which serve to evaluate the adequacy of mockups employing a reduced number of fuel plates. An experimental estimate of the SM-1 boron loading was determined. The measurements consisted of reactivity, uranium reactivity worth, boron worth, effect of substituting fuel elements, and heterogeneity effects.

The measurements[33] made during a zero-power experiment on the SM-1 core 2, the second operational core produced for the Army's Ft. Belvoir plant, included an element-by-element reactivity check of fuel elements and control-rod absorber sections and an estimate of the burnable nuclear poison loading in stationary fuel elements. An approach to critical was made by the inverse multiplication method, and critical rod bank position was obtained as a function of fuel loading up to full core loading. Minimum and maximum core reactivity measurements were obtained by selective loading of stationary fuel elements, and the total excess reactivity of the core was established. Power-distribution measurements were taken in the regions of the core-reflector interface and the fuel-absorber interface in the control-rod assemblies. The effectiveness of europium flux suppressors in the tops of control-rod fuel elements was determined, and power peaking was measured in stationary elements adjacent to control-rod-assembly water gaps. Survey measurements investigated the worth of spikes, consisting of SM-2 elements, in the SM-1 core, as well as the reactivity worth of water holes in the SM-1 core 2. A zero-power experiment of reduced scope, performed on SM-1A core 1, included an element-by-element uniformity check of stationary fuel elements, a core assembly test, comparison of Eu_2O_3 and B_4C absorber sections, and the development of initial core loading procedures for the SM-1A plant.

A group of papers on fast-neutron critical-assembly measurements and related topics appeared in the December 1960 issue of *Nuclear Science and Engineering*.[34–42] The following paragraphs give only the briefest summary of their contents.

Two of the plutonium metal critical assemblies that have been studied at the Pajarito site in Los Alamos are described in reference 34. The design features of Jezebel, the bare plutonium critical assembly, are given, as well as the observed characteristics such as critical mass, effective delayed-neutron fraction, Rossi-alpha values, prompt-neutron mean life, spectral indices, and reactivity coefficients. The second assembly is Popsy, a plutonium metal core in a thick normal uranium reflector. The design features of the assembly, and the experimental results, consisting of measurements of critical mass, Rossi-alpha values, reactivity calibrations, and a few spectral indices, are described.

Reference 35 presents the results of material replacement measurements made within the past 10 years on five critical assemblies at Pajarito by Los Alamos Scientific Laboratory. Three of the critical assemblies were set up on the Topsy machine: one (Topsy oralloy-uranium) was enriched uranium in a thick natural-uranium reflector; the second was a variant and had a core at one-half normal density; and in the third (Topsy oralloy-nickel), thick nickel was substituted for the uranium reflector. The fourth assembly, Godiva, was a nearly spherical enriched-uranium system without a reflector, and the fifth assembly was Jezebel, a bare delta-phase (low-density) plutonium system. The reactivity contribution measurements were made by determining the reactivity change when a small cavity within the system was filled by a

sample of the material of interest. A second group of measurements on Godiva was designed to give more precise data on the relative effective absorption cross sections for various elements, with particular attention to the apparent periodicity against Z for the isotopically simple odd Z–odd A elements. Reactivity contributions were also determined for large samples sealed in an aluminum can and placed in the cylindrical cavity at the center of Godiva. The interpretation of the material replacement data for Godiva is given as apparent absorption cross section, capture cross section, and scattering effect for each of the sample elements. The reactivity contributions of samples of plutonium, oralloy (93.5 per cent U^{235}), and uranium placed just beyond the Godiva surface were measured in an attempt to improve the information on the relative transport cross sections of these materials.

Some experimental information[36] on the shape dependence of critical size has been obtained at the LASL Critical-Assembly Laboratory. Critical configurations were established with enriched uranium and plutonium metal in the forms of squat and elongated cylinders with various reflectors. The elongated, 3.24-in.-diameter enriched-uranium cylinders were reflected by depleted uranium, graphite of various thicknesses, polyethylene, or water. The squat, 15.0-in.-diameter enriched-uranium cylinders were unreflected, and reflected by beryllium of various thicknesses, normal uranium, graphite, polyethylene, or water. The elongated, 2.25-in.-diameter plutonium cylinders were reflected by depleted uranium, graphite, polyethylene, water, or a combination of polyethylene and water. The squat, 6.0-in.-diameter plutonium cylinders were reflected by normal uranium, two thicknesses of graphite, or water. The observed critical heights and diameters were corrected to correspond to standard enriched-uranium and plutonium densities and concentrations. Specifications of the critical configurations are tabulated for the different cases. Critical data for a reasonably complete range of height-to-diameter values for water-reflected U^{235} cylinders are presented graphically, along with the less extensive data for water-reflected plutonium and for bare U^{235} assemblies.

The critical masses of 6-in.-diameter cylinders of plutonium diluted in various volume ratios with steel, aluminum, thorium, air, and depleted uranium were established in a series of measurements[37] performed at LASL. The critical parameters were determined for the diluted plutonium cores unreflected, and reflected with uranium or thorium reflector thicknesses of 2, 4.5, or 7.5 in. The resulting data are intended to help establish the effects of representative structural and fertile materials on the size of plutonium-fueled fast reactors. The equivalent spherical critical masses of plutonium have been estimated for each cylinder measurement. End-reflector savings for $\frac{1}{2}$-in.-thick disks of various reflector materials on an otherwise unreflected plutonium cylinder were determined. Reflector savings for $\frac{1}{2}$-in. thicknesses of these materials on uranium cores are included for comparison.

Critical mass measurements[38] have been obtained at the Pajarito Remote-Control Laboratory for cylindrical enriched-uranium cores unreflected, and reflected on both ends and one end only by multiple layers of two and three of the metals copper, iron (mild steel), zinc, nickel, and stainless steel. Similar measurements were conducted with the core partially moderated with graphite and with polyethylene in order to determine the effect of the decreased neutron energy upon the reflector savings of the multiple reflectors. The purpose of these measurements was to provide more information about the influence of the resonance scattering structure of the medium-Z elements in fast-neutron systems and, in particular, to determine the extent to which such resonance structure affects the validity of neutron calculations using linear mixing of multigroup element cross sections. The experimental results included the critical masses of an enriched-uranium core with one end reflected by each of the two-element reflectors, the critical masses of the graphite-diluted enriched-uranium core with one end reflected by a multiple reflector of zinc-iron and nickel–stainless steel and of the polyethylene-diluted enriched-uranium core with one end reflected by a multiple reflector of zinc-iron and nickel–stainless steel, and the critical masses of an enriched-uranium core reflected on one end and on both ends with reflectors composed of nickel, iron, and copper simulating a range of ternary alloys.

Reference 39 reports some criticality measurements that have been made by LASL on solid spherical core-reflector systems. Three different cores were used in the experiments (two of U^{233} and one of Pu^{239}), in conjunction with re-

flector materials of enriched uranium, normal uranium, beryllium, and tungsten alloy. The thickness of each of the various reflector materials required to obtain criticality with each of three cores was determined. Actual experimental measurements were modified to account for the nonideal experimental configurations.

An experiment[40] has been performed at the Pajarito Critical Assemblies Facility by LASL to measure the neutron-flux parameters in the equilibrium spectrum of natural uranium. The purpose of this experiment was to resolve the conflicting results reported from previous measurements at various laboratories, by measuring the buckling and spectral indices in a natural-uranium-metal exponential column system by means of several independent detectors under various source spectrum conditions and for different masses of uranium. Two exponential columns of natural uranium, each 30.7 in. high, with diameters of 15 and 21 in. were used with the small fast-reactor source (Hydro). The experiments were performed outdoors, about 11 ft above the ground level, in order to reduce flux perturbations due to backscattering of neutrons. The parameters investigated were the material buckling, the diffusion length, the U^{235}-to-U^{238} fission cross-section ratio, the Pu^{239}-to-U^{238} fission cross-section ratio, the Np^{237}-to-U^{238} fission cross-section ratio, and the U^{238} cross section for inelastic scattering of fission-spectrum neutrons across the U^{238} fission threshold. A summary of results of previous experiments is presented along with the results of the Pajarito survey.

The leakage neutron spectrum[41] of a bare Pu^{239} critical assembly (Jezebel) has been measured at LASL with nuclear emulsions. The leakage neutron spectrum from Godiva, a bare U^{235} critical assembly, is presented for comparison. Neutron spectrum measurements[42] have been made at the center of the bare U^{235} and Pu^{239} critical assemblies, Godiva and Jezebel, by means of the activation detectors $P(n,p)$, $Al(n,p)$, $Fe(n,p)$, $Al(n,\alpha)$, and $Cu(n,2n)$. The measured response ratios provide the basis for a comparison of high-energy portions of the Godiva-Jezebel spectra as well as comparisons with the corresponding fission-neutron spectra.

References

1. R. A. Egen et al., VMR Critical-Assembly Studies, USAEC Report BMI-1482, Battelle Memorial Institute, Dec. 2, 1960.
2. M. V. Davis et al., An Enriched UO_2-ZrH Critical Assembly, USAEC Report NAA-SR-5610, Atomics International, Nov. 1, 1960.
3. G. A. Price et al., Single Rod Fast Effects and Related Measurements, USAEC Report BNL-616, Brookhaven National Laboratory, May 1960.
4. I. H. Coen, Multi-Region Reactor Lattice Studies, Quarterly Progress Report for the Period July 1 to September 30, 1960, USAEC Report WCAP-1423, Westinghouse Electric Corp., Atomic Power Dept., October 1960.
5. G. H. Bidinger et al., Nuclear Safety Experiments on Plutonium and Enriched Uranium Hydrogen Moderated Assemblies Containing Boron, USAEC Report RFP-201, The Dow Chemical Co., July 7, 1960.
6. C. L. Schuske et al., Plexiglas Reflected Assemblies of Plutonium, USAEC Report RFP-213, The Dow Chemical Co., Jan. 10, 1961.
7. R. C. Lloyd et al., Critical Approach and Exponential Measurements with 3.1 Per Cent Enriched Uranium Rods in Light Water, in Nuclear Physics Research Quarterly Report for January, February, and March 1960, USAEC Report HW-64866, p. 143, Hanford Atomic Products Operation, Apr. 20, 1960.
8. R. C. Lloyd, Exponential Measurements of Natural Uranium-Water Systems, in Nuclear Physics Research Quarterly Report for January, February, and March 1960, USAEC Report HW-64866, p. 150, Hanford Atomic Products Operation, Apr. 20, 1960.
9. R. C. Lloyd, Exponential Measurements of Natural Uranium-Water Systems, in Nuclear Physics Research Quarterly Report for April, May, and June 1960, USAEC Report HW-66215, p. 34, Hanford Atomic Products Operation, July 20, 1960.
10. G. W. R. Endres and D. E. Wood, Material Bucklings of Graphite Uranium Lattices, in Nuclear Physics Research Quarterly Report for January, February, and March 1960, USAEC Report HW-64866, p. 65, Hanford Atomic Products Operation, Apr. 20, 1960.
11. W. A. Reardon and R. C. Lloyd, Shape Perturbations in Critical Experiments, in Nuclear Physics Research Quarterly Report for April, May, and June 1960, USAEC Report HW-66215, p. 27, Hanford Atomic Products Operation, July 20, 1960.
12. W. A. Reardon and R. C. Lloyd, Shape Perturbations in Critical Experiments, in Nuclear Physics Research Quarterly Report for October, November, and December 1959, USAEC Report HW-63576, pp. 70–76, Hanford Atomic Products Operation, Jan. 20, 1960.
13. R. C. Lloyd et al., Critical Approach and Exponential Measurements with 2.00 Per Cent Enriched Uranium Rods in Light Water, in Nuclear Physics Research Quarterly Report for April, May, and June 1960, USAEC Report HW-66215,

p. 30, Hanford Atomic Products Operation, July 20, 1960.

14. R. C. Lloyd, Exponential Experiments with Poisoned Moderator, in Nuclear Physics Research Quarterly Report for January, February, and March 1960, USAEC Report HW-64866, p. 148, Hanford Atomic Products Operation, Apr. 20, 1960.
15. V. I. Neeley et al., Neutron Multiplication Measurements with Pu-Al Alloy Rods in Light Water, in Nuclear Physics Research Quarterly Report for January, February, and March 1960, USAEC Report HW-64866, p. 137, Hanford Atomic Products Operation, Apr. 20, 1960.
16. J. R. Worden and P. F. Nichols, Lattice Parameters for the Experimental Gas Cooled Reactor, in Nuclear Physics Research Quarterly Report for April, May, and June 1960, USAEC Report HW-66215, p. 14, Hanford Atomic Products Operation, July 20, 1960.
17. P. F. Nichols, EGCR Lattice Radial and Angular Power Distribution–2.6 Wt.% Enrichment, in Nuclear Physics Research Quarterly Report for April, May, and June 1960, USAEC Report HW-66215, p. 24, Hanford Atomic Products Operation, July 20, 1960.
18. P. F. Nichols and R. E. Heineman, PCTR Measurements of Control Rod Strength, in Nuclear Physics Research Quarterly Report for January, February, and March 1960, USAEC Report HW-64866, p. 105, Hanford Atomic Products Operation, Apr. 20, 1960.
19. P. F. Nichols and J. R. Worden, PCTR Measurement of the Reactivity Effect of a Stainless Steel Loop Tube in the EGCR, in Nuclear Physics Research Quarterly Report for April, May, and June 1960, USAEC Report HW-66215, p. 18, Hanford Atomic Products Operation, July 20, 1960.
20. R. A. Bennett, Neutron Rethermalization in Graphite in Cylindrical Geometry, in Nuclear Physics Research Quarterly Report for January, February, and March 1960, USAEC Report HW-64866, p. 114, Hanford Atomic Products Operation, Apr. 20, 1960.
21. J. K. Fox et al., Solution Experiments in a Flux-Trap Critical Assembly: Preliminary Study for High Flux Isotope Reactor, in Neutron Physics Division Annual Progress Report for Period Ending September 1, 1960, USAEC Report ORNL-3016, pp. 59–70, Oak Ridge National Laboratory, Dec. 13, 1960.
22. J. T. Mihalczo and J. J. Lynn, Homogeneous Critical Assemblies of 2% U^{235}-Enriched UF_4 in Paraffin, in Neutron Physics Division Annual Progress Report for Period Ending September 1, 1960, USAEC Report ORNL-3016, p. 71, Oak Ridge National Laboratory, Dec. 13, 1960.
23. J. T. Mihalczo and J. J. Lynn, Homogeneous Critical Assemblies of 2% U^{235}-Enriched UF_4 in Paraffin, in Neutron Physics Division Annual Progress Report for Period Ending September 1, 1959, USAEC Report ORNL-2842, p. 85, Oak Ridge National Laboratory, Nov. 16, 1959.
24. J. J. Lynn et al., Homogeneous Hydrogen-Moderated Critical Assemblies with 2% U^{235} Enriched Uranium, in Neutron Physics Division Annual Progress Report for Period Ending September 1, 1958, USAEC Report ORNL-2609, p. 40, Oak Ridge National Laboratory, Oct. 28, 1958.
25. J. K. Fox and L. W. Gilley, Critical Dimensions of Random Arrays of ThO_2-UO_2 Pellets, in Neutron Physics Division Annual Progress Report for Period Ending September 1, 1960, USAEC Report ORNL-3016, p. 72, Oak Ridge National Laboratory, Dec. 13, 1960.
    Oak Ridge National Laboratory, Dec. 13, 1960.
26. J. T. Mihalczo and J. J. Lynn, Critical Parameters of Bare and Reflected 93.4 Wt.% U^{235}-Enriched Uranium Metal Slabs, in Neutron Physics Division Annual Progress Report for Period Ending September 1, 1960, USAEC Report ORNL-3016, pp. 73–75, Oak Ridge National Laboratory, Dec. 13, 1960.
27. E. B. Johnson and K. M. Henry, Jr., Critical Experiments with PRNC Research Reactor Fuel Elements, in Neutron Physics Divisicn Annual Progress Report for Period Ending September 1, 1960, USAEC Report ORNL-3016, pp. 76–80, Oak Ridge National Laboratory, Dec. 13, 1960.
28. R. Gwin and D. W. Magnuson, Determination of the Thermal Value of η of U^{233} and U^{235} by Direct Comparison of Critical Parameters of Aqueous Solutions, in Neutron Physics Division Annual Progress Report for Period Ending September 1, 1960, USAEC Report ORNL-3016, p. 81, Oak Ridge National Laboratory, Dec. 13, 1960.
29. R. L. Macklin et al., Measurements of η of U^{233} and U^{235} by a Manganese-Bath Technique, in Neutron Physics Division Annual Progress Report for Period Ending September 1, 1960, USAEC Report ORNL-3016, p. 81, Oak Ridge National Laboratory, Dec. 13, 1960.
30. R. L. Macklin et al., Manganese Bath Measurements of η of U^{233} and U^{235}, USAEC Report CF-60-2-84, Oak Ridge National Laboratory, Mar. 15, 1960.
31. W. J. McCool et al., SM-2 Flexible Critical Experiments, *Nuclear Sci. and Eng.*, 9(1): 47–54 (January 1961).
32. J. W. Noaks et al., SM-2 Critical Experiments—CE-1, USAEC Report APAE-54, Alco Products, Inc., Nov. 30, 1959.
33. R. A. Robinson et al., SM-1 Research and Development Task XV, Zero Power Experiments for SM-1 Core II and SM-1A Core I, USAEC Report APAE-58(Rev.), Alco Products, Inc., Oct. 12, 1960.
34. G. A. Jarvis et al., Two Plutonium-Metal Critical Assemblies, *Nuclear Sci. and Eng.*, 8(6): 525–531 (December 1960).

35. L. B. Engle et al., Reactivity Contributions of Various Materials in Topsy, Godiva, and Jezebel, *Nuclear Sci. and Eng.*, 8(6): 543–569 (December 1960).

36. G. E. Hansen et al., Critical Plutonium and Enriched-Uranium-Metal Cylinders of Extreme Shape, *Nuclear Sci. and Eng.*, 8(6): 570–577 (December 1960).

37. D. P. Wood et al., Critical Masses of Cylinders of Plutonium Diluted with Other Metals, *Nuclear Sci. and Eng.*, 8(6): 578–587 (December 1960).

38. G. E. Hansen et al., Critical Masses of Enriched-Uranium Cylinders with Multiple Reflectors of Medium-Z Elements, *Nuclear Sci. and Eng.*, 8(6): 588–594 (December 1960).

39. E. A. Plassmann and D. P. Wood, Critical Reflector Thicknesses for Spherical U^{233} and Pu^{239} Systems, *Nuclear Sci. and Eng.*, 8(6): 615–620 (December 1960).

40. C. G. Chezem, A Uranium-Metal Exponential Experiment, *Nuclear Sci. and Eng.*, 8(6): 652–669 (December 1960).

41. L. Stewart, Leakage Neutron Spectrum from a Bare Pu^{239} Critical Assembly, *Nuclear Sci. and Eng.*, 8(6): 595–597 (December 1960).

42. J. Grundl and A. Usner, Spectral Comparisons with High Energy Activation Detectors, *Nuclear Sci. and Eng.*, 8(6): 598–607 (December 1960).

Section III

HEAT TRANSFER AND FLUID FLOW

Shutdown Cooling of Steam-Cooled Superheating Elements

As discussed in Sec. X, several nuclear superheat reactor designs employ superheating fuel elements which are insulated, by stagnant steam or other insulating material, from the surrounding water moderator. Although the insulating layer is necessary under normal operating conditions, to prevent a large flow of heat from the hot superheater elements to the surrounding liquid water, it becomes a liability at shutdown when there is no coolant flow in the superheating elements. In the absence of forced convection, the superheater fuel must cool by radiation and conduction across the insulating gap, and by whatever natural convection of steam may be established. Two reports have been written on the subject of shutdown cooling of superheating elements.[1,2]

Shutdown cooling experiments of superheater elements performed by the General Electric Company's Atomic Power Equipment Department (APED) were done with a resistance cartridge heater encased in a tube liner.[1] Coaxial to this was another tube, the process tube, which trapped an annulus of saturated steam 0.030 in. thick. The cartridge heater was made from type 321 stainless steel, and the two remaining tubes were fabricated from type 304. The assembly, which had a heated length of 15 in., was immersed in a tank of water at atmospheric pressure, which simulated the water moderator. Thermocouples were fastened to the heater, the liner, and the process tube to obtain pertinent temperature data.

To obtain data of general applicability, it is necessary to evaluate separately the heat transfer by convection, conduction, and radiation. The approach was to determine how much heat was transferred by convection and conduction and to assign the remainder of the total to radiation. The APED experiments studied the relative importance of convection and conduction by placing helium, nitrogen, or a vacuum in the 0.097-in. annulus between the heating element and the tube liner. The heat transferred by natural convection is proportional to $kY^{0.25}$, where:

k = thermal conductivity in consistent units
Y = (Grashof number)/$(D^3 \times \Delta T)$
D = characteristic dimension of system
ΔT = temperature difference between surface and fluid

On the other hand, the amount of heat transferred by conduction is proportional to the thermal conductivity, k. The operating pressures for the tests involving nitrogen and helium were chosen so that the terms $kY^{0.25}$ were about the same, whereas the values of k for helium were three to four times greater than for nitrogen. Analysis of the data revealed that convection played a very minor role in the total transfer of heat. The steady-state heat transfer between the liner wall (surface 3) and the process tube wall (surface 4) was given by

$$q = \frac{k\left(\frac{A_3 + A_4}{2}\right)}{r_4 - r_3}(T_3 - T_4) + \frac{A_3\sigma}{\frac{1}{\epsilon}\left(1 + \frac{r_3}{r_4}\right) - \frac{r_3}{r_4}}(T_3^4 - T_4^4) \quad (1)$$

The symbols A, r, and T refer to the area, radius, and temperature of the two walls; q is the power input to the heater; and σ is the Stefan-Boltzmann constant. A similar equation with different subscripts applies to heat trans-

ferred from the heating element to the liner. These equations were solved for the emissivity, ϵ; a value of 0.495 was determined for all stainless-steel surfaces, and this was taken to be independent of temperature. The temperatures attained during the experimentation ranged from 1167 to 1237°F for the heater surface and from 556 to 636°F for the liner.

Surface conditions affect emissivity and are important in radiant heat transfer. The two heating elements used in the APED experiments exhibited a "high coloration" after removal from the test rig; the high coloration was attributed to the formation of an oxide film. The film was present even in the evacuated runs. The oxidation was attributed to moisture in the pressurizing gases and to the presence of low-pressure air in the evacuated runs. The viscosity and thermal-conductivity values used in reference 1 for superheated steam are not those recommended by ANL[3] (discussed in the March 1961 issue of *Power Reactor Technology*, Vol. 4, No. 2). At 1000 psia and 900°F, the recommended Russian thermal-conductivity value is approximately 28 per cent higher than the corresponding value from the data of Keyes (1952), which were apparently utilized. This is not an important point, however, since steam was not used in the APED experiments and since the steam data were used only to compute a Grashof number for comparison with helium and nitrogen.

A comparable experiment done by General Nuclear Engineering Corporation (GNEC) is reported in reference 2. The geometry of the test assembly is given in Fig. III-1. The heater was fabricated of type 304 stainless steel and had an outside diameter of $\frac{5}{8}$ in. This was placed in a tube having a 0.75-in. outside diameter and a 65-mil wall thickness, representing the cladding of the fuel element. The coolant tube or liner (1.065-in.-OD by 35-mil wall) was positioned around the mocked-up element to form the coolant channel. The coaxial pressure tube (1.250-in.-OD by 49-mil wall) completed the assembly. The heated length was 14 in., and the tubes were fabricated from type 304 stainless steel. Runs were made at pressures of 380 and 900 psig and with heater outside wall temperatures ranging from roughly 900 to 1500°F. The radiant heat transfer was computed using equations similar to the last term of Eq. 1, except that the emissivities of two surfaces

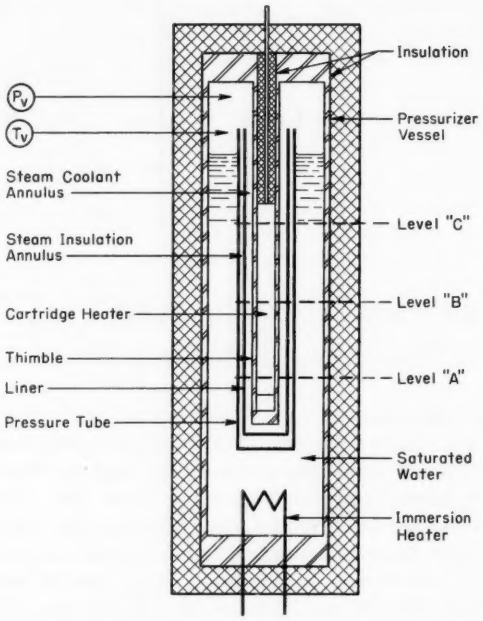

Fig. III-1 Schematic diagram of test assembly.[2]

"seeing" each other were not taken to be the same.

The method of accounting for heat not transferred by radiation was to employ the correlation discussed in Sec. 25-3 of Jakob.[4] This technique uses an equivalent film coefficient which includes the effect of conduction and convection; the correlation is based on Figs. 25 to 27 of Jakob. Reference 2 used the steam thermal-conductivity data given in *National Bureau of Standards Circular No. 564*, and these data are very close to those of Keyes (1952). Figure III-2 contains the results of the experiments, and Fig. III-3 shows the comparison of experimental data with calculated temperatures using the emissivity values given in Fig. III-2. Values shown in Fig. III-2 represent the "upper-limit emissivity values for stably oxidized surfaces." The reference recommends that the values ranging from 0.50 to 0.65 be used for new fuel elements. Although the emissivities indicated by references 1 and 2 do not agree, it is hard to identify a discrepancy, for surface condition plays an extremely important role in determining the emissivity. Figure III-4, taken from reference 2, illustrates the wide range of emissivities reported for various surfaces.

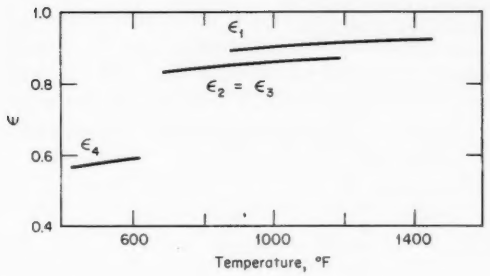

Fig. III-2 Total normal emissivity for test element No. 1 at level B.[2]

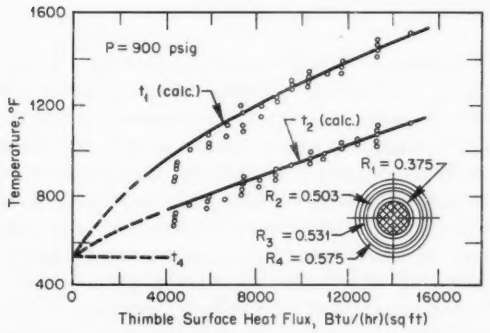

Fig. III-3 Variation of test-element temperatures with thimble surface heat flux.[2]

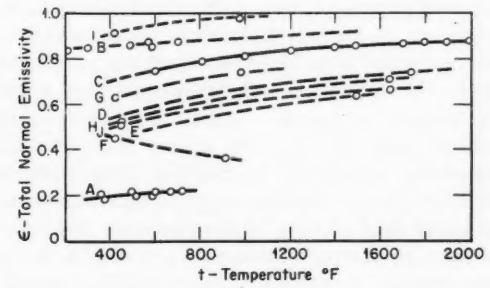

Fig. III-4 Total normal emissivity of various stainless steels.[2] *A*, 18-8 unpolished (Snyder et al.). *B*, 18-8 oxidized at 1500°F, weathered (Snyder et al.). *C*, AISI 303 oxidized at 2000°F in air for 60 min (Wade). *D*, AISI 303 oxidized at 1800°F in air for 60 min (Wade). *E*, AISI 303 oxidized at 1500°F in air for 60 min (Wade). *F*, AISI 304 light silvery brown after heating (Rice). *G*, AISI 304 after 42-hr heating at 980°F (Rice). *H*, AISI 301 after repeated heating and cooling (Wilkes). *I*, AISI 310 after furnace service (Rice). *J*, AISI 347 after repeated heating and cooling (Wilkes).

Liquid Metals

A recent report deals with an analytical and experimental treatment of heat transfer to mercury flowing parallel to a bundle of heated rods.[5] The conditions of the experiment are given in Table III-1. The experimental data were compared to two theoretically derived equations. The Dwyer and Tu correlation[6] is given as Eq. 2, and the correlation of Friedland and Bonilla,[7] as Eq. 3.

$$N_{Nu} = 0.93 + 10.81\,(P/D) - 2.01\,(P/D)^2 + 0.0252\,(P/D)^{0.273}\,(\mathrm{Pe})^{0.8} \quad (2)$$

$$N_{Nu} = 7.0 + 3.8\,(P/D)^{1.52} + 0.027\,(P/D)^{0.27}\,(\mathrm{Pe})^{0.8} \quad (3)$$

where

N_{Nu} = Nusselt number
P/D = pitch-to-diameter ratio
Pe = Peclet number

Surface temperatures were measured by thermocouples on the central heating element only. This center element was replaceable, and a total of eight heater elements were used*; the heater sheath was either nickel and copper plated for runs wherein the coolant wetted the surface, or chromium plated for nonwetting runs.

The experimental results indicated "rather poor" reproducibility of the data. Some of the runs agreed with the theoretical equations, whereas others gave results from 70 per cent above to 50 per cent below. In addition, at a given axial position, a relatively large circumferential variation in heater surface temperature was observed. After analytical and experimental work, it was concluded that the difficulties were due to some extent to the existence of slight deviations from true straightness. Quoting the reference: "... appreciable changes in peripheral temperatures and Nusselt number can result from misalignments."

Another heat-transfer rig was constructed to examine the problem further. Although the rig had dimensions different from those given in Table III-1, its major difference was that all

*Five heaters in first bundle and three in second bundle assembly.

Table III-1 SCOPE AND EXPERIMENTAL CONDITIONS OF INVESTIGATION OF HEAT TRANSFER BY MERCURY[5]

	Bundle design No. 1	Bundle design No. 2
Tube size, OD, in.	0.498	0.500
Tube spacing	Equilateral triangular	Equilateral triangular
No. of tubes	19	13
Pitch-to-diameter ratio	1.380	1.750
Heated length, in.	40	54
Shell ID, in.	3.39	3.96
Flow	Vertically upward	Vertically upward
Heat flux, Btu/(hr)(sq ft)	13,500	37,000
Reynolds number range	8000–80,000	35,000–175,000
Temp., °F	120–260	~100
Prandtl number range	0.016–0.021	~0.0227
Peclet number range	190–1700	800–4000
Linear velocity, ft/sec	0.16–2.0	0.41–2.04

the rods were kept under tension to prevent possible bowing from the thermal expansion. Preliminary results indicated no significant circumferential surface temperature variations with the new rig. Figure III-5 illustrates data

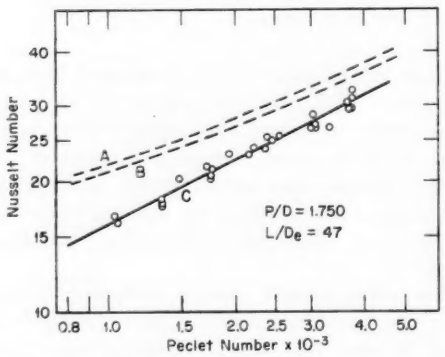

Fig. III-5 Nusselt number versus Peclet number.[5] Curve *A*, Friedland and Bonilla equation. Curve *B*, Dwyer and Tu equation. Curve *C*, experimental.

taken on the new rig. It is significant that the experimental points fall below the theoretical equations. The authors recommend that the theoretical equations be reduced by a factor Y to bring them into agreement with the experimental data; a table of Y versus Peclet number is presented for the various theoretical equations.

Gas Suspension Coolants

The use of solid particles suspended in a gaseous coolant was discussed in the September 1960 issue of *Power Reactor Technology*, Vol. 3, No. 4. Additional reports from Babcock and Wilcox have recently become generally available.[8,9] Additional data are presented, including the heat-transfer results from the annular-flow heating element. Results of a fission-product distribution study are also presented. The purpose of these latter experiments was to determine the distribution of fission products in a system composed of powdered graphite, a gas, and stainless steel. The data taken with the turbulence promoter incorporated in the test rig were correlated with equations different from those given in the earlier Review (Table III-2 of the September 1960 issue of *Power Reactor Technology*, Vol. 3, No. 4); of significance, however, is the fact that no one equation serves to correlate data from test sections employing different diameters and different pitches of the turbulence promoter. Also, the correlations which apply for heating do not yield Nusselt numbers applicable to cooling. This multiple number of correlations suggests that the mechanism of heat transfer in a suspension flowing in a tube employing turbulence promoters is not understood. Accordingly, the combined analytical and experimental approach to the problem given in reference 10 is of interest.

The University of California study[10] was on the problem of heat transfer to an air stream containing solid glass beads flowing upward in a vertical tube. Heat balance and energy equations were integrated subject to various assumptions, the most important being that the air and solids act as a homogeneous mixture with nearly equal local temperatures and with the same velocity distribution as the unladen air.

The experiments employed 30- and 200-μ spheres at two superficial-air Reynolds numbers: 13,500 and 27,400. No turbulence promoters were utilized. Figure III-6 presents the local Nusselt number as a function of the solids loading ratio,* and Fig. III-7 illustrates the local Nusselt number as a function of axial distance. These figures apply to the 30-μ spheres; the results using the 200-μ spheres indicated "practically no effect due to the solids."†

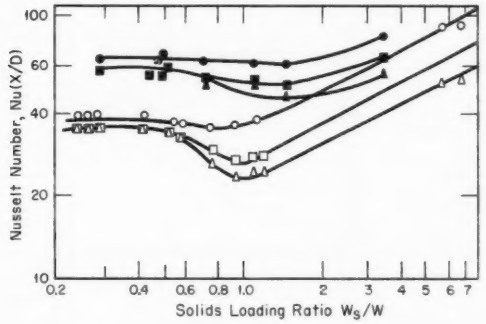

Fig. III-6 Local Nusselt number versus solids loading ratio, using 30-μ particles.[10] Solid symbols are for Re = 27,400. Open symbols are for Re = 13,500. ○ and ●, X/D = 8.4. □ and ■, X/D = 25.4. △ and ▲, X/D = 46.9.

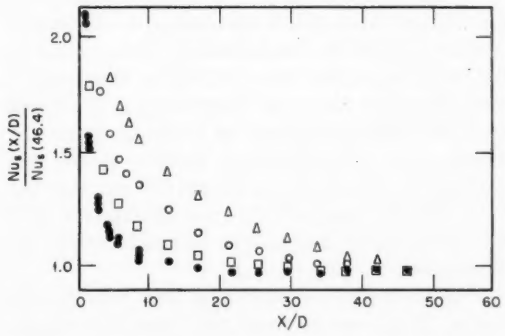

Fig. III-7 Local Nusselt number ratio versus axial distance at different loading ratios.[10] Reynolds number = 13,500. Particle diameter = 30 μ. ●, W_S/W = 0. □, W_S/W = 0.58. ○, W_S/W = 0.78. △, W_S/W = 1.17.

In considering Fig. III-6, it is evident that below a solids loading ratio of about 0.5 the solids have no effect. At loading ratios between 1 and 2, the solids hinder the transfer of heat, and lower Nusselt numbers result. As solids loading increases, heat transfer improves, and Nusselt numbers increase above the values for air alone. From Fig. III-7 it is evident that the thermal entry length increases with increasing solids loading.

The author[10] expresses dissatisfaction with the model used to derive the analytical results; the assumptions of equal phase temperatures and velocity distribution are evidently not valid. Another assumption employed was that the solid phase was uniformly distributed across the tube, and this is open to question. The reference[10] recommends that further study be done on the effect of the solids on the motion of the coolant and on the development of a better approximation for the difference between the gas and solid temperatures.

Burnout in Water-Cooled Systems

Reference 11 is a report on work done at ORNL on a natural-circulation system. The initial purpose of the program was to determine burnout heat fluxes for the HFIR to be built at ORNL, under conditions in which the reactor was shut down and the fuel elements were being removed. In addition, data were obtained pertinent to the core removal of the Oak Ridge Research Reactor (ORR). Other coolant channel geometries were also studied, including empty tubes and tubes with full-length internal twisted-tape swirl-flow generators. The experimental apparatus is shown in Fig. III-8, and the test conditions are given in Table III-2. The infinite values given in the last column of Table III-2 denote that the downcomer was completely restricted or had a zero-flow area. Power was determined from the current and voltage drop of the electrically heated test section, with suitable corrections to account for system losses. Inlet and outlet water temperatures were measured, and outside surface temperatures of the test section were measured at unspecified locations. As burnout approached, metal temperatures increased, and this resulted in a decreased current flow due to increasing resistance: the burnout criterion was taken as the power corresponding to the observed maximum value of current. Apparently the test section was destroyed in one or more runs, since the authors state that "maximum

*Pounds of solid per pound of air.

†The Babcock and Wilcox experiments[8] were done with particles ranging from 0.70 to 2.0 μ.

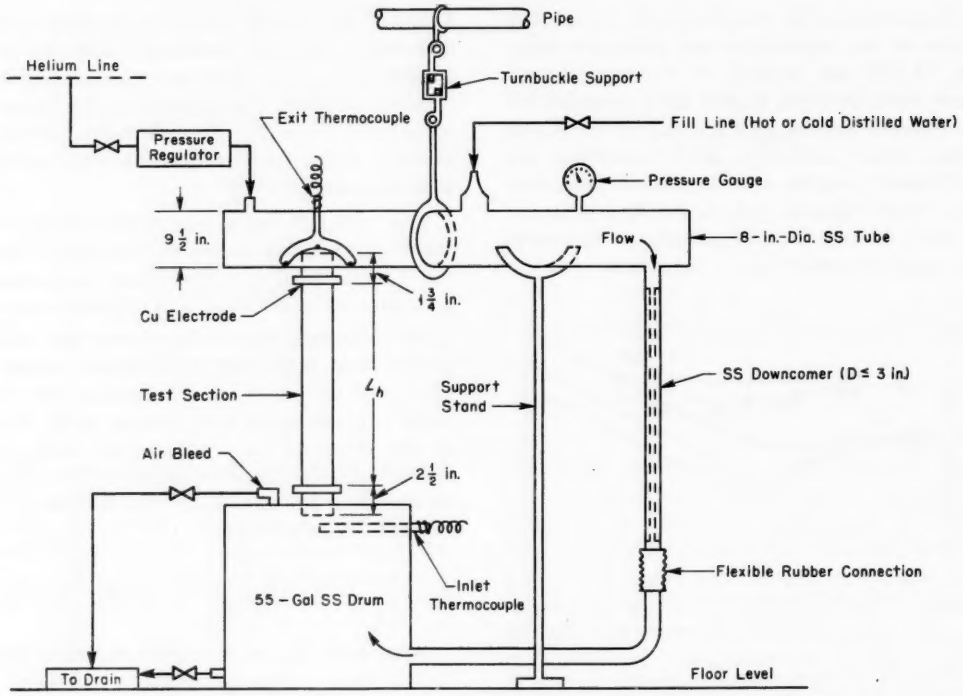

Fig. III-8 Experimental system for natural-circulation heat-transfer tests.[11]

temperatures (or metal failure) occurred at the top of the test section when the coolant was externally recirculated and at the bottom of the section when no return leg was used." Power was then corrected from an average to a maximum value using the resistivity values corresponding to the measured average and maximum wall temperatures. The resulting axial power profiles for the various runs are not illustrated, and the axial maximum-to-average value is given for only two runs—run 13 had a value of 2.19, and run 11 had a value of 1.007. The value for run 13 was chosen to represent ORR conditions, but whether a cosine-like distribution was attained is not mentioned.

Table III-3 presents the natural-circulation burnout data test results. As stated in the table footnote, the experimental burnout fluxes were calculated from the measured wall temperatures. The reference does not state that the experimental values of ϕ_{BO} given in column 4 of the table are actually at the axial position where burnout occurred. Presumably a definition of a limiting heat flux would be the heat flux at the geometrical location where the limitation occurred. If this were the definition, then the values listed would correspond to the power transferred to the coolant at the exit portion of the tube, neglecting the runs with no downcomer, where burnout occurred elsewhere. It is evident from the second column of Table III-3 that the system was producing high-quality steam; the exit quality was between 95 and 100 per cent for 11 of the 15 runs with the rectangular test section wherein the downcomer was not completely restricted.

The predicted burnout heat flux (column 5 in Table III-3) comes from the "semitheoretical prediction method" illustrated in the reference. The flow equation for natural circulation is derived assuming that the phases flow homogeneously, i.e., with no slip. This results in an equation relating the mass flow in the system to the densities in the heated section and downcomer and to the physical dimensions of the system. The correlation of Lowdermilk et al.[12] for straight-flow burnout is used for the runs wherein no swirl promoter was utilized; this equation relates the burnout heat flux to mass velocity and system dimensions. These two

TABLE III-2. NATURAL-CIRCULATION BURNOUT DATA TEST CONDITIONS[11]

Test No.	Flow Channel Dimensions (in.)	L_h (in.)	L_t (in.)	y (dia/180-deg twist)	Material	P_2[a] (psia)	t_{b_1} (°F)	$(\Delta t_{sub})_1$ (°F)	Downcomer ID (in.)	A_{TS}/A_D[b]
1	0.056 x 1.06	17.99	22.0	---	0.057 A-nickel	20.2	75 – 77	151	2.870	0.0092
2	0.053 x 1.06	17.94	22.0	---	separated by	15.4	68 – 75	140	2.870	0.0087
3	0.052 x 1.08	17.80	22.0	---	0.050 Inconel	25.7	122 – 125	117	2.870	0.0087
4	0.054 x 1.06	17.94	22.0	---	spacers	20.6	75	154	2.870	0.0088
5	0.052 x 1.11	17.92	22.0	---	"	25.7	124 – 128	114	0.000	∞
6	0.052 x 1.06	17.92	22.0	---	"	25.7	124	118	0.137	3.72
7	0.052 x 1.06	17.92	22.0	---	"	25.2	122	119	0.095	7.65
8	0.052 x 1.06	17.92	22.0	---	"	25.0	123	117	0.000	∞
9	0.116 x 2.07	23.38	27.0	---	0.059 A-nickel	25.5	121	120	0.000	∞
10	0.119 x 2.07	23.33	27.0	---	separated by	20.0	86	142	2.870	0.0381
11	0.119 x 2.07	23.33	27.0	---	0.116 Inconel spacers	26.3	127	116	2.870	0.0381
12	0.119 x 2.07	23.33	27.0	---	"	15.0	129	84	2.870	0.0381
13	0.113 x 2.09	23.65	35.5	---	0.057 A-nickel	26.1	115	127	0.180	8.86
14	0.066 x 2.26	33.28	37.0	---	separated by	24.5	176	63	2.870	0.0231
15	0.066 x 2.26	33.28	37.0	---	0.060 Inconel spacers	15.8	78	137	2.870	0.0231
16	0.066 x 2.26	33.28	37.0	---	"	14.7	176	46	2.870	0.0231
17	0.066 x 2.26	33.28	37.0	---	"	15.2*	184	40	2.870	0.0231
18	0.066 x 2.26	33.28	37.0	---	"	14.7	84	138	2.870	0.0231
19	0.249 ID	9.99	14 0	---	0.249 x 0.354	15.0	74	149	2.870	0.0076
20	0.249 ID	10.05	14.0	---	copper tubes	25.0	76 – 78	162	2.870	0.0076
21	0.249 ID	10.09	14.0	---	"	24.5	169 – 174	65	2.870	0.0076
22	0.249 ID	10.00	13.5	2.30	0.249 x 0.354	24.7	71 – 73	166	2.870	0.0070
23	0.249 ID	10.09	13.5	2.30	copper tubes	15.0	71 – 73	140	2.870	0.0070
24	0.249 ID	10.06	13.5	4.94	with full-length	15.0	78	135	2.870	0.0070
25	0.249 ID	10.09	13.5	8.03	0.015 Inconel twisted tapes	15.0	82	131	2.870	0.0070
26	0.249 ID	10.09	13.5	4.94	"	24.6	64	175	2.870	0.0070
27	0.249 ID	10.08	13.5	4.94	"	24.8	177 – 180	59	2.870	0.0070
28	0.249 ID	10.12	13.5	8.03	"	24.8	69	170	2.870	0.0070
29	0.249 ID	10.12	13.5	8.03	"	25.1	176 – 179	61	2.870	0.0070

[a] Pressure at top of heated length of test section.

[b] Ratio of the test-section coolant-flow area to that of a section of the downcomer having the same total length as the test section. The rest of the downcomer had a coolant-flow area much larger than that of the test section.

* At burnout, the liquid level was 10-3/4 in. below the heated exit.

TABLE III-3. NATURAL-CIRCULATION BURNOUT DATA TEST RESULTS[11]

Test No.	$(x_e)_{bo}$[c] Calculated (%)	$(t_i)_{max}$[d] (°F)	$(\phi_{bo})_{exptl}$[e] (Btu/hr·ft^2)	$(\phi_{bo})_{pred}$[f] (Btu/hr·ft^2)	$(\phi_{bo})_{exptl}/(\phi_{bo})_{pred}$
1	96	232	48,800	68,000	0.718
2	100	214	52,200	63,600	0.833
3	98	433	83,100	83,000	1.001
4	99	226	50,100	71,500	0.700
5	--	293	13,000	---	---
6	97	277	70,600	78,000	0.905
7	100	260	61,500	69,500	0.885
8	--	402	19,700	---	---
9	--	242	18,500	---	---
10	82	244	127,100	122,000	1.043
11	76	266	127,100	136,000	0.930
12	77	--	95,200	111,000	0.863
13	27	254	151,400[g]	153,000	0.990
14	100	286	67,700	63,500	1.066
15	100	225	59,300	57,100	1.039
16	100	239	51,100	49,400	1.034
17	100	232	49,000	43,400	1.114
18	100	221	30,500	39,600	0.770
19	80	259	118,900	137,000	0.868
20	75	271	137,100	166,000	0.826
21	85	246	218,500	158,000	1.383
22	100	273	144,200	164,000	0.879
23	100	257	135,500	144,000	0.941
24	97	246	114,700	156,000	0.735
25	80	239	126,900	167,000	0.760
26	75	248	139,100	196,000	0.710
27	89	228	198,900	188,000	1.058
28	73	259	143,900	205,000	0.702
29	84	255	175,900	193,000	0.911

[c] Exit quality calculated from the semitheoretical burnout prediction method presented in this report (homogeneous flow model).

[d] Defined as the maximum surface temperature reached just before the sharp rise in temperature at burnout.

[e] Corrected from an average to a maximum value by using the electrical resistivities corresponding to the measured maximum and average wall temperatures.

[f] Predicted using the semitheoretical burnout prediction method presented in this report (homogeneous flow model).

[g] $\phi_{max}/\phi_{avg} = 2.19$.

equations are then solved for several assumed values of the exit quality, and a graph is made of $\phi_{BO}/\phi_{av.}$ vs. ϕ_{BO}, where $\phi_{av.}$ is the average heat flux necessary to produce the assumed exit quality. The burnout heat flux is then determined as that flux for which $\phi_{BO}/\phi_{av.}$ equals the axial peak-to-average power ratio for the channel under consideration. Implicit in this technique appears to be the assumption that burnout is not a very strong function of local enthalpy, since no mention is made of how various axial power distributions affect the accuracy. In any case there is good agreement between the analytical and experimental data (see Table III-3).

Flow oscillations were noted in many of the runs. This was studied indirectly by measuring outlet coolant temperature fluctuations, and the heat-flux thresholds for various degrees of flow instability are given in Table III-4.

Table III-4 HEAT-FLUX THRESHOLDS FOR FLOW OSCILLATION[11]

Test No.	Lower* Btu/(hr)(sq ft)	Upper† Btu/(hr)(sq ft)
1	1,700	11,700
2	1,540	11,400
3		10,600
4	1,800	13,200
5		5,200
9	2,140	
20	94,000	
21	33,900	54,400
22	52,500	63,500
23		68,600
24		62,300
25		95,500
26	77,000	
27	74,600	

*The heat flux at which the exit water temperature began a stable oscillation of low frequency (<1 cps) and small amplitude (±9 to 15°C maximum).

†The heat flux at which the exit water temperature began a stable oscillation of higher frequency (>1 cps) and larger amplitude (±19 to 25°C maximum).

The Savannah River Operations Office of the USAEC has been supporting basic experimental studies on boiling fluid flow and heat transfer at elevated pressures, at the Engineering Research Laboratories of Columbia University.[13,14] The basic apparatus is a flow loop designed to operate up to 1000 psi at a maximum flow rate of 250 gal/min. The test section can house elements up to 10 ft in length, heated by direct current, and the system has a heat-removal capacity of 10^7 Btu/hr. Burnout detection is accomplished by comparing the resistances of various portions of the heated test section. The apparatus is described in detail in reference 14.

Preliminary data were taken on a type 304 stainless-steel heater tube 40 in. in length and 1.38 in. in outside diameter. These data are given in Table III-5 and are shown in Fig. III-9. Also shown in Fig. III-9 are other burnout data and some burnout correlations. A striking feature of Fig. III-9 is the spread of the data. The Columbia and General Electric APED data taken with annular test sections group together, whereas the ANL and MIT data taken with tubular geometry tend to group together. For the two Columbia runs marked "27," the data give both the onset of burnout as indicated by a signal from the burnout detector (lower point) and the point of physical destruction of the heating tube (upper point). Runs 25 and 26 were made under nearly identical conditions but yielded slightly different burnout values; this is tentatively attributed by the experimenters[14] to deterioration of the surface finish of the heater tube.

Other test sections are planned that will more nearly approximate reactor fuel elements. The test section to be used next is a cluster of seven type 347 stainless-steel rods. The individual rods are 0.55 in. in outside diameter, on a 0.633-in. pitch, and have heated lengths of 37 in. A second cluster of seven rods is planned, similar in detail to the first, except that the outer six rods are to be wrapped with 83-mil-OD tubing to maintain the tube-to-tube spacing. Helical spacers such as these have been specified for use in the Heavy-Water Components Test Reactor (HWCTR), and the test loop data will determine whether the presence of the spacers results in a reduction of the burnout heat flux due to centrifugal separation of steam and water in the vicinity of the rod surface. A 19-rod test section is also being fabricated by Nuclear Development Corporation of America.

A paper given at the Reactor Heat Transfer Conference in 1956 has been declassified.[15] It reports on boiling burnout at high pressure in horizontal annuli, and, because the geometry was somewhat specialized, only the abstract will be quoted here.

TABLE III-5. BURNOUT DATA FOR INTERNALLY HEATED ANNULUS[13]
(Data Obtained by Columbia University Engineering Center)

1000 psia, 1.902" ID Housing,
1.380" OD x 1.14" ID Heater Tube (Type 304 Stainless Steel),
42" Heated Length

			Burnout Detector Trip-Point[c]	
Run No	Mass Velocity, lb/(hr)(ft^2)	Test Section Inlet Temp., °C	Heat Flux, pcu/(hr)(ft^2)	Exit Quality, %
1	0.507×10^6	267	3.4×10^5	21.4
2	0.518×10^6	257	3.9×10^5	20.0
3	0.527×10^6	239	4.1×10^5	14.9
4	0.539×10^6	208	4.2×10^5	5.6
5	0.315×10^6	222	3.3×10^5	20.4
6	0.312×10^6	237	3.0×10^5	21.9
7	0.296×10^6	257	2.7×10^5	25.1
8	0.328×10^6	203	3.8×10^5	18.3
9[a]	0.514×10^6	234	3.4×10^5	9.1
10	0.504×10^6	272	3.6×10^5	22.9
11	0.529×10^6	231	3.8×10^5	10.5
12[a]	0.317×10^6	216	3.4×10^5	19.0
13	0.758×10^6	272	3.5×10^5	13.4
14	0.774×10^6	253	3.9×10^5	8.7
15	0.771×10^6	239	4.2×10^5	6.1
16[b]	0.783×10^6	223	4.2×10^5	(9°C subcooled)
17	0.537×10^6	208	4.6×10^5	8.0
18	0.995×10^6	273	4.4×10^5	12.9
19	1.018×10^6	261	4.5×10^5	8.9
20	1.043×10^6	246	4.7×10^5	4.5
21	0.310×10^6	253	2.8×10^5	24.6
22	0.316×10^6	205	3.7×10^5	20.2
23	0.514×10^6	246	4.2×10^5	18.4
24	0.527×10^6	214	4.6×10^5	10.9
25	0.748×10^6	258	4.7×10^5	15.1
26	0.744×10^6	257	4.9×10^5	15.9
27[c]	0.511×10^6	263	4.0×10^5	22.7

(a) These data were obtained by holding the power constant and decreasing the inlet subcooling.

(b) In this run the burnout detector trip-point occurred before there was any net steam generation.

(c) All runs except Run 27 were terminated before the heater melted, but after conditions were reached at which the burnout detector sensed heat transfer instabilities. In Run 27 the power was increased at constant inlet coolant conditions until the heater melted. Melting occurred at a heat flux of 4.3×10^5 pcu/(hr)(ft^2) and an exit steam quality of 24.8%.

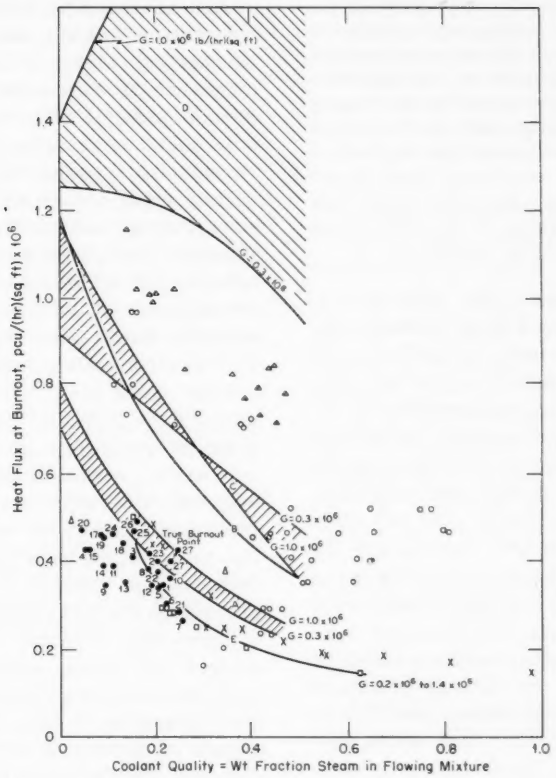

Data for water in the range 950 to 1050 psia and 300,000 to 1,400,000 lb/(hr)(sq ft) mass velocity

Symbol	●	△	○	Δ	□	X
WAPD-188 Table No.		3	10	12	*	*
Source	Columbia	MIT	ANL	ANL	Vertical	45° incline
Channel, in.	1.902 OD 1.380 ID	0.1805 ID	0.306 ID	0.226 ID	0.875 OD 0.540 ID	
Hydraulic diameter, in.	0.522	0.1805	0.306	0.226	0.335	
Length, in.	42	9	23.2	24.6	110	
Length/diameter ratio	80	50	76	109	328	
Boiling length, in.	7.8–35.4	2.1–8.5	4.5–23.2	0.7–16.7		42–102

A: WAPD-188 correlation, flow inside tubes 2000 psia
B: WAPD-188 correlation, rectangular channels 1000 psia
C: D. W. Bell's correlation, rectangular channels 2000 psia [see *Nuclear Sci. and Eng.*, 7: 245-251 March(1960)]
D: Griffith correlation, 1000 psia (MIT Tech. Report No. 9, March 1957)
E: Levy and Swan correlation, upflow in vertical annulus 1000 psia [GEAP-3228(Rev.1)]

*From GEAP-3228(Rev.1).

Fig. III-9 Boiling burnout data and correlations.[13]

Boiling burnout test results are described for forced circulation, bulk boiling heat transfer to high purity water in a 0.192 inch horizontal annulus of 1.43 inches inside diameter and 21-foot heated length. A description is provided of the electrically heated experimental facility used and of details of test procedure which cover conditions of pressure from 590 to 2010 psia, heat fluxes from 133,000 to 378,000 Btu/(hr)(sq ft), mass flow rates from 610,000 to 1,700,000 lb/(hr)(sq ft), and outlet steam qualities up to 44.4 per cent by weight.

Reference 16 presents some preliminary burnout data taken using a 9-ft by 0.540-in.-OD electrically heated rod inside a 0.875-in.-OD tube. The rod was modified to give an axial power distribution approximated by $q/A = (q/A)_{max.} \cos (y/139)$. The axial coordinate y is measured in inches from the mid-point of the heated section. Mass flow rates and subcooling were varied, but the reference does not state what the operating pressure was during the tests. The experimental burnout heat fluxes are compared with predicted heat fluxes based on a uniform power distribution. The reference concludes as follows: "... burnout with non-uniform power distribution may be reliably predicted from uniform power distribution data." The reference does not, however, state which uniform power distribution data were utilized in the comparison.

Boiling Water

Interest in two-phase flow continues to be high, as evidenced by the number of papers recently published on the subject. Reference 17 is a survey of bulk-boiling studies in pressurized-water reactor systems and is a review primarily of recent Westinghouse-Bettis documents on departure from nucleate boiling (DNB), two-phase pressure drop, and flow redistribution and transients. The author[17] recognizes that data such as those shown in Fig. III-9 are disconcerting when one is designing a boiling-water reactor that is burnout limited. He suggests[17] that there is an "urgent need to expand fundamental studies at universities and other laboratories" and recommends that a detailed statistical evaluation of all DNB data be undertaken by a qualified independent laboratory. More data are needed on the effects of (1) non-uniform heat flux on DNB and (2) transient operation in the film- and transition-boiling regions. The reference also recommends that data should be obtained using nuclear heating for comparison with the data obtained with electrical heating, to see if there is any significant difference. It would seem, however, that if DNB is not fundamentally understood, this latter step might be premature until such time as the various experimental discrepancies can be adequately explained. However, many experimenters studying natural-circulation burnout have reported flow perturbations preceding physical burnout, and if these were accompanied by wall temperature fluctuations (and corresponding heat-flux fluctuations due to resistivity changes in the electrically heated rigs), then nuclear heating might yield different results. Experimenters at Battelle,[18] for example, report an apparent resonance phenomenon in a boiling test section heated by alternating current; subsequently a d-c generator was utilized, and data exhibiting less scatter were obtained. Conceivably there might have been some coupling between bubble "behavior" and the frequency impressed on the test section during the a-c runs.

Three ANL reports[19–21] deal with some basic studies of boiling phenomena. Reference 19 contains analyses of data taken on the Armadilla test apparatus at ANL. The first portion of the report is devoted to bubble hydrodynamics and presents a mathematical description of the generation of a bubble, its growth, and subsequent movement through the fluid. The second section of the report presents and analyzes the experimentally determined void-fraction data. The model did not predict sufficiently high steam-bubble slip velocities. Underestimation of the degree of bubble coalescence was recognized as a possible explanation. Drag coefficients for spheres were utilized in the calculation, and the applicability of these coefficients is uncertain.

Reference 20 also discusses a model of nucleate boiling but is directed not to a discussion of slip ratio, but rather to a prediction of the boiling curve. This curve is the familiar plot of heat flux versus the difference between the wall temperature and the saturation temperature and is illustrated in Fig. 14-1 in the third edition of McAdams' *Heat Transmission*. Reference 20 deals with the region between simple convection and DNB. The film boiling regions are to be treated in subsequent papers. The author postulates that the bubbles exert a "pumping" action on the liquid; as the bubbles form, they push hot liquid away from the heated surface and into the bulk of the coolant. Heat is

also transferred from the surface by transport of latent heat by the vapor phase. The equations of motion and energy are formulated, and an equation is obtained for heat transfer during vigorous nucleate boiling by applying dimensional analysis and an empirical modification of nucleation theory. The equation is compared to experimental nucleate boiling data for 15 organic liquids and water under various pressures and using various materials for the boiling surface. The agreement between the analytical equation and the experimental data appears to be very good, and the following conclusions are quoted from reference 20:

1. The high heat-transfer rate in nucleate boiling is due principally to the pumping action of bubbles at the earlier stage of their growth.
2. The sizes of bubbles at which they leave the surface have practically no effect to the heat transfer at earlier stage of vigorous boiling.
3. Due to the intensive turbulence caused by bubbles, the transport properties dependent upon the molecular character of the liquid, namely, thermal conductivity and viscosity, have little effect to the heat transfer.
4. Liquids that possess larger values of density, specific heat, boiling point, and lower values of surface tension give higher heat-transfer rate. Liquids which have larger variations of vapor pressure with temperature are always desirable for boiling heat transfer.

The effect of liquid viscosity on the slip ratio and pressure drop in two-phase flow has been experimentally investigated.[21] A glycerine-water mixture (glycerol) was used for the aqueous phase, and air was used as the gaseous phase for flow studies in a rectangular, horizontal plastic flow channel. The apparatus was operated at approximately atmospheric conditions with the viscosity of the glycerol controlled by temperature and glycerine concentration. The voids were measured by the attenuation of gamma rays from a Tm^{170} source. The source-detector could be positioned along the channel length and made to traverse the channel in a vertical direction. Twenty-five experimental runs were made using five liquid flow rates and five qualities for each. A pictorial study of the various flow regimes (i.e., bubble, plug, stratified, wavy, and slug) is presented, and the effect of the liquid viscosity on the cross-sectional distribution of void-volume fraction is illustrated. It is shown that:[21]

a) as the liquid viscosity is decreased from 500 to 1 cp, the void volume fraction tends to envelop a greater cross-sectional area of the channel; b) as the gas and liquid flow rates are increased ... the void volume fraction appears to "round out" to an approximate semi-circular distribution along the (vertical) width of the channel.

Void-volume-fraction and two-phase pressure-drop data were compared to the Lockhart and Martinelli correlation. Figure III-10 shows the comparison of void-volume-fraction data; there apparently is a relatively large viscosity effect that is not accounted for in the Lockhart-Martinelli correlation. It is recognized that runs should be made at given values of viscosity that encompass a wider range of X to confirm this deviation. Pressure-drop data also were compared with the Lockhart-Martinelli correlation; the data agreed "reasonably well" up to a viscosity of 150 centipoises. From a viscosity of 150 to 500 centipoises the data fell about 15 per cent lower than predicted by the Lockhart-Martinelli correlation. Although this could be a viscosity effect, it should be noted that the liquid was in laminar flow at these viscosities, and the hydraulic radius, which was used in the calculations, may introduce errors. This is because the friction forces act throughout the fluid in laminar flow as contrasted to turbulent flow in which friction is primarily a wall effect.

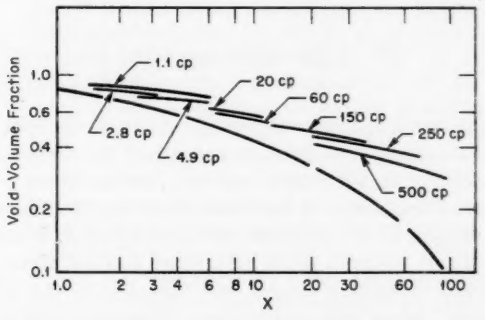

Fig. III-10 Proposed void-volume correlation on the basis of the slip ratio correlation, $\sigma = 80\ \mu^{0.30}\ X^{0.77}$ (reference 21). Values are in centipoises (cp). The lower curve is the Lockhart-Martinelli correlation.

Several reports are useful for design purposes.[22–25] Reference 22 deals with the experimental determination of local pressure gradients for subcooled boiling of water in vertical tubes. The experimental parameters covered

Table III-6 VALUES OF EXPERIMENTAL PARAMETERS[22]

	Run VII	Run IV
Test section ID, in.	0.1181	0.1824
Test section length, in.	15	16
q/A range, Btu/(hr)(sq ft)	$2.74-12.7 \times 10^5$	$2.14-4.58 \times 10^5$
Mass flow, lb/(sec)(sq ft)	305–1090	234–355
Pressure, psia	100–400	50–400

are shown in Table III-6.* The following equation correlated the data with a deviation (maximum) of +27 to −31 per cent:

$$\Psi^2 = 0.97 + 0.028 \exp 6.13\left(\frac{l}{L}\right) \qquad (4)$$

The term l/L represents the ratio of the local heated length to the total length of the element undergoing subcooled boiling, and the term Ψ^2 gives the ratio of the total subcooled pressure gradient to the gradient with liquid flowing alone without boiling. Both frictional and accelerational pressure drops are included in the Ψ^2 term. Runs were made under nonboiling conditions to correlate nonisothermal (f_{HT}) and isothermal (f_{ISO}) friction factors with the following result:

$$f_{HT} = f_{ISO} \frac{\mu_w^{0.4}}{\mu} \qquad (5)$$

Film coefficients were also determined during the nonboiling runs and were correlated satisfactorily by Colburn type equations.

Reference 23 considers the expansion losses in two-phase flow. Four different recipes for this form loss are examined, and the method of F. Romie, American-Standard, is recommended, although there is a lack of definitive experimental data at present. A bibliography on two-phase heat transfer has recently been published.[24]

In high-power boiling reactors the pressure-vessel size may be dictated by steam separation requirements, provided that no mechanical separators are to be incorporated within the vessel. Accordingly, reference 25, which discusses the problem of liquid entrainment, is of interest. The purpose of the reference is primarily that of a literature survey, and it encompasses a great deal of Russian literature. The report discusses the mechanism of formation of liquid drops above liquid-vapor interfaces, and the characteristics of rising liquid jets, since the breakup of such a jet often results in entrainment. The equations of motion for small and large drops are formulated, and the applicability of two theoretical methods for the entrainment of solids by gaseous phases is discussed. Although the problem has been analytically formulated, experimental data on drop size distribution and the initial velocity distribution of the drops are needed to evaluate the constants appearing in the equations. Most of the reported experimental work pertinent to steam-water separation has been done in Russia: reference 25 cites approximately 30 articles appearing in the Russian technical literature on the subject. These correlations give the effects of pressure, disengagement height, and superficial vapor velocity on the entrainment, but the original articles lack information on the experimental procedure and the accuracy of the correlations and experimental data. Also, there is disagreement in the Russian literature on the functional relation between the void fraction and the superficial vapor velocity in the bubbling mixture. As discussed in Sec. X of this issue of *Power Reactor Technology*, there is an experimental program on steam-water separation being conducted in this country in connection with the AEC program on nuclear superheat. It is hoped that, when this latter program is concluded, a comprehensive review of all the data will lead to satisfactory correlations.

*Table III-6 is reprinted here by permission from the American Society of Mechanical Engineers.[22]

Short Notes

A number of studies have recently been published which are primarily of a mathematical nature. Formal heat-transfer solutions to several transient problems are given in reference 26. Three general cases are studied:

1. The coolant inlet temperature is time dependent, and an infinite film coefficient is assumed.
2. The coolant flow rate decreases with time.
3. The coolant inlet temperature is time dependent, and a finite film coefficient is assumed.

A similar study is reported in reference 27, entitled Axial Temperature Distribution for a Nuclear Reactor with Sinusoidal Space and Exponential Time-Varying Power Generation. The

bibliographies of these reports contain a collection of pertinent papers on transient performance. The static and dynamic behavior of natural-circulation systems is treated mathematically in references 28 and 29. A small, naturally circulating, boiling pentane loop was constructed for one of the studies[29] and was used to demonstrate the predicted instabilities. Reference 30 and 31 present computing-machine programs for use in deriving internal temperature distributions in fuel elements. The steady-state temperature distribution in concentric fuel tubes is covered,[30] as is the transient temperature distribution in a bare or clad fuel pin cooled on the surface by coolant flowing axially along the pin.[31] The release of Wigner energy in graphite is treated in reference 32.

References

1. E. Janssen, Superheat Process Tube Heat Transfer Tests, Nuclear Superheat Project, USAEC Report GEAP-3319, General Electric Co., Atomic Power Equipment Dept., Jan. 5, 1960.
2. General Nuclear Engineering Corp., Zero-Flow Shutdown Cooling Test for BONUS Type Superheater Elements, USAEC Report GNEC-144, Nov. 21, 1960.
3. E. S. Nowak and R. J. Grosh, An Investigation of Certain Thermodynamic and Transport Properties of Water and Water Vapor in the Critical Region, USAEC Report ANL-6064, Argonne National Laboratory, October 1959.
4. M. Jakob, *Heat Transfer*, Vol. 1, John Wiley & Sons, Inc., New York, 1950.
5. A. J. Friedland et al., Heat Transfer to Mercury in Parallel Flow Through a Bundle of Circular Rods, USAEC Report BNL-5111, Brookhaven National Laboratory, November 1960 (revised Mar. 10, 1961).
6. O. E. Dwyer and P. S. Tu, Analytical Study of of Heat Transfer Rates for Parallel Flow of Liquid Metals Through Tube Bundles: Part 1, *Chem. Eng. Progr. Symposium Ser. No. 30*, 56: 183–193 (1960).
7. A. J. Friedland and C. F. Bonilla, Analytical Study of Heat Transfer Rates for Parallel Flow of Liquid Metals Through Tube Bundles, accepted for publication in the *A.I.Ch.E. Journal*.
8. Babcock and Wilcox Co., Gas-Suspension Task III Final Report, USAEC Report BAW-1201, July 31, 1960.
9. Babcock and Wilcox Co., Supplement to the Gas-Suspension Task III Final Report, USAEC Report BAW-1207, Oct. 31, 1960.
10. C. A. Depew, Heat Transfer to Flowing Gas-Solids Mixtures in a Vertical Circular Duct (thesis), USAEC Report UCRL-9280, University of California Lawrence Radiation Laboratory, July 11, 1960.
11. W. R. Gambill and R. D. Bundy, Burnout Heat Fluxes for Low-Pressure Water in Natural Circulation, USAEC Report ORNL-3026, Oak Ridge National Laboratory, Dec. 20, 1960.
12. W. H. Lowdermilk et al., Investigation of Boiling Burnout and Flow Stability for Water Flowing in Tubes, Report NACA-TN-4382, National Advisory Committee for Aeronautics, September 1958.
13. D. F. Babcock et al., Heavy Water Moderated Power Reactors Progress Report for October 1960, USAEC Report DP-555, E. I. Du Pont de Nemours & Co., December 1960.
14. Columbia University, Engineering Research Laboratories, Basic Experimental Studies on Boiling Fluid Flow and Heat Transfer at Elevated Pressures for Month of September 1960, USAEC Report TID-6689, Sept. 30, 1960.
15. Nuclear Development Corp. of America, Reactor Heat Transfer Conference of 1956, USAEC Report TID-7529, November 1957.
16. W. H. Cook, Fuel Cycle Program, A Boiling Water Reactor Research and Development Program, Quarterly Report No. 1, August to September 1960, USAEC Report GEAP-3558, General Electric Co., Atomic Power Equipment Dept., Oct. 10, 1960.
17. H. Susskind, A Survey of Bulk-Boiling Studies in Pressurized Water Reactor Systems, USAEC Report BNL-636, Brookhaven National Laboratory, August 1960.
18. R. W. Dayton and C. R. Tipton, Jr., Progress Relating to Civilian Applications During January 1961, USAEC Report BMI-1496, Battelle Memorial Institute, Feb. 1, 1961.
19. Argonne National Laboratory, A Study of the Variation of Steam Velocity in Vertical Boiling Channels, USAEC Report ANL-6251, November 1960.
20. Yan Po Chang, An Empirical Modification of Nucleation Theory and Its Application to Boiling Heat Transfer, USAEC Report ANL-6304, Argonne National Laboratory, February 1961.
21. M. J. Fohrman, The Effect of the Liquid Viscosity in Two-Phase, Two-Component Flow, USAEC Report ANL-6256, Argonne National Laboratory, November 1960.
22. W. L. Owens and V. E. Schrock, Local Pressure Gradients for Subcooled Boiling of Water in Vertical Tubes, ASME Paper 60-WA-249, Aug. 22, 1960.
23. P. A. Lottes, Expansion Losses in Two-Phase Flow, *Nuclear Sci. and Eng.*, 9(1): 26 (1961).
24. G. W. Maurer, Bibliography on Two-Phase Heat Transfer, USAEC Report WAPD-TM-249, Westinghouse Electric Corp., Bettis Atomic Power Laboratory, August 1960.

25. G. C. K. Yeh et al., On the Problem of Liquid Entrainment, USAEC Report ANL-6244, Argonne National Laboratory, October 1960.
26. C. F. Bonilla et al., Formal Heat Transfer Solutions, *Nuclear Sci. and Eng.*, 9(3): 323 (1961).
27. W. O. Doggett and E. L. Arnold, Axial Temperature Distribution for a Nuclear Reactor with Sinusoidal Space and Exponential Time-Varying Power Generation, ASME Paper 60-WA-194, Aug. 22, 1960.
28. T. R. Bump, Steady-State Fluid Flow in a Closed Loop with Two Parallel Channels, ASME Paper 60-WA-287, Sept. 6, 1960.
29. G. B. Wallis and J. H. Heasley, Oscillations in Two-Phase Flow Systems, ASME Paper 60-WA-209, Aug. 22, 1960.
30. J. C. Jensen, IBM 650 Routine VI, Temperature Distribution in Fuel Elements, USAEC Report DP-512, Savannah River Laboratory, September 1960.
31. J. Heestand et al., The Calculation of Transient Temperature Distributions in a Solid Cylindrical Pin, Cooled on the Surface, USAEC Report ANL-6237, Argonne National Laboratory, October 1960.
32. A. J. E. Foreman and A. R. Curtis, Propagation of Thermal Waves Through Graphite with Uniform Cooling, British Report AERE-R-3500, October 1960.

Section IV

REACTOR DYNAMICS

Boiling-Water Reactors

The following review covers recent papers on theoretical boiling-water-reactor dynamics, which consider the behavior of the Experimental Boiling-Water Reactor (EBWR) as an illustrative case. It may be helpful to refer to a review of some earlier work on the EBWR which appeared in the December 1959 issue of *Power Reactor Technology*, Vol. 3, No. 1, pages 42 to 47.

In a 1958 Geneva paper,[1] and elsewhere,[2] Thie has presented a simplified transfer-function analysis which agrees with the general features of the dynamic behavior of the EBWR. A more recent paper by Kirchenmayer[3] discusses some of the approximations used and their significance.

The general simplifying assumptions used by Thie were the following:

1. Only first-order deviations of quantities from their equilibrium values were taken into account.

2. Effects due to changes in pressure, saturation temperature, coolant velocity, and slip ratio were neglected.

In the derivation of transfer functions for the specific case of the EBWR, these additional simplifications were made:

3. Steam velocity, power density, and nuclear importance were assumed independent of position.

4. Certain transcendental functions appearing in the transfer-function expressions were approximated by their Taylor series.

Reference 3 deals with the latter two approximations.

In the notation of reference 3, the reactivity feedback loop of a boiling-water reactor, under assumptions 1 and 2 above, can be represented as in Fig. IV-1.* Here the notation $\bar{f}(p)$ denotes the Laplace transform, in the complex variable p, of the function of time, $f(t)$. The transfer function for each element of the feedback circuit, which is the Laplace transform solution of the differential equation relating the output to the input for the element, is designated by $Y(p)$, with an appropriate subscript. The significance of the diagram (described in transform space) is as follows: The net reactivity, $\bar{k}_{ex}(p)$, applied to the neutron kinetics, produces a reactor power change $\bar{y}(p)$. Part of the power change $[\bar{y}_1(p)]$ occurs in the boiling region of the reactor, and part $[\bar{y}_2(p)]$ in the nonboiling region; in each region the transfer of heat from the fuel elements to the coolant is described by a transfer function (Y_{T_1} and Y_{T_2}), with a characteristic time constant (θ_{T_1} and θ_{T_2}). In the boiling region a change in the volume fraction of steam $[\bar{\delta}_{\gamma_1}(p)/\gamma_0]$ results from the new balance of steam generation with steam flow out of the region. A further change in the average steam fraction in the reactor $[\bar{\delta}_{\gamma_2}(p)/\gamma_0]$ results from the changed heat input to the nonboiling region, which causes a shift in the boundary between the boiling and nonboiling regions. The two components of the change in void fraction are added and act together on the (negative) steam-void coefficient of reactivity to determine the feedback reactivity $[\bar{\delta}k_\gamma(p)]$ which is added algebraically to the input reactivity to determine the net reactivity applied to the neutron chain reaction.

Reference 3 directs attention to the transfer functions $Y_{\gamma_1}(p)$ and $Y_{\gamma_2}(p)$, connecting the heat flux into the coolant with the change in steam fraction. For the case of position-independent

*Figure IV-1 is reprinted here by permission from the *Journal of Nuclear Energy: Part A, Reactor Science*.[3]

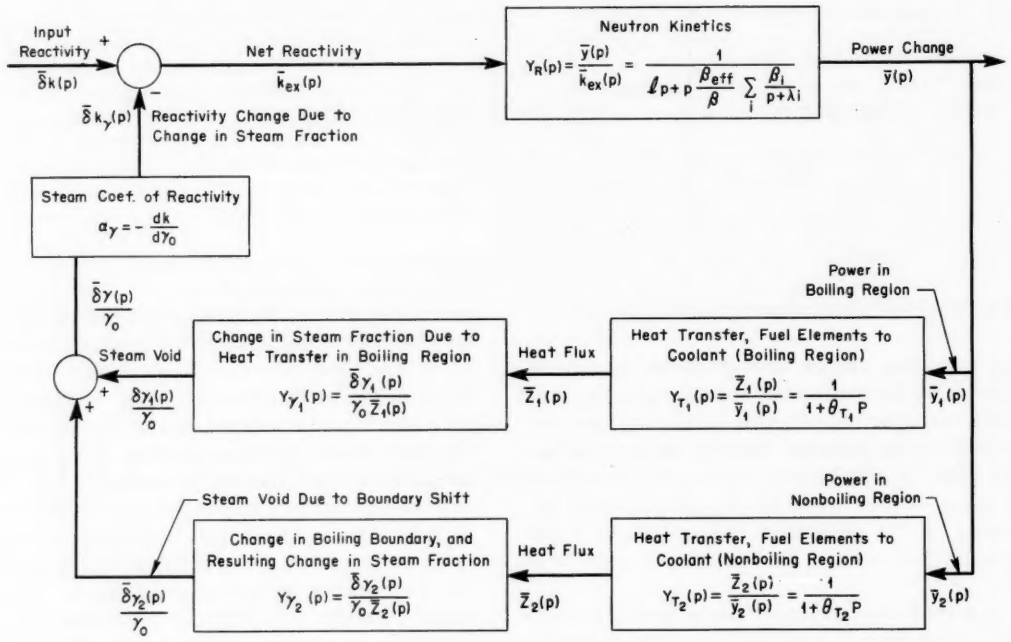

Fig. IV-1 Internal reactivity feedback through boiling and nonboiling regions of a boiling-water reactor.[3]

power density, these are given by

$$Y_{\gamma_1}(p) = 2\left[\frac{1}{\theta_1 p} - \frac{1}{\theta_1^2 p^2}(1-e^{-\theta_1 p})\right] \qquad (1)$$

$$Y_{\gamma_2}(p) = 2\,\frac{H_2}{H_1}\left(\frac{1-e^{-\theta_1 p}}{\theta_1 p}\right)\left(\frac{1-e^{-\theta_2 p}}{\theta_2 p}\right) \qquad (2)$$

where H_1 is the steady-state height of the boiling region of the core, H_2 is the height of the nonboiling region, θ_1 is the transit time of steam through the boiling region ($= H_1/v_s$), and θ_2 is the transit time of water through the nonboiling region ($= H_2/v_w$). For straightforward handling of these expressions, the exponential functions must be replaced by a power series; the reference[3] demonstrates that considerably better approximations to the experimental EBWR frequency-response results are obtained if an additional term, beyond that used in reference 1, is retained in the Taylor expansion of the exponential.

For $Y_{\gamma_1}(p)$, Thie[1] uses the approximation

$$\frac{1}{1+\frac{1}{3}\theta_1 p}$$

and Kirchenmayer[3] uses the approximation

$$\frac{1+\frac{1}{6}\theta_1 p}{1+\frac{1}{2}\theta_1 p+\frac{1}{12}\theta_1^2 p^2}$$

For $Y_{\gamma_2}(p)$, Thie[1] uses the approximation

$$\frac{2H_2}{H_1}\left(\frac{1}{1+\frac{\theta_1 p}{2}}\right)\left(\frac{1}{1+\frac{\theta_2 p}{2}}\right)$$

and Kirchenmayer[3] uses the approximation

$$\frac{2H_2}{H_1}\left(\frac{1}{1+\frac{\theta_1 p}{2}+\frac{\theta_1^2 p^2}{12}}\right)$$

Kirchenmayer uses as a criterion for selecting his approximation the fact that it yields the correct asymptotic value for Y_{γ_1}—a value of $2/\theta_1 p$ (compare Eq. 1)—as $p \to i\,\infty$. The main effect of the improved approximation is to decrease the damping of the reactor response in the frequency range above about 1 cps.

Kirchenmayer also considers approximations for $Y_{\gamma_1}(p)$ and $Y_{\gamma_2}(p)$ for the case of nonuniform axial distribution of the reactor power density. He approximates the power distribution, $q(x)$, by

$$q(x) = q\left(\frac{H}{2}\right)\left[\sin\frac{\pi}{H_e}\left(x+\frac{H_e-H}{2}\right) - \epsilon \sin\frac{2\pi}{H_e}\left(x+\frac{H_e-H}{2}\right)\right]$$

where $q(x)$ is the rate of heat flow crossing the surfaces of all fuel elements per unit of core height (steady state), H is the actual height of the core, and H_e is the extrapolated height. The second term of the equation, by proper choice of the coefficient ϵ, will approximate asymmetries in the power distribution due to steam-void distribution, partial insertion of control rods, etc.

The reference gives approximate expressions for the transfer functions Y_{γ_1} and Y_{γ_2} of the same form as those for the uniform power case but with the addition of six coefficients that are the functions ϵ, H_1/H_e, and H/H_e. Parametric curves of the coefficients, covering ranges of ϵ and H_1/H_e, are given for $H/H_e = 0.9$.

The agreement between calculated and measured frequency-response curves for the EBWR is improved further by use of the distributed-power transfer functions Y_{γ_1} and Y_{γ_2}. The significance of this improvement is not quickly apparent since it would seem that an acknowledgment of the nonuniformity of power distribution is incomplete unless the spatial variation of the steam-void coefficient of reactivity is also taken into account.

Reference 4 is a more comprehensive consideration of the boiling-water reactor which takes into account all the obvious processes that may affect the internal dynamics of a natural-circulation direct-cycle boiling-water reactor. The feedback circuit for such a reactor is shown schematically in Fig. IV-2. As a representation of the processes involved, the diagram is quite general, although the form of some of the transfer functions is affected by certain simplifying assumptions that were made in the analysis. The purpose of the diagram in this review is simply to show the general relations of the phenomena to one another. Consequently the gain terms (G) in the transfer functions, some of which are rather complicated expressions, are not specified, whereas the time constants are expressed as accurately as possible in descriptive terms. The notation of reference 4 has been preserved, and the expressions for the various quantities in the diagram can be obtained by reference to the report.

As indicated in the diagram, three reactivity feedbacks are taken into account: the fuel temperature coefficient of reactivity (the major component of which is usually the Doppler effect), the water temperature coefficient of reactivity, and the steam-void coefficient of reactivity. In reactors having an important fuel temperature coefficient, the temperature drop in the fuel itself and in the jacket is usually the important factor involved; consequently no allowance is made for the slight difference in film temperature drop in the boiling and nonboiling regions of the reactor. The reactivity changes due to the water temperature coefficient of reactivity result from changes of heat flow into the nonboiling region of the reactor, and from any changes in the saturation temperature of the water that may be produced by pressure variations. The net production rate of steam is affected by the power input to the boiling region of the reactor and by flashing or condensation of steam in the reactor core due to changes in pressure. In addition, the steam-void content of the core varies as the boundary between the boiling and nonboiling regions shifts upward and downward. This shift in turn depends on the heat input to the nonboiling region, on the pressure, and on the inflow of feed water. In the formulation described by the diagram, all these effects on steam-void content are computed as though the recirculation velocity of the water and the slip ratio of the steam remained constant. Actually, an increase of void in the core increases the circulating head, and, in the stable region, leads to an increase in recirculation velocity. This effect is taken into account by the internal feedback loop shown in the lower left-hand corner of the diagram. The result is a "net" steam void (perhaps more accurately described as the true steam void) which acts upon the reactivity through the steam-void coefficient of reactivity.

Akcasu[4] approximates the axial distribution of power in the reactor by a single sine distribution but chops off a portion of the core length, at the top, to approximate the effect of asymmetry in the power distribution in the actual reactor. He assumes that the reactivity worth of a local perturbation is proportional to the power (P). This is a compromise between the P^2 weighting that should apply to changes in

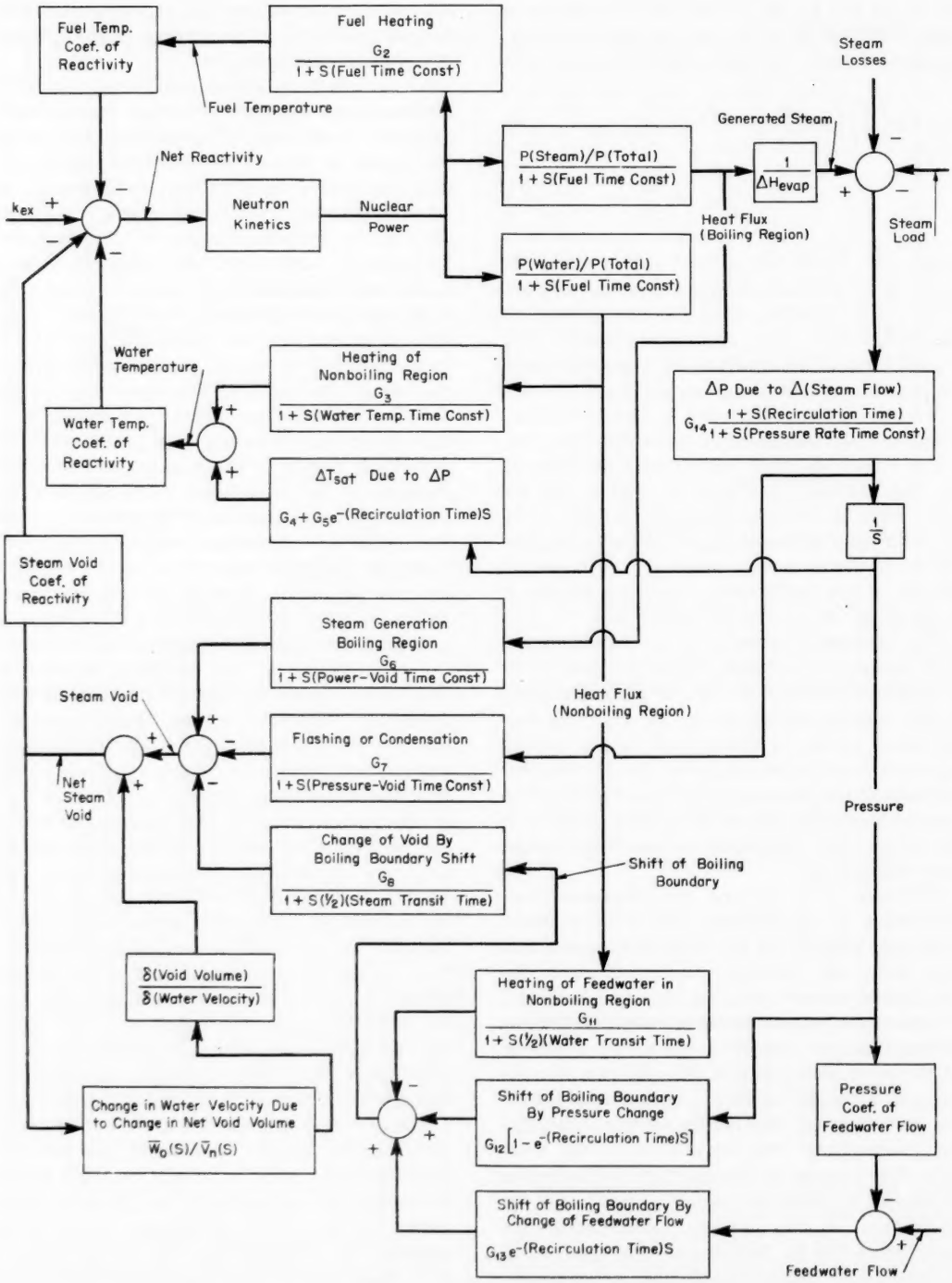

Fig. IV-2 Internal reactivity feedback in a boiling-water reactor.[4]

migration lengths and the $(dP/dx)^2$ weighting that should apply to changes in diffusion coefficients. Other approximations which affect the transfer functions indicated in Fig. IV-2 are the approximations of certain multiple time constants by single time constants. In cases where this is done, the exact formulation is also discussed in the reference.

The applicable portions of the analyses indicated by Fig. IV-2 are applied in the reference to two experimental results: the power-void transfer function of an electrically heated natural-circulation circuit, and the measured transfer function of the EBWR at 20 Mw and 41 atm.

The power-void transfer-function measurements were performed at the Ramo-Wooldridge Research Laboratory on an electrically heated boiling channel simulating the SPERT-IA reactor (atmospheric pressure). Descriptions of the experiment and the experimental results are given in reference 5. The theoretical analysis gave good agreement with the experiment up to a frequency of about 2 cps and reproduced a minimum in the amplitude function which was observed in the experiments. Deviations at higher frequencies may have been due to uncertainties in the fuel time constant in the boiling region.

In the analysis of the EBWR behavior, the effects of feed-water variations and the effects of water acceleration by changes in void content were ignored. The reactivity effect of water temperature changes was also ignored because it is small relative to void effects except at very low frequencies. The results of the analysis are compared with the experimental transfer functions in Figs. IV-3 and IV-4. The reference states that the agreement at low frequencies could probably have been improved by adjustment of the estimate of the water recirculation time, which involves considerable uncertainty.

Other Oscillation Measurements

Reference 6 is a report of transfer-function measurements on the Kinetic Experiment on Water Boilers (KEWB) reactor at power levels of 10^{-2} and 4 kw. The analysis is directed mainly toward the neutron kinetics at high frequencies. The oscillation frequency was carried up to 260 cps, and at frequencies above 10 cps the results deviated from those to be expected from the

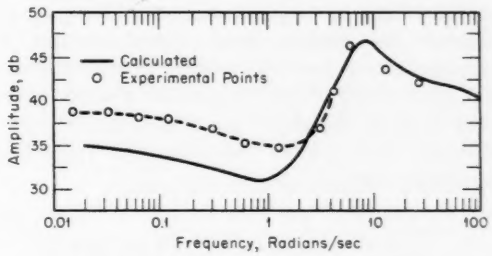

Fig. IV-3 Amplitude response of EBWR transfer function at 20 Mw and 41 atm.[4]

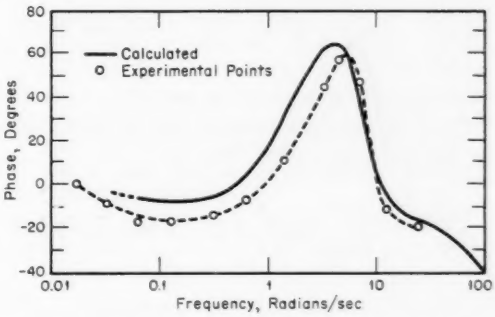

Fig. IV-4 Phase response of EBWR transfer function at 20 Mw and 41 atm.[4]

usual reactor kinetics equations based on six groups of delayed neutrons. The experimental transfer function can be fitted by adding a seventh group of delayed neutrons having a decay constant of about 625 sec^{-1} and an effective β of about 0.020. These neutrons are identified as neutrons returned to the core from the reflector after having spent some time there.

References 7 and 8 describe oscillation experiments on the Sodium Reactor Experiment (SRE). The reactor response is characterized by a relatively fast negative power coefficient of reactivity that is due to the net effect of fuel temperature and coolant temperature—both having nearly the same time response—and by a much slower positive coefficient that results from the temperature of the graphite moderator. The fast response coefficient affects the amplitude function noticeably up to frequencies of about 0.01 cps and affects the phase angle noticeably up to a frequency of about 0.2 cps. The moderator temperature coefficient has a time constant of many minutes and could not be measured accurately by the oscillation technique.

The values of the power coefficients depend on whether the coolant flow is held constant or whether it is varied to maintain a constant coolant temperature rise through the reactor. The steady-state values for the fast-response components of the power coefficient for these two conditions are

$$\frac{\delta k_{\text{eff}}}{\Delta P} = -1.24 \times 10^{-4} \pm 10\% \text{ per Mw(t)}$$

for a constant coolant flow of 1400 gal/min and

$$\frac{\delta k_{\text{eff}}}{\Delta P} = -\left(\frac{7.3}{n_0} + 0.88\right) \times 10^{-4} \pm 20\% \text{ per Mw(t)}$$

for a constant coolant ΔT of 335°F.

The over-all steady-state power coefficients for the same two cases are

$$\frac{\delta k_{\text{eff}}}{\Delta P} = +\left(\frac{3}{n_0} - 0.37\right) \times 10^{-4} \pm 50\% \text{ per Mw(t)}$$

for a constant flow of 1400 gal/min and

$$\frac{\Delta k_{\text{eff}}}{\Delta P} = \frac{-3.5 \times 10^{-4}}{n_0} \pm 50\% \text{ per Mw(t)}$$

for a constant ΔT of 335°F. In these expressions, n_0 is the initial reactor power in thermal megawatts. The above equations are straight-line approximations of experimentally determined curves of the reactor power coefficient. The lower limit of application is about 5 Mw(t). The components of the isothermal temperature coefficient of reactivity are $\alpha_f = -1.1 \times 10^{-5} \pm$ 10 per cent per degree Fahrenheit for fuel temperature and $\alpha_c = +0.3 \times 10^{-5} \pm 30$ per cent per degree Fahrenheit for coolant temperature. The moderator temperature coefficient decreases with increasing temperature, from a value of about $+2.2 \times 10^{-5}$ per degree Fahrenheit at 400°F to about $+0.6 \times 10^{-5}$ per degree Fahrenheit at 800°F.

The reference[8] states that the negative power coefficient of reactivity is the important one in characterizing the controllability of the reactor, and that the very slow positive component of the power coefficient acts much like the reactivity coefficient due to xenon concentration so far as control behavior is concerned.

Reference 9 reports the results of control-rod calibrations in the SRE by the oscillation method. The possibility of the method is well known, but its application has not previously been described in a comprehensive way. The method makes possible rapid rod calibrations, provided that the necessary equipment for oscillation of the rods is available. The biggest advantage of the method is that calibrations can be made under power operating conditions, provided that the frequency of rod oscillation is high enough that feedback through the power coefficients of reactivity is negligible. Such a calibration technique can be of great value, for control-rod worths are not necessarily the same under power operating conditions as under zero-power conditions, and there is no other straightforward method of rod calibration at operating power.

Kinetics of TREAT

References 10 and 11 give experimental reactor physics information and kinetics information on the Transient Reactor Test Facility (TREAT). The questions of the effective prompt-neutron lifetime and effective delayed-neutron fractions are treated at some length, by low-power transfer-function measurements and by period measurements in the super-prompt-critical range, since these quantities are essential to the application of the reactor. Of somewhat more general interest is the comparison of theoretical and experimental power burst shapes generated by the pulsed reactor. The reactor is a nearly homogeneous mixture of graphite and enriched uranium oxide, and hence the questions involved in its transient behavior relate primarily to the processes of the neutron chain reaction rather than to thermal processes. The power-limiting mechanism in self-limiting bursts is the temperature coefficient of reactivity, which is stated to result mainly from the effect of neutron temperature on neutron leakage. It was found that this characteristic could be predicted theoretically with adequate precision to duplicate the shapes of the power bursts. The calculation utilized 26 neutron energy groups, of which 20 groups were used to cover the energy range from 2 ev downward, and the remaining six groups were used for the higher energy ranges. For the energy range below 2 ev, the gas model was used for energy exchange between the graphite and the neutrons.

References

1. J. A. Thie, Theoretical Reactor Statics and Kinetics of Boiling Reactors, *Proceedings of the Second United Nations International Conference on the Peaceful Uses of Atomic Energy, Geneva, 1958*, Vol. 11, p. 441, United Nations, New York, 1958.
2. J. A. Thie, Dynamic Behavior of Boiling Reactors, USAEC Report ANL-5849, Argonne National Laboratory May 1959.
3. A. Kirchenmayer, On the Kinetics of Boiling Water Reactors, *J. Nuclear Energy: Pt. A, Reactor Sci.*, 12(4): 155 (August 1960).
4. A. Z. Akcasu, Theoretical Feedback Analysis in Boiling Water Reactors, USAEC Report ANL-6221, Argonne National Laboratory, October 1960.
5. Ramo-Wooldridge Div., Thompson Ramo Wooldridge, Inc., Kinetic Studies of Heterogeneous Water Reactors, Annual Summary Report, 1959, USAEC Report RWD-RL-167, Feb. 29, 1960.
6. R. N. Cordy, Kinetic Experiments on Water Boilers—"A" Core Report—Part III, Pile Oscillator Results, USAEC Report NAA-SR-5417, Atomics International, Dec. 1, 1960.
7. J. G. Lundholm, Jr., et al., Measurement of Zero Power Frequency Response of the SRE, USAEC Report NAA-SR-3762, Atomics International, Nov. 1, 1960.
8. C. W. Griffin et al., Measurement of the SRE Power Coefficients and Reactor Parameters Utilizing the Oscillation Techniques, USAEC Report NAA-SR-3763, Atomics International, Nov. 1, 1960.
9. C. W. Griffin et al., Calibration of the SRE Shim Rods by the Oscillation Method, USAEC Report NAA-SR-3764, Atomics International, Nov. 1, 1960.
10. F. Kirn et al., Reactor Physics Measurements in TREAT, USAEC Report ANL-6173, Argonne National Laboratory, October 1960.
11. D. Okrent et al., The Reactor Kinetics of the Transient Reactor Test Facility (TREAT), USAEC Report ANL-6174, Argonne National Laboratory, September 1960.

Section V

SHIELDING

Shielding Data

In a review of recent information on capture gamma spectra, in the March 1961 issue of *Power Reactor Technology*, Vol. 4, No. 2, it was mentioned that the report containing the latest compilation of data[1] did not present the material in the most convenient form for the shield designer. A more recent report by other workers (Troubetzkoy and Goldstein[2]) is in a more convenient format. The intensities of the capture gamma rays are given in seven energy intervals. The gammas included are those emitted instantaneously and those decay gammas characterized by half lives shorter than a few hours. Nuclei for which no capture gamma spectra are available are also listed in the table. Although most of the unmeasured nuclei are relatively unimportant in shielding work, U^{235} and plutonium, for which information is missing, are notable exceptions.

In reference 3, a table of gamma rays emitted by radioactive nuclei is presented, arranged in the order of increasing energy. The half life and the mode of decay are given; in most cases the entire spectrum is given, and when possible the intensities are presented. When possible, the percentage intensity is given, whereas, for other nuclei, relative intensities are listed. Use of the table for specific nuclides is laborious unless the energy of at least one of the gammas is known approximately to facilitate finding the nuclide of interest. A quantity called the occurrence ratio is given as an indication of the reliability of observation of individual gamma lines. The denominator of this ratio is the number of investigators of the nuclide, and the numerator is the number of investigators that listed the particular gamma ray. A specific reference is not given for each nuclide, but the bulk of the information is taken from two sources.[4,5]

In reference 6 the status of the measurements of neutron cross sections for elements pertinent to shielding analysis is presented. Eighteen materials are reviewed. Included are the cross sections important in the energy ranges from thermal to 20 Mev. For each element, and in some cases for specific isotopes, a reference survey is included along with a bar graph of the available data.

Nuclear Merchant Ship Reactor Shield Design

A summary report on the nuclear merchant ship (Savannah) reactor shield has been issued by the Babcock and Wilcox Company.[7] The report describes the shielding arrangement and the calculated dose rates in the vicinity of the shield. Included are the various sources of radiation and the methods of calculating the expected source strengths. The methods of calculating the shield penetrations are briefly outlined or referenced. Also presented are the dose-rate design criteria for the various regions of the ship. The materials used in the shield are described, as is their placement, although, as stated by the authors, weight optimization was not attempted in the design. The report gives a rather thorough review of all the problem areas expected in the shield design of a pressurized-water reactor, as well as a method for calculating the shielding required.

References

1. L. V. Groshev et al., *Atlas of γ-Ray Spectra from Radiative Capture of Thermal Neutrons*, Pergamon Press, New York, London, Paris, and Los Angeles, 1959.
2. E. Troubetzkoy and H. Goldstein, A Compilation

of Information on Gamma-Ray Spectra Resulting from Thermal-Neutron Capture, USAEC Report ORNL-2904, Oak Ridge National Laboratory, Jan. 18, 1961.

3. E. der Mateosian and M. McKeown, Table of Gamma Rays Emitted by Radioactive Nuclei Arranged in Order by Increasing Energy, USAEC Report BNL-605, Brookhaven National Laboratory, May 1960.
4. D. Strominger et al., Table of Isotopes, *Revs. Modern Phys.*, 30: 585 (1958).
5. Nuclear Data Sheets, Printing and Publishing Office, National Academy of Sciences, National Research Council.
6. A. Prince, The Status of Neutron Cross Sections and Related Data, Report XDC-60-11-164, General Electric Co., Aircraft Nuclear Propulsion Dept., Nov. 30, 1960.
7. W. R. Smith and M. A. Turner, Nuclear Merchant Ship Reactor Shield Design Summary Report, USAEC Report BAW-1144-1, Babcock and Wilcox Co., Aug. 1, 1959.

Section VI

FUEL CYCLES: ECONOMIC POTENTIAL OF THE SEED-BLANKET REACTOR

Reference 1 is a report on a study in which several variants of the Pressurized-Water Reactor (PWR) seed-blanket concept were investigated and were compared with slightly enriched designs. Much of the work reported was undertaken during the period (1957 to 1959) prior to selection of the reference design for PWR (Shippingport) core No. 2. Fuel-cycle costs were estimated for many of the variants on each type of design, and the effects of possible future changes in prices of fuel and fabrication were calculated. Uncertainties in these prices and in the metallurgical and reactivity limits on fuel lifetime led the author to conclude that the eventual relative power costs from the two reactor types can be determined only by construction and operation of both types. Since none of the H_2O reactors after Shippingport has utilized the seed-blanket concept, it would appear that design practice has answered the question, at least for the present; nevertheless the study is of interest as an investigation of a rather wide range of possibilities.

A seed-blanket reactor utilizes a "seed" region of high infinite multiplication factor (k_∞) to produce excess fast neutrons which leak into a surrounding "blanket" of low k_∞ to make it critical. The objective of the seed-blanket concept is to obtain a large fraction of the total reactor power from an inexpensive natural-uranium (or very slightly enriched) blanket which has a high conversion ratio and, consequently, a long reactivity lifetime.

The attainable reactivity in the blanket, considered as a separate multiplying region, basically determines how much can be accomplished in the way of achieving a high blanket-power-to-seed-power ratio. Consider, for example, a blanket which alone has an effective multiplication constant (k_{eff}) of 0.99. One might consider "spiking" it with individual plates of Zr-U^{235} alloy. Each plate would return to the blanket approximately two neutrons (η minus the small parasitic absorption) for every neutron supplied to it by the blanket. The k_{eff} of the combined system would then be 1.00, provided that enough "spikes" were used to give one net fission neutron, or approximately two total fission neutrons, for every 99 fission neutrons produced in the blanket. The blanket-power-to-seed-power ratio would be 99/2. Reference 3 generalizes this sort of consideration by the approximate equation

$$\frac{\text{Blanket power}}{\text{Seed power}} \doteq \left(\frac{k_b \epsilon}{1 - k_b}\right)\left(\frac{k_s - 1}{k_s}\right) \qquad (1)$$

where k_b is k_∞ for the blanket, k_s is k_∞ for the seed, and ϵ is the fast-fission factor in the blanket.

It is evident that the attractiveness of the seed-blanket concept can be evaluated only in terms of the characteristics and limitations of a particular system. The H_2O system, in which the typical range of k_b (for natural uranium) may be 0.90 to 0.75 (reference 3), may perhaps be considered borderline, and k_s must be made rather high to yield a favorable power split. However, the appropriate value for k_s in Eq. 1 is the effective value including the effect of any control rods that may be in the seed during operation. As a result of the control-rod effects and other effects discussed in reference 3, the practical range for k_s appears to extend up to only about 1.6. In the studies of reference 1, various methods of attaining high blanket-power-to-seed-power ratios have been considered. In general, the values of k_s are high, and the seeds in the seed-blanket cores described occupy less than one-fourth of the core volume, but it appears to be difficult to reduce their power frac-

tion to much less than one-half of the core power in practical designs.

Some of the characteristics of the system comprising a small, high k_∞ region surrounded by a large, low k_∞ region are:

1. Concentration of fissionable material in the high-power-density seed regions (which also have high statistical worth for neutrons) reduces the total amount of fissionable isotope necessary for criticality.

2. The high rate of burnup of seed fissionables is not compensated by plutonium production. Thus the seed loses reactivity rapidly and must be replaced two or more times during the reactivity life of the high-conversion-ratio blanket.

3. The temperature coefficient of the undermoderated, leaky seed is strongly negative and largely determines the temperature coefficient of the entire core.

4. A control rod inserted into the high-k, high-power-density, high-statistical-worth seed is far more effective than one inserted into the blanket; control poison in the blanket would also decrease the power fraction in the blanket. Thus all seed-blanket cores considered in the study contain control rods and burnable poison in seed regions only.

5. Control elements in the seed must compensate not only for the burnup, xenon transients, and temperature defect of the seed but also for those reactivity changes of the blanket which occur during the lifetime of the seed in question. If control rods alone are used for burnup control, they must be deeply inserted into the seed at the beginning of life when the seed power fraction is highest. A resulting power peaking at the lower end of the seed may amplify an already severe thermal design problem. Moreover, the total absorption of seed neutrons in the clean core must be very large for control, and many control rods must be closely spaced in the seed. The use of lumped burnable poison in the seed to compensate for the bulk of long-term reactivity variations is virtually mandatory in order to obtain tolerable power distributions and acceptable seed life.

6. The highly absorbing seed with low water content contains control-channel water gaps (which may be partially filled by control-rod followers) and is adjacent to the lightly absorbing blanket of high water fraction. The consequent high current of thermal neutrons into the seed may result in extreme peaks in the thermal flux at the perimeter of the seed subassemblies; when these peaks are superimposed on the already high over-all seed power density, the thermal design problems may become especially severe. The seed is therefore built as a plate type core with both fuel plates and water channels less than 0.1 in. thick, to provide the maximum heat-transfer capability in a limited core volume.

7. Seed-blanket cores may contain one or more thin seed annuli or many individual, unconnected spikes. The core is "poorly coupled"; i.e., the effects of a perturbation occurring in one part of the seed must pass around a long, thin, curved path in the seed or through a highly attenuating blanket before being felt in the seed at the opposite side of the core. Two consequences of this poor coupling may be a tendency to xenon oscillation and difficulty in meeting the "stuck rod" shutdown criterion.

Simple considerations indicate that the cost of power produced by a seed-blanket reactor can be reduced by increasing the lifetimes of the seed and blanket and by increasing the fraction of power generated in the blanket. These objectives, however, are in conflict. As the fuel loading in the seed is increased to obtain increased lifetime, the seed becomes a stronger absorber of thermal neutrons, the current of thermal neutrons from the blanket increases, and a larger fraction of power is generated within the seed. To explore this point further, a set of calculations was performed for cores that were essentially extrapolations of the first Shippingport core to a rating of 100 Mw(e) and to longer lifetime.

The first Shippingport core[2] has a seed arranged in the general form of an annular ring that occupies 22 per cent of the core volume and is located at about 55 per cent of the full core diameter. A core of this geometry with a highly enriched seed containing 250 kg of U^{235} and a natural-uranium blanket will generate slightly more than 50 per cent of the power in the blanket.

As the seed life was varied by varying the U^{235} loading of the seed from 90 to 365 kg, it was apparent that the fuel-cycle cost dropped rapidly with increasing seed lifetime until the seed lifetime reached about 20,000 effective full-power hours (EFPH). It was also observed that, when the average irradiation of the blanket exceeds about 5000 Mwd/ton, the poisoning ef-

fect of accumulated fission products results in a decrease of blanket reactivity, in deterioration of the fraction of power generated in the blanket, and in reduced seed lifetimes.

For subsequent studies the fuel loading in the seed was fixed at 250 kg, the amount indicated to be necessary for a seed lifetime of 20,000 EFPH, and the geometry and material compositions of seed and blanket were varied, but the over-all core size was held constant at 6.8 ft in diameter by 7.5 ft in height. The objectives of this parametric study were, first, to maximize the blanket power fraction at start of life and, second, to keep the blanket reactivity essentially constant up to an average irradiation of about 35,000 Mwd/ton.

Several geometric arrangements involving multiple seeds were investigated in an attempt to find the configuration that would provide the maximum power fraction in the blanket. The geometric arrangements were:

1. A double-annular seed, with the mean radii of the two seeds at 0.4 and 0.8 of the core radius and with an inner seed volume 0.43 times that of the outer seed.
2. A four-pancake seed, in which the midplanes of the seeds were located at $\frac{1}{8}$, $\frac{3}{8}$, $\frac{5}{8}$, and $\frac{7}{8}$ of the core length.
3. A 24-spike seed, in which 8 seed modules were placed at 0.4 of the core radius and 16 were placed at 0.8 of the core radius.

All these concepts ideally increase the power fraction in the blanket over that obtained with the single-annular reference design by 5 to 10 per cent, at the expense of additional fuel loading. Each of these geometries produced its unique difficulties. The multiple-pancake design was unpromising for the reason, among others, that no control system was found which gave adequate reactivity control without inserting rods into the blanket, thus reducing blanket power fraction to a value below that of the reference (single-annular) design.

Both the double-annular and multiple-spike concepts show an inherent shift in power from the inner seed regions to the outer regions as burnup progresses. A sophisticated operating procedure involving the use of burnable poisons with different self-shielding factors and an elaborate programming of control rods can minimize this power shift and the resulting problems in thermal design. The more highly separated these seed regions are and the less the neutron coupling between them is, the more sensitive will the power distribution be to changes in blanket reactivity, xenon oscillations, stuck rods, etc., and the greater will the difficulty be in controlling power distribution. Thus the multiple-spike arrangement appears to present more difficult problems than does the double-annular design.

If the conversion ratio of the blanket is sufficiently high, k_∞ of the blanket can be maintained essentially constant over some 35,000 Mwd/metric ton exposure. The higher conversion ratio may be obtained by reducing the water-to-uranium volume ratio from about 3 to 1 (at which initial k_∞ is maximum) to about 1.5 to 1 (where initial k_∞ is quite low and where the blanket fraction of the power is low). Enrichment of the blanket to 1 per cent, however, raises its initial k_∞ to 0.95 and maintains it at nearly that level for 35,000 Mwd/metric ton. The blanket power fraction is increased about 10 per cent, the seed life is increased by a still greater percentage, and power is flattened in both seed and blanket, resulting in improved thermal performance. Control requirements increase, however, because of an increased temperature defect in the relatively dry blanket and because of the reduced statistical worth in the seed region.

As the blanket enrichment is continuously increased, the necessary size and U^{235} loading of the seed decrease, and the reactor acts progressively more like a homogeneously enriched reactor. The power distribution becomes continuously flatter, the reactivity lifetime increases, as does the total U^{235} content, and the required control surface increases.

After one seed lifetime, some 50 per cent of the initial U^{235} still remains, and the k_∞ may still be about 1.4. These depleted seeds can substitute for blanket modules in the subsequent fuel cycle, and the depleted seeds can be located in two annuli, one near the center of the inner blanket and one at the outer boundary of the outer blanket. Power in the blanket is increased significantly, seed lifetime increases, and the over-all power distribution is flatter. A corresponding increase in control requirement and in the change of core reactivity with time can be partially negated, at least in principle, by the insertion of appropriately self-shielded burnable poison in the depleted seed. The core lifetime obtainable with sufficient control is roughly

equal to that obtained using a high-conversion-ratio blanket.

Another method of utilizing depleted-seed modules is to alternate them with fresh-seed modules in the original annular seed ring. Each seed module, for example, may remain in place for two cycles, and after each cycle only those seed modules which have remained in place for two cycles may be replaced with new modules. This procedure results in a one-third increase in seed lifetime over that obtained with single-batch reloading. Power peaking within the seed is increased somewhat, and flow reorificing within the seed is necessary after each cycle.

The economic studies[1] were based on a 100-Mw(e) Shippingport type, single-annular core. Variations were reported as perturbations on the base cost. The study covered fuel costs only.

In the base case, three seeds loaded with 250 kg of U^{235} each were used successively with one natural-uranium blanket containing about 15 metric tons of uranium. Average irradiation of the blanket was about 13,000 Mwd/metric ton, the average of the three seed lives was about 10,400 EFPH, and the corresponding fuel cost was estimated at about 6.4 mills/kw-hr averaged over the blanket lifetime.

A 50 per cent increase in seed fuel loading (to 375 kg) provided a 38 per cent increase in average seed life and a 19 per cent reduction in fuel cost to 5.2 mills/kw-hr. When the base fuel load was nearly doubled, to 475 kg, average seed lifetime increased 73 per cent to 18,000 EFPH, and fuel cost decreased 25 per cent to 4.8 mills/kw-hr. In each case it was assumed that the blanket would last successfully for three core lifetimes. If blanket lifetime were limited by metallurgical considerations to less than 20,000 Mwd/metric ton, advantages of the heaviest seed loadings would disappear since one blanket would have to be supplied for each two seeds. In any case the seed-blanket core is no exception to the general rule that increasing fuel lifetime is the most effective means of decreasing fuel cost.

Other design variants were capable of much smaller improvements. The use of a double-annular seed decreased cost about $2\frac{1}{2}$ per cent. The high-conversion-ratio blanket gained, at most, $3\frac{1}{2}$ per cent, as did the use of depleted seeds in the blanket. The cyclically loaded seed was more effective, decreasing cost about $6\frac{1}{2}$ per cent.

Slightly enriched converter reactors were designed for comparison purposes. In general, they were substantially smaller than the seed-blanket reactors because of their better power distribution, and they required more control rods because the rods were located in regions of lower statistical worth. The base cost of a homogeneously loaded, slightly enriched reactor appears comparable to that of the reference seed-blanket design of comparable design life. It would appear, however, that the use of a three-cycle loading, with corresponding power flattening and increased fuel utilization, decreases the cost of the base fuel cycle by 12 to 15 per cent, and it is not clear that the slightly enriched concept does not have the greater potential for cost improvement.

Fuel-cycle costs were recomputed assuming a 43 per cent decrease in fabrication cost and assuming the reduction of the natural-uranium price to $15 per kilogram with consistent reductions in enriched-uranium prices. Under these conditions, the minimum fuel cost estimates approached 2.8 mills/kw-hr for both seed-blanket and slightly enriched designs.

References

1. F. Schwoerer, Economic Potential of the Seed-Blanket Reactor, USAEC Report WAPD-237, Westinghouse Electric Corp., Bettis Atomic Power Laboratory, December 1960.
2. *The Shippingport Pressurized Water Reactor*, Addison-Wesley Publishing Co., Inc., Reading, Mass., 1958.
3. A. Radkowsky and S. Krasik, Physics Aspects of the Pressurized Water Reactor (PWR), *Proceedings of the International Conference on the Peaceful Uses of Atomic Energy, Geneva, 1955*, Vol. 5, p. 229, United Nations, New York, 1956.

Section VII

MATERIALS

Preferred Orientation in Extruded Zircaloy-2 Tubing

The highly anisotropic nature of zirconium, and the directionality of mechanical properties resulting from the highly oriented structures usually encountered with its alloys, has given rise to several problems affecting the use of Zircaloy-2. However, it has been shown that control of the amount of cold working and the annealing conditions can greatly affect the texture of the final product. The amount of control possible is great enough that it has been suggested that "ideally, it should be possible to determine the texture which results in optimum properties and then modify the fabrication schedule to produce this texture."[1] The factors influencing final textures are (1) the original texture, (2) the extrusion ratio, (3) the extrusion temperature, (4) ram speed, (5) type of cold work, (6) amount of cold work, and (7) annealing temperature and time. The texture of an extrusion will vary from the lead, through the center, to the trailing end. Small amounts of alloying elements will also affect the texture.

In a recent study Laidler[1] has investigated the textures produced in seven specimens of Zircaloy-2 tubing. These specimens represented material extruded at three reduction ratios (14 to 1, 36.9 to 1, and 11 to 1) and subsequently cold worked and annealed under various conditions. Pole figures were constructed from data obtained from a Cummings goniometer employing a spiral scan. The textures were analyzed in their relation to the prior histories of the materials studied and to the deformation mechanisms likely to be encountered. Although the deformation behavior of polycrystalline materials cannot be precisely predicted from data of this type, it was indicated that textures which should result in a reasonable balance of ductility and strength should be obtainable with the proper selection of processing methods. It was indicated, for instance, that, for Zircaloy-2 tubing, satisfactory strength and ductility under axial stresses would be found in both annealed and cold-worked tubing but that annealed tubing would have better ductility, although slightly less strength, under circumferential, or combined circumferential and axial, stress.

Irradiated Zircaloy-2 Hot-Water Loop Tube

Recent work at Hanford[2] has thrown new light on the question of irradiation damage to Zircaloy, a matter of pressing importance in regard to the use of the alloy in pressure-tube designs as well as in fuel-element cladding.

Hanford, fortunately, was able to test twin Zircaloy tubes, one from an in-pile loop and one from an out-of-pile loop. The initial condition of the tubes was identical, as were the operating conditions of the loops. The tubes were hot extruded and then cold reduced by the "Rockrite" process to receive 70 per cent cold work. Nominal dimensions were: outside diameter, 2.41 in., and wall thickness, 0.145 in. The irradiated tube had received an integrated flux believed to "be high in the 10^{20} nvt range." Times of operation were not given. Both tubes were exposed to water at temperatures in the 175 to 235°C range, and the in-pile tube had a CO_2-helium atmosphere on the outside. As an indication of the relative neutron exposures, a gamma survey was made along the length of the tube. The intensities measured are given in Table VII-1.

The in-pile tube was removed from the reactor and chopped into sections on a guillotine.

Table VII-1 300°C TENSILE PROPERTIES OF ZIRCALOY-2 SPECIMENS CUT FROM UNIRRADIATED AND IRRADIATED TUBES[2]

Specimen No.	Tube section	Gamma activity	Ultimate strength, psi × 10^3	Total elongation, %
B-2*	Control	0	53.4	4.7
B-8*	Control	0	58.9	4.7
E-4	Control	0	61.7	4.2
1-4	1	500 mr	44.8	3.3†
1-5	1	500 mr	47.8	3.7
4-4	4	3 r	50.9	2.4
4-5	4	3 r	60.8	2.5
5-3	5	10 r	63.4	4
5-4	5	10 r	54.9	3.3
2-3	2	15 r	55.3	3.5
2-4	2	15 r	47.6	7.4†
3-4	3	25 r	65.3	2.6
3-5	3	25 r	66.0	3.5

*Tested at 275°C.
†Partially recrystallized.

Some of the lengths shattered during this operation. No significant corrosive attack was found in either tube, but a few 0.005-in. pits were found on the irradiated tube. Tensile specimens were prepared on a template-following milling tool. Testing was done at room temperature and at 300°C. Although room-temperature properties of the unirradiated tube were quite uniform, with an average yield strength of $86{,}000 \pm \frac{1800}{900}$ psi, an ultimate strength of $100{,}500 \pm \frac{2000}{2300}$ psi, and a total elongation of $5.8 \pm \frac{0.7}{0.3}$ per cent for five specimens, the irradiated specimens showed relatively large variations. For six specimens in the highest flux zones, the yield strength varied between 82,000 and 102,000 psi, the ultimate strength varied between 96,000 and 109,000 psi, and elongations for three of the specimens were below 3.7 per cent. Some of the irradiated specimens fractured with negligible necking. The results for the 300°C tests of both tubes are given in Table VII-1. Some specimens evidently were subject to localized heating from the supporting graphite and underwent partial recrystallization. It is evident that increasing the testing temperature decreased the ultimate strength, but it had no great effect on total elongation. In general, the radiation effects as found at 300°C can be said to be those expected from normal radiation hardening, provided the behavior of the partially recrystallized samples can be regarded as irrelevant.

Metallographic examination revealed that the hydride content of both tubes was low, probably below 50 ppm, as would be expected at the water temperature used.

Corrosion by Helium Impurities

Although pure helium is chemically inert, the use of helium as a reactor coolant does not avoid all corrosion problems. The impurities to be found in any practical grade of helium are always to some extent corrosive; and if the reactor is moderated with bare graphite, the impurities contained in it, or those produced by the reaction of the oxygen in the helium with the graphite, may result in an important corrosion problem, particularly at high temperature. Because one of the General Dynamics designs for the Maritime Gas-Cooled Reactor (MGCR) utilized unclad graphite as the moderator with helium as the coolant, a study was undertaken[3] to determine the extent of corrosive attack to be expected and to investigate the transport of carbon. The program had four objectives: (1) to screen the heat-resistant nickel- and iron-base alloys for resistance to oxidation and carburization by CO, CO_2, and H_2 at different partial pressures, (2) to rank the alloys according to their catalytic influence on the disproportionation of CO, (3) to study the effect of H_2 additions on the carburization of the alloys and on the decomposition of CO, and (4) to investigate niobium and its alloys and to determine the limiting amount of CO_2 that could be tolerated without important corrosion of these alloys.

The materials investigated included types 316 and 430 stainless steel, four chromium-molybdenum steels containing up to 9 per cent chromium and 1 per cent molybdenum, A nickel, Monel, Inconel, Inconel X, Inconel 702, molybdenum, niobium, copper, and six binary alloys of niobium with zirconium and titanium. These materials were tested in five atmospheres:

1. Helium containing $P_{CO} + P_{CO_2}$ at 2×10^{-4} atm.
2. Helium containing the above at 10^{-2} atm.
3. Carbon monoxide at 1 atm.
4. A mixture of 0.5 atm CO and 0.5 atm CO_2.
5. Helium containing 5×10^{-3} atm CO plus 10^{-3} atm H_2.

During testing, the specimens were held in quartz tubes in a resistance furnace. The entering gas passed over a heated graphite (AGOT) plug before touching the specimens. Before entering the furnace the helium was purified by passage through a 5-A "molecular sieve" tower and then through heated titanium and uranium traps. The gas additions entered the system through variable leaks, and additive contents were determined by gas chromatograph analysis. Test temperatures were as high as 1700°F, and most of the tests were for 500 hr.

Within the limits of the experiments, it was indicated that, of the conventional stainless steels, type 316 would be usable only below 1100°F. However, the ferritic stainless steel, type 410, might be used to 1300°F and was found to be not only the most carburization-resistant steel tested but also to be superior in that it did not catalyze CO disproportionation. It might be assumed, however, that the low strength of type 410 above 1000°F might militate against its use for some purposes. The low-alloy steels were found to carburize badly above 1000° and were only considered usable for the MGCR piping at temperatures below 900°F.

Of the nickel-base alloys, Monel had the attractive property of not undergoing "graphitization" and embrittlement when thermal cycled in a carburizing atmosphere. Its high-temperature solubility for carbon is much lower than that of nickel, which absorbs and precipitates carbon on thermal cycling. Inconel X was the most promising high-strength nickel-base alloy since it was found to resist both carburization and oxidation. It did catalyze the CO disproportionation reaction. Although they are possibly not a hindrance to the MGCR design, the high cross sections of Monel (67 per cent nickel, 30 per cent copper) and Inconel X (73 per cent nickel, 15 per cent chromium, and 7 per cent iron) make them rather unattractive as reactor core materials.

Results of the molybdenum tests were promising, but the metal does form a carbide layer at 1200°F which causes severe embrittlement. It was concluded that niobium and its alloys would not be suitable for use in the unclad, graphite-moderated version of MGCR. Niobium has too low a tolerance for oxygen and was embrittled in 100 hr at impurity contents as low as 2×10^{-4} atm ($P_{CO} + P_{CO_2}$). The results of the carbon transport tests were encouraging. It was found that little methane is formed below 1300°F by the reaction of carbon with hydrogen. At hydrogen contents below 10^{-2} atm, little carbon transport should occur at 1300°F in the reactor.

Decontamination of Pressurized-Water Systems

Two types of contamination can exist in the primary system of a UO_2-fueled nuclear reactor. One type, in which the contaminants are fission products and uranium dioxide, occurs only after a fuel-element rupture or a cladding failure. The other type is a result of normal operation and is caused by the gradual buildup of activated corrosion-product films on the internal surfaces of the system. The methods of removal of the two types of contamination are generally different: for the fuel-element rupture products, an oxidizing medium is used to change the valence of uranium so that dissolution and removal may be accomplished; for the corrosion products, descaling is required.

A program is being conducted at Hanford to evaluate decontamination processes for high-temperature recirculating-water-cooled reactor systems. The processes are judged principally on the bases of decontamination effectiveness and corrosion of the material being decontaminated, as determined by a series of tests ranging from laboratory beaker tests to high-temperature circulating loop tests. Reference 4 is a report of the work accomplished under the program for the period June 1959 to January 1960.

Results of tests indicate that a hydrogen peroxide–carbonate solution, used as a pretreatment for alkaline permanganate acid or acid salt processes, very effectively increases the efficiency of decontamination for fuel-element rupture products. For corrosion-product-film removal, an alkaline permanganate conditioning solution is used to complete the oxidation of the film so that it may be removed by a subsequent acid process.

The processes studied, and some conclusions concerning the processes, are as follows:

1. *Sodium Bisulfate Processes.* These processes give good decontamination factors. The uniform corrosion rates of carbon steel, stainless steel, Zircaloy-2, and Inconel X are low. Galvanic corrosion of carbon steel coupled to stainless steel is relatively high—as much as 0.7 to 0.9 mil per decontamination cycle.

2. *Ammonium Citrate Process.* This process is effective in removing rupture products from 300 series stainless steels, Inconel X, and Monel but is less effective as a decontaminant for carbon steel. The uniform corrosion rates of carbon steel, stainless steel, Zircaloy-2, Inconel X, and Monel are low. Galvanic corrosion of carbon–stainless steel couples is comparatively high, as much as 0.5 to 0.7 mil per decontamination cycle.

3. *Oxalic Acid Processes.* These processes give high decontamination factors and low corrosion rates on mixed carbon and stainless-steel systems. However, chemical films form on loop surfaces, and methods must be developed for preventing the formation of these films or for removing them after they form.

4. *Nitric Acid Process.* This process is usable in systems that are predominantly stainless steel. It is compatible with zirconium but causes severe corrosive attack on carbon steel and Stellite.

5. *Phosphoric Acid Process.* This process yields acceptable decontamination factors and corrosion rates on stainless steel and carbon steel.

6. *COD(S-4) Process.* This process, which was devised at Bettis for corrosion-product decontamination, is not intended for use with carbon steel. It is less effective than the above processes in removing fission products from both stainless and carbon steel and, as expected, gives unacceptably high corrosion rates when used with carbon steel.

Table VII-2 TEST CONDITIONS[5]

Test designation	Water temp., °F		Water condition	Flow rate, ft/sec	Alloy type	Time, hr
	Inlet	Outlet				
A-2*	149	190	Deionized	32	1100	240
A-3	149	190	Deionized	32	1100	129
A-4	149	190	Deionized	33	1100	240
A-5	149	190	Deionized	37	1100	42
A-6	149	190	Deionized	33	1100	240
A-7	156	193	*p*H 5	36	1100	240
A-8	156	195	*p*H 5	35	1100	240
A-9	186	223	*p*H 5	33	1100	240
A-11	152	196	*p*H 5	34	6061	240
A-12	166	192	*p*H 5	48	6061	240
A-13	131	176	*p*H 5	34	6061	240

*300 psi; all others, 900 psi.

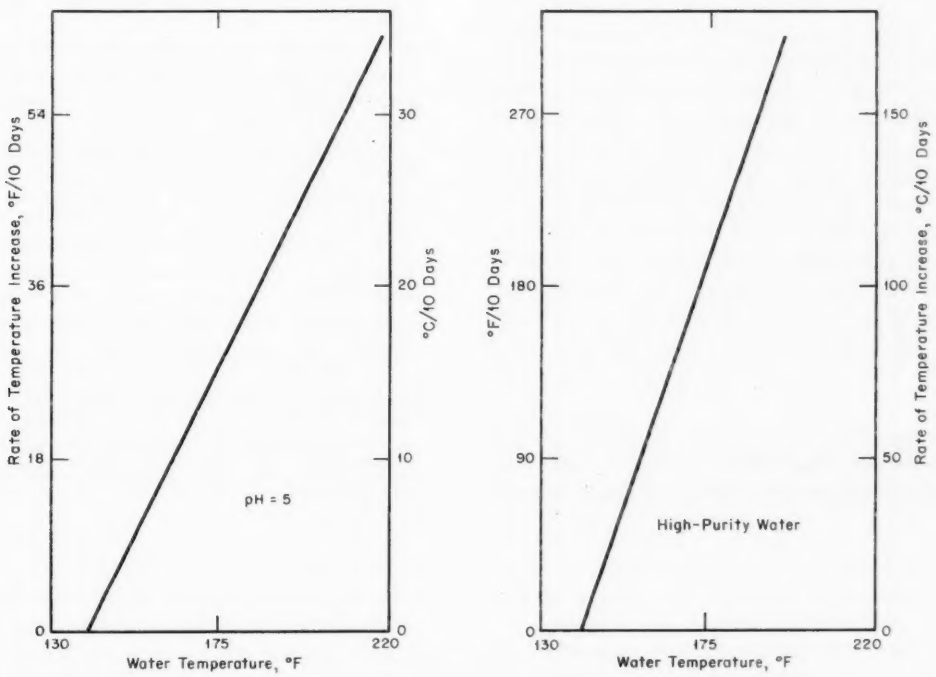

Fig. VII-1 Correlation of rate of temperature increase and water temperature.[5]

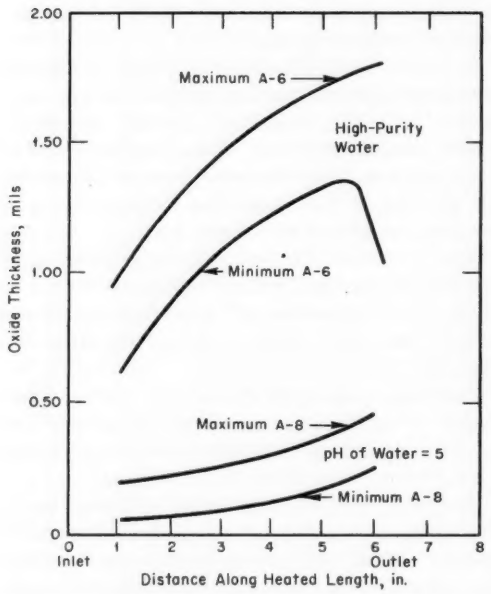

Fig. VII-2 Oxide thickness on test specimens[5] at the end of tests A-6 and A-8.

Corrosion of Aluminum

The preliminary results of an experiment designed to study the behavior of aluminum cooled by water and subjected to a very high heat flux were reported in the September 1960 issue of *Power Reactor Technology*, Vol. 3, No. 4. Additional data have become available from subsequent tests and are reported in reference 5. The test equipment was described previously, and the test conditions studied are given in Table VII-2. Run A-2 is the run that was reviewed previously in this journal. In all tests after run A-2, heat flux through the side of the channel was 1.5×10^6 Btu/(hr)(sq ft) ± 5 per cent.

The benefits accruing from control of *p*H are illustrated in Figs. VII-1 and VII-2. The data points are not shown in either of these figures. Experiment A-10, not shown in the table, was conducted to determine the effect of thermal cycling, bulk coolant flow rate, and use of carbon dioxide rather than nitric acid to control *p*H. The conclusions after the above series of experiments are quite different than the conclusions presented previously in *Power Reactor Technology*. The localized attack reported for run A-2 appears to be peculiar to that run and was not found in the remaining 11 experiments. The use of coolant adjusted to *p*H 5 results in wall-temperature increases that are tolerable at least for the application envisioned in reference 5. No coolant velocity effects were noticed within the velocity range studied, and thermal cycling produced no loss of oxide when the layer was less than 1 mil thick; some loss occurred when the oxide thickness was in excess of 1 mil. Within the limits of reproducibility, the rate of surface-temperature increase appeared to be the same for both the 1100 and 6061 aluminum specimens, all other conditions being identical.

References

1. J. J. Laidler, Preferred Orientation in Extruded Zircaloy-2 Tubing, USAEC Report HW-64815, Hanford Atomic Products Operation, Apr. 15, 1960.
2. A. L. Bement, Examination of an Irradiated, Zircaloy-2, Hot Water Loop Tube, USAEC Report HW-65999, Hanford Atomic Products Operation, July 8, 1960.
3. J. C. Bokros and H. E. Shoemaker, Reactor Materials Compatibility with Imputiries in Helium, USAEC Report GA-1508, General Atomic Div., General Dynamics Corp., Jan. 12, 1961.
4. T. F. Demmitt et al., Decontamination Studies for HAPO High Temperature Reactor Circulation Systems, Progress Report for June 1959 to January 1960, USAEC Report HW-62806, Hanford Atomic Products Operation, Mar. 28, 1960.
5. J. C. Griess et al., Effect of Heat Flux on the Corrosion of Aluminum by Water. Part II. Influence of Water Temperature, Velocity, and *p*H on Corrosion-Product Formation, USAEC Report ORNL-3056, Oak Ridge National Laboratory, Feb. 27, 1961.

Section VIII

DESIGN PRACTICE: YANKEE NUCLEAR POWER STATION

Until a number of nuclear power plants have been constructed for commercial applications, there will be no established body of design practice with which the particular design features of a new plant can be compared. The Yankee Nuclear Power Station, for example is the first large pressurized-water plant that can be considered typical of a purely commercial application. The extent to which the design practice embodied in such an early representative of the class will become general practice can only be determined after later plants have reached the construction stage. At this point it appears that the most useful treatment that can be made of the design practice in these early models is to summarize as briefly as possible those features and design principles which result from fundamental design decisions, and to summarize those items of plant performance which illustrate how well the practice has worked out in the particular case in question. Such summarization is herein presented for the Yankee plant; the information was extracted from the final Hazards Summary Report.[1] The Yankee plant completed its 500-hr test run at the thermal power level of 392 Mw on Feb. 8, 1961, and operational information should be forthcoming soon which will make possible further evaluation of the design. Summaries of this kind will be made in *Power Reactor Technology* for new operating reactors as the information becomes available.

The basic design features that characterize the Yankee reactor are the use of steel-jacketed oxide fuel in a noncompartmented core in which surface boiling (but not bulk boiling) is permitted. A high degree of fuel subdivision is used, and close attention is paid to the minimization of local power-peaking factors through the close packing of fuel assemblies and minimization of water holes. The thermal design appears to be quite conservative, at least for the initial operating power of 392 Mw(t). The reactor is to be operated, at least initially, with single-batch reloading, and the design does not appear to have been directed toward ease of reloading to facilitate the use of any partial reloading scheme. The rather large amounts of excess reactivity required, because of the large temperature defect of the reactor and because of the large burnup requirement associated with single-batch reloading, pose a problem of reactivity holddown by the control rods. This problem has been circumvented by the use of dissolved boric acid for cold shutdown: the clean reactor would be supercritical in the cold condition if control rods alone were used for shutdown. A limited departure has been made from the pressurized-water practice exemplified by the Shippingport reactor in that gasket sealing of the pressure-vessel closure will be attempted; provisions are made for seal welding, however, if this should prove unsatisfactory. The approach to containment is unusual in that the spherical containment vessel for the reactor and the primary coolant circuit is supported on columns, entirely aboveground. Access to the containment vessel — except for certain special tests — is prohibited when the reactor is critical.

Fuel Elements

The fuel element for the first core is composed of a closed stainless-steel tube which contains uranium dioxide fuel in the form of cylindrical ceramic pellets. The pellets of 3.4 per cent enriched UO_2 are placed in the fuel tubes in groups of 25. Each group is separated from the next by a perforated stainless-steel disk (0.1205 in. thick) coated with braze ma-

terial. Each disk has a circumferential groove into which the tube is crimped during the loading process to fix its position until the entire subassembly is brazed. The disks are so spaced that each group of 25 pellets is allowed a free expansion space (approximately 0.2 in.). The disks are provided to prevent progressive distortion of the fuel which might be caused by repeated differential expansion between a long uninterrupted fuel column and its surrounding stainless-steel jacket.

Pellet density	10.10 g/cm^3
Pellet dimensions	0.294 in. diameter by 0.60 in. long
No. of pellets per element	150
Jacket	348 S.S., 0.021 in. thick, free standing
Jacket thickness/diameter ratio	0.062
Pellet-jacket clearance (assembly)	0.002 in. on radius
Additional gas space	About 1 in. of fuel-element length on assembly
Filling gas	Air, plus H_2 that diffuses through jacket wall during hydrogen brazing of fuel assemblies
End closures	S.S. plugs, tungsten inert-gas-shielded arc welded
Element dimensions	0.340 in. diameter by 93.6 in. long (between end plates of fuel-element assembly)
Length of UO_2 per element	90 in.
Total elements in core	23,142
Total UO_2 pellets in core	3.47×10^6
Total length of UO_2 pellet column in core	1.74×10^5 ft
Total "active" heat-transfer surface in core	15,500 sq ft

Fuel Assemblies

The fuel rods (elements) are assembled on a square lattice into assemblies that would be 18 by 18 rods square in cross section but for the omission of parts of the outer rows to make channels for the vanes of the cruciform control rods (Fig. VIII-1). Each assembly is composed of nine subassemblies; a standard subassembly is made up of a 6 by 6 square of fuel rods held together by brazing to tubular spacers, or ferrules, ½ in. long, which are located at 8-in. intervals along the length of the subassembly, in each channel formed by four adjacent fuel rods. Those subassemblies which occupy outside positions in the assembly also have rubbing straps brazed to their outer elements at four intervals along the length. Nine subassemblies are joined between end plates to form a complete assembly. The end plates are fixed to the ends of the center subassembly by captive machine screws which engage the end plugs of the fuel rods. The eight subassemblies surrounding the center one are free to "float" axially between the end plates, which they engage by slip fits with the end plugs of their fuel tubes. All subassemblies are tied together at a number of points along their length by means of tie straps which join the rubbing straps of subassemblies on opposite sides of the assembly.

The assemblies are of the open type, i.e., not contained in boxes. They are positioned by their end nozzles, round in cross section, which engage upper and lower core support plates. When a control-rod vane intrudes into the space between adjacent assemblies, it is accommodated by omitting a row of elements from one of the assemblies (Fig. VIII-1). Two types of assemblies are required to meet all the geometrical requirements (Fig. VIII-1), one containing 304 fuel rods and the other, 305.

No. of elements per assembly	305 (type A); 304 (type B)
Fuel-element lattice	Square
Lattice pitch in	0.422 in. (standard); 0.454 in. (in line with control-rod vanes)
Cross-sectional dimensions	About 7.61 by 7.61 in.
Length	111.25 in. total; 93.583 in. between end plates
Method of spacing elements	Brazing to ferrules and rubbing straps [electroless nickel-phosphorus (Kanigen)] plated onto ferrules, and furnace brazed
Total number of assemblies	76

Control Rods

The regular pattern of the core structure provides 32 cruciform rod positions (Fig. VIII-2). Twenty-four are occupied by control rods, and the remaining eight are filled by shims that can be moved when the vessel head is removed. The movable rods are of silver-indium-cadmium alloy, plated with nickel to a nominal thickness of 0.3 mil, heat-treated to give a diffusion bond between the nickel and the silver-indium-cadmium. They have Zircaloy-2 followers, attached by a disconnect joint. The shims are reversible, of double core length, one end being of stainless steel containing 1.2 wt.% natural boron, and the other being of Zircaloy-2.

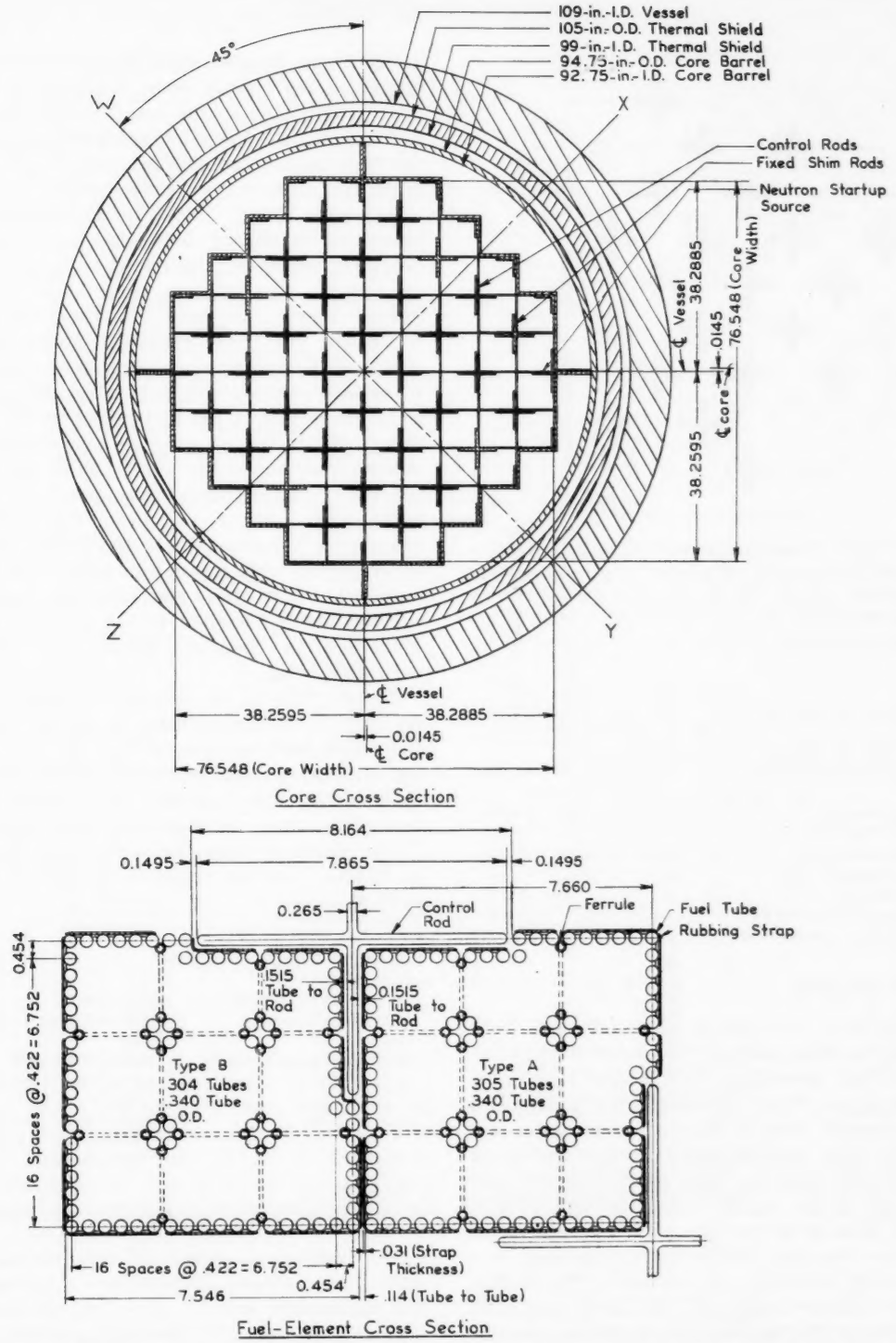

Fig. VIII-1 Yankee core configuration.[1] The 76 fuel assemblies include 38 of type A and 38 of type B. The 32 cruciform slots are for 24 control rods and 8 shim rods. The total number of fuel tubes (full core) is 23,218.

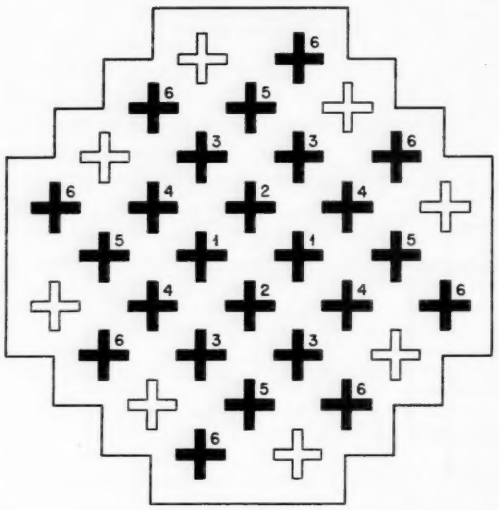

Fig. VIII-2 Diagram of Yankee core showing relative positions of control-rod groups.[1] The solid symbols represent control rods, and the open symbols represent stationary shims. The numbers 1 through 6 are group designations.

Control-rod material	80% Ag; 15% In; 5% Cd, plated with 0.3-mil Ni
Control-rod follower	Zircaloy-2
Control-rod dimensions	Cruciform, 7.865 in. span by 0.265 in. thick
Shim material	1.2 wt.% natural B in S.S.
Shim "follower"	Zircaloy-2
Shim dimensions	Same as control rod
No. of control rods	24
No. of shims	8
Control rods driven from	Top
Downward motion of rod	Decreases reactivity

Core Structure

The core structure is an "open" one, there being no walls between fuel assemblies or between fuel assemblies and control rods in the core proper. The positioning of fuel assemblies and control rods is determined by lower and upper core support plates, both of which are suspended from the same internal flange, near the top of the reactor vessel, by support barrels. Each of the two support plates is fabricated of two separate plates that are spaced, in a sandwich structure, for stiffness. The bottom plate contains holes for the lower end-plate nozzles of the fuel assemblies and has shrouds for the control-rod followers suspended downward from it. The upper plate contains holes for the upper end-plate nozzles of the fuel assemblies and supports guide blocks and dashpot stops for the control rods. It serves as both upper positioning means and holddown for the fuel assemblies. A core baffle fits closely around the core outline and confines the upward pass of the coolant flow to the core region.

Referring to Fig. VIII-3, the mechanical assembly is as follows: The lower core support barrel is suspended, by its upper flange, from the internal support ledge near the top of the reactor vessel. The core barrel and the core baffle are suspended (bolted) from the lower flange of this lower core support barrel, and the irregularly shaped baffle is strengthened by webs connecting to the cylindrical core barrel (Fig. VIII-1). The bottom core support plate is attached (bolted) to the lower end of the core barrel. The upper flange of the upper core support barrel rests on the upper flange of the lower core support barrel. The function of the upper barrel is to support the upper core support plate. Both upper and lower core support barrels are held down by a core holddown ring, which acts as a Belleville spring, held down by the vessel head.

Coolant flow is downward, in parallel flow through the spaces between the thermal shield and vessel wall, between the thermal shield and the core barrel, and between the barrel and the core baffle; then upward, in a single pass through the core, confined by the core baffle.

The effective diameter of the core (fueled) is 75.4 in., and the height of the core (fueled) is 91.86 in.

Fuel and Control Program

Fuel reloading program	Single batch
Average fuel exposure	7830 Mwd/metric ton
Fuel shuffling	None
Program of control-rod withdrawal	Banks of rods, in order 6-4-2-5-3-1 (see Fig. VIII-2)
Shim program	Shims inserted initially if needed; no fixed removal program

Power Distribution and Hot-Channel Factors

The estimated values of engineering and nuclear hot-channel factors are combined in the appropriate ways, to give the total factors $F_{\Delta T}$, F_Q, and F_θ. The factor $F_{\Delta T}$ is the ratio of the enthalpy rise of the coolant in traversing the hot channel to the average enthalpy rise of the coolant in traversing the core. F_θ is the

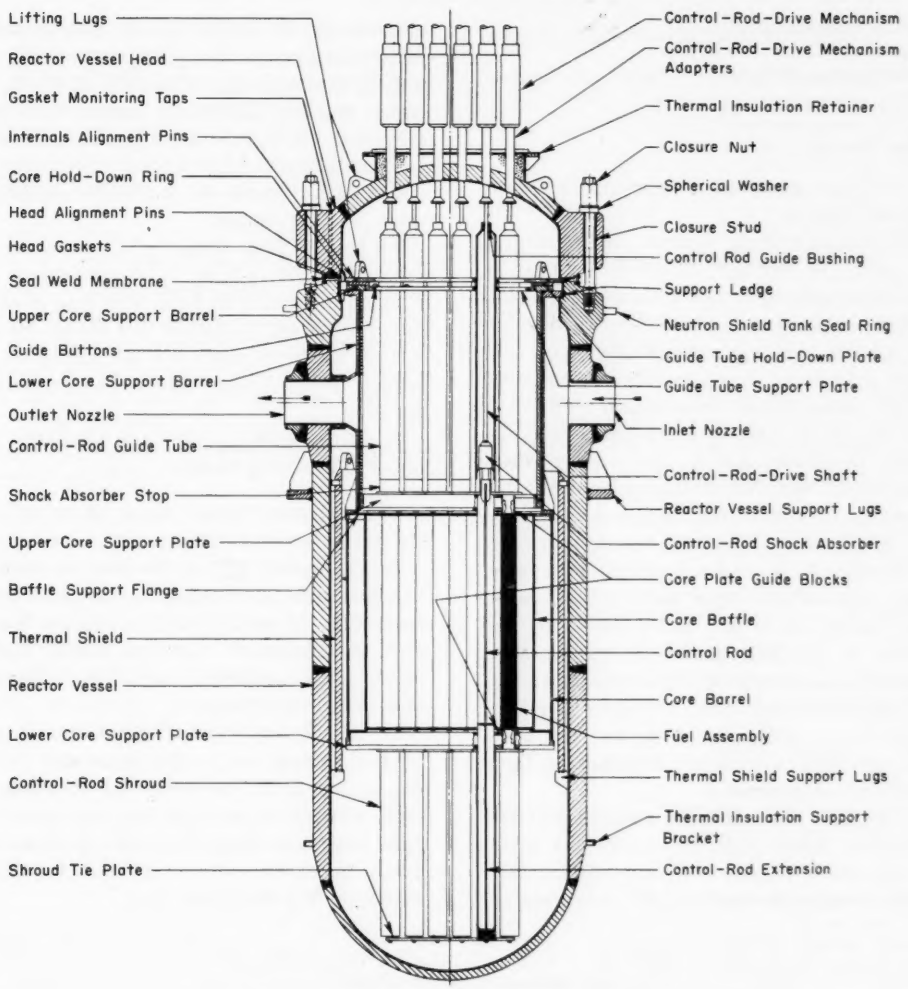

Fig. VIII-3 Yankee reactor vessel assembly.[1]

ratio of the maximum film temperature drop to the average film drop. F_Q is the ratio of the maximum heat flux to the average heat flux. The values are listed in Table VIII-1. The design values used (for core heat output of 392 Mw) were higher than the estimated values for initial operation. No artificial means of power flattening are used, other than control-rod programming. The possibility of using the chemical control during operation, to reduce power distortion by control rods, is mentioned.

Heat Removal

Fuel, max. center temp., °F	4330
Conductivity assumed for UO_2, Btu/(hr)(ft)(°F)	1.0
Fuel-to-jacket contact conductance assumed, Btu/(hr)(sq ft)(°F)	1000
Av. heat flux, Btu/(hr)(sq ft)	86,300
Max. heat flux (design assumption), Btu/(hr)(sq ft)	446,000
Av. film coefficient, Btu/(hr)(sq ft)(°F)	6050
$[(Q/A)_{burnout}/(Q/A)_{max.}]$ at point of burnout by Bettis correlation	2.3
Surface boiling of subcooled liquid	Permitted
Bulk boiling	Not permitted
Coolant temp., vessel inlet, °F	499
Av. coolant temp. rise in core, °F	33
Av. film drop, °F	14.3
Max. cladding-surface temp., °F	663
Coolant temp., outlet of hot channel, °F	603
Minimum saturation temp. in core, °F	621
Orificing for flow distribution	None
Coolant flow velocity in core, ft/sec	14.0
No. of core passes	1
Pressure drop across core, psi	16

Pressure drop across vessel, psi	34
Av. power density in core, kw(t)/liter	58.4
Av. specific power, Mw(t)/metric ton of uranium	18.8

Pressure Vessel

The reactor vessel is a welded assembly of the following parts:

1. The hemispherical bottom head of the reactor vessel is formed of SA-302, grade B, carbon-steel plate of $3\frac{7}{8}$ in. minimum thickness and is clad on the inside with a sheet of type 304 stainless steel of 0.109 in. thickness.

2. The cylindrical shell section of the reactor vessel is made up of two rolled courses of SA-302, grade B, carbon-steel plate of $7\frac{7}{8}$ in. minimum thickness and is clad on the inside with sheets of type 304 stainless steel of 0.109 in. thickness. Each rolled course has a longitudinal weld seam, and the two courses are joined together by a circumferential weld seam.

3. The cylindrical upper shell section of the reactor vessel is made up of three formed segments of SA-302, grade B, carbon-steel plate of $9\frac{5}{8}$ in. minimum thickness and is clad on the inside with type 308L stainless steel weld deposited to a thickness of $\frac{1}{4}$ in. The three formed segments are joined together by three longitudinal weld seams.

4. Four main coolant inlet nozzles and four main coolant outlet nozzles are welded to the upper shell section. The inlet and outlet nozzles alternate around the vessel at 45° intervals and are all at the same level. The nozzles are hollow forgings of SA-182 carbon steel, modified to the requirements of SA-302, grade B, carbon steel, and are clad on the inside with type 308L stainless steel weld deposited to a thickness of $\frac{1}{4}$ in. Stainless steel is weld deposited to the end of each nozzle to facilitate welding to the main coolant piping.

5. The bolting flange of the reactor vessel is an SA-105, grade 2, carbon-steel forging clad on the inside and top with type 308L stainless steel weld deposited to a thickness of $\frac{1}{4}$ in.

6. A support ledge for the internals is machined on the inside of the bolting flange near the top.

7. Two gasket grooves are machined into the top of the bolting flange.

The reactor vessel head is a welded assembly of the following parts:

1. The center disk of the reactor vessel head is approximately hemispherical in shape and is formed of SA-302, grade B, carbon-steel plate of 7 in. minimum thickness and is clad on the inside with a sheet of type 304 stainless steel of 0.109 in. thickness.

2. The thirty-two adapters for supporting control-rod-drive mechanisms are welded to the center disk. Each adapter is made up of a type 304 stainless-steel top and a coextruded tube which, in turn, is made up of an SA-106, grade C, carbon-steel tube clad on the inside with type 304 stainless steel.

Table VIII-1 TABULATION OF INITIAL* OVER-ALL HOT-CHANNEL FACTORS[1]

	$F_{\Delta T}$	F_Q	F_θ
Engineering Hot-Channel Factors			
Fuel rod characteristics:			
Pellet diameter	1.002	1.003	1.003
Pellet density	1.027	1.05	1.05
Pellet enrichment	1.011	1.022	1.022
Rod diameter pitch and bowing	1.097		1.134
Coolant-flow characteristics:			
Flow distribution in lower plenum	1.07		1.07
Flow redistribution due to local boiling	1.05		1.05
Product of engineering subfactors	1.28	1.08	1.37
Nuclear Hot-Channel Factors			
Local power peaking	1.3	1.3	1.3
Over-all maximum to average	1.8	2.9	2.9
Product of nuclear factors	2.4	3.8	3.8
Initial over-all factor*	3.07	4.10	5.21
Design over-all factor	3.36	5.17	7.36

*Initial implies maximum values for 0 to 500 hr of full-power operation.

3. The bolting flange of the reactor vessel head is an SA-105, grade 2, carbon-steel forging clad on the inside and bottom with type 308L stainless steel weld deposited to a thickness of $\frac{1}{4}$ in.

4. Two gasket monitoring taps penetrate the bolting flange and exit at the top.

The reactor vessel head is held to the reactor vessel by 52 closure studs with nuts and spherical washers. The $5\frac{1}{4}$-in.-diameter closure studs are made of SA-193, grade B16, carbon steel, and the closure nuts are made of SA-194, grade 2HB, carbon steel. Each set of spherical washers consists of two halves: a lower half with a concave upper surface and an upper half with a convex lower surface. The washers are made of special nitrided alloy.

The closure joint between the reactor vessel head and the reactor vessel is sealed by two self-energizing stainless-steel O-ring gaskets. The two gasket monitoring taps monitor the leakage past both the inner and outer O-ring gaskets. A backup provision for sealing is provided in the form of a seal-weld membrane. Operating experience will show whether seal welding of the seal-weld membrane is required.

The reactor vessel and head are designed in accordance with the ASME *Boiler and Pressure Vessel Code*, Section VIII, Unfired Pressure Vessels, 1956 Edition and Latest Addenda, and Code Case No. 1234.

Vessel height (with head)	31 ft 6 in.
Vessel internal diameter	9 ft 1 in.
Operating pressure (max.)	2300 psig
Operating pressure (min.)	1800 psig
Design pressure	2500 psig
Design temperature	650°F
Hydrostatic test	3750 psig, 90 to 200°F
Max. heating or cooling rate	50°F per hour (in heating up, the vessel must be held in the 150 to 250°F range until an isothermal condition is reached)
Material between core and vessel wall (effective thermal shield)	4.5 in. of steel, plus 8 to 11 in. of water
Ratio, cross-sectional area of core to internal cross-sectional area of pressure vessel	0.365

Reactor Instrumentation and Control

Internal instruments	Coolant outlet temperature thermocouples on selected fuel-assembly nozzles; unspecified number of flux wires in core — removable without depressurizing
Failed-fuel-element detection	None as such; main coolant water is sampled and monitored
Neutron source	Po-Be for initial operation; Sb-Be for self-activation. Multiple sources (4?) near edge of core
Location of nuclear operating instruments	Vertical thimbles in shield tank
Source-range instruments	2 BF_3 proportional counters: 4.5 cps/nv; range 1 to 10^5 cps
Intermediate-range instruments	3 compensated ion chambers: 4×10^{-14} amp/nv; 3×10^{-13} amp-hr/r; range 2.5×10^2 to 2.5×10^{10} nv
Power-range instruments	3 uncompensated ion chambers: 4.4×10^{-14} amp/nv; 5×10^{-11} amp-hr/r; range 2.5×10^4 to 2.5×10^{10} nv
Control-rod drives	24 positive-grip magnetic jacks
Rod travel	90 in.
Lifting capacity	750 lb (min.)
Normal rod speed	10 in./min in $\frac{3}{8}$-in. steps
Scram speed	Rods fully inserted in less than 2 sec
Scram delay	0.20 sec or less
Scram deceleration	Dashpots on top of upper core support plate
Shims	8 cruciform boron-steel shims, movable only when reactor head is off; to be used if needed (Fig. VIII-2)
Chemical control	Boric acid, added to coolant as a 12 wt.% aqueous solution before cooldown, to provide shutdown for the cold reactor
Method of boric acid removal	95% removed in 11 hr by dilution; remainder removed in 9 hr by ion exchange
Δk, cold to hot	7.2%
Δk, Doppler (zero to full power)	2.5%
Δk, fuel burnup	6.9%
Δk, equilibrium Xe and Sm	3.2%
Total	19.8%
k_{eff}, cold, clean	1.198
k_{eff}, cold, clean, all rods in	1.044
k_{eff}, cold, clean, all rods in, 950 ppm boron	0.950
k_{eff}, hot, clean, zero power	1.126
k_{eff}, hot, clean, zero power, 1 rod out	0.970
k_{eff}, hot, clean, zero power, 950 ppm boron	1.041

k_{eff}, hot, clean, full power	1.101
k_{eff}, hot, full power, equilibrium Xe and Sm	1.069
k_{eff}, hot, 10,000 hr at 392 Mw(t), equilibrium Xe and Sm	1.000

Primary Coolant Circuit

Total volume of primary coolant system	2940 cu ft
No. of independent loops	4
No. of steam generators per loop	1
No. of pumps per loop	1
Valves per loop	2 gate (remote operated), 1 check; also 1 gate and 1 relief in bypass line
Main piping size	24 in., steam generator to pump; 20 in. elsewhere
Flow velocity in pipe	26 ft/sec in 24 in.; 38 ft/sec in 20 in.
Pipe construction and material	Hollow forged and bored, ASTM-A-376-55T-TP-304 material specification
Main circulating pumps	Canned motor, 23,700 gal/min each
Steam generators	Shell and U-tube evaporator with 3-stage moisture separator; primary coolant in tubes
Log mean ΔT in steam generator	37°F at full load
Method of pressurization	Electric heaters in a separate steam-pressurizer vessel
Relief valves	Solenoid-operated relief valve on pressurizer, set at 2385 psig; 2 code safety valves (self-actuated) on pressurizer, set at 2485 psig and 2560 psig
Provision against loss of coolant flow	Independent power sources for pairs of the main circulating pumps (2 fed from main generator, 2 from incoming 115-kv lines)
Provision against loss of coolant	117,000-gal borated-water emergency injection system

Primary System Water

Additives, during reactor operation	Hydrogen injected into vapor phase of surge tank as necessary to control oxygen concentration, as indicated by analysis of primary water samples
Additives, during subcritical operation of primary system	35 wt.% solution of hydrazine in water injected by feed pump as needed to control oxygen concentration
Purification method	Bypass of cooled depressurized coolant to two mixed-bed ion exchangers; normal flow 25 gal/min, maximum flow 125 gal/min
Water chemistry, shutdown:	
Boron (as boric acid)	950 ppm
Hydrogen	25–45 ml (STP) per kg
Chloride	<0.1 ppm
pH	Approximately 5.2
Water chemistry, normal operation:	
Boron (as boric acid)	<5 ppm
Total solids (other than boric acid)	Approximately 2 ppm
Hydrogen	25–45 ml (STP) per kg
Oxygen	<0.1 ppm
Chloride	<0.1 ppm
pH	7.5 ± 1
Specific resistivity	0.5 megohm-cm

Shielding

The reactor vessel is surrounded by an annular water-filled shield tank, the thickness of the annulus being 36 in. This attenuates the neutrons to a thermal flux of approximately 5×10^3 neutrons/(cm^2)(sec) and a fast flux of approximately 1×10^3 neutrons/(cm^2)(sec). The primary shield, of ordinary reinforced concrete, surrounds the water tank and attenuates the radiation from the reactor to a level about equal to that emanating from the primary coolant system. The concrete thickness varies between 4.5 and 5.0 ft. A secondary concrete shield surrounds the entire reactor plant within the vapor container and reduces the radiation to tolerable levels outside the container. Portions of this concrete perform structural, as well as shielding, functions. The thickness varies from 5 to 2 ft.

Fuel Handling

A water pit is provided above the reactor vessel, its concrete walls being upward extensions of the main biological shield. The pit is empty during reactor operation. For refueling, the nuts are first removed from the reactor vessel studs, and the head seal weld, if any, is cut. The pit is then flooded with borated water to a level approximately 25 ft above the top flange of the vessel. The vessel head and other parts are then removed by crane and handling tools and are stored under water in the pit. With the magnetic jack control-rod drives deenergized, the vessel head, with the control-rod-drive magnets attached, can be lifted off, leaving the control rods and their drive shafts in place. The following equipment must then be

removed and then stored under water before fuel assemblies are removed: control-rod guide-tube holddown plate and holddown ring; 24 control-rod shaft guide tubes and 24 control-rod-drive shafts; guide-tube support plate; and upper core support barrel with attached core support plate. The fuel assemblies and control rods can then be removed as desired. Spent fuel assemblies are placed, under water, in a discharge chute, which transfers them, by gravity, out of the containment vessel to an external water-filled fuel transfer pit, whence they can be loaded into coffins for shipping. After reloading of the reactor, reassembly of the internals proceeds as above, but in reverse order.

Steam Plant

No. of turbines	1
Type	Saturated steam, 1800 rpm, tandem compound, with 3 points of automatic extraction for feed-water heating, exhausting to an 85,000-sq ft single-pass divided-water-box condenser
Rating	145,000 kw at 3½ in. Hg backpressure
Reactor thermal power (ultimate)	530 Mw
Gross electrical output	160 Mw
Net electrical output	150 Mw
Net efficiency	28.3%
Heat rate (turbine)	11,345 Btu/kw-hr at backpressure of 1.5 in.
Heat rate (plant)	12,270 Btu/kw-hr at backpressure of 1.5 in.
Steam conditions	465 psia, 459.6°F, ¼% moisture
Maximum throttle flow	2×10^6 lb/hr

Plant Arrangement

The plant is housed in two main structures: the vapor container and the adjacent turbine building. The control room is in the turbine building, on the side nearest the vapor container. In the vapor container are located the reactor, the steam generators, the primary coolant circuit, and all auxiliary systems servicing the primary circuit. The fuel transfer pit and the adjacent storage vault for new fuel are located just outside the vapor container; all other major components are located in the turbine building.

Containment

The reactor, its shielding, and the primary coolant system are located in the spherical, steel, vapor container, which is held entirely above ground level on concrete support columns. The pressure in the container is maintained slightly above atmospheric during reactor operation. Personnel are not allowed in the vapor container when the reactor is critical, except for special test reasons.

Diameter of vapor container	125 ft
Minimum wall thickness	⅞ in.
Gross volume of vapor container	1.02×10^6 cu ft
Net volume of vapor container	0.84×10^6 cu ft
Design pressure	31.5 psig
Design membrane stress for welded plate	13,500 psi
Material	ASTM spec. A-300, class A-201, grade B
Permissible leakage rate	0.1 wt.% of contained air in 24 hr (= 70 cu ft/hr, STP) at 15 psig
Postulated condition determining design pressure	Rupture of one 20-in. primary coolant line and in one secondary steam line

Plant Control

Reactor startup is manually controlled. In the power range from 10 per cent to full power, load matching control may be either manual or automatic. The automatic system acts to maintain a constant average reactor temperature by movement of the control rods. Normally the reference temperature is set at 514°F. When the average reactor temperature deviates from this value by as much as 3°F, the control rods are set in motion in the proper direction, and the motion is continued until the deviation is reduced by 0.5°F. The reference temperature, the magnitude of deviation at which rod motion begins, and the degree of correction before rod motion is stopped are all manually adjustable.

Reference

1. Yankee Atomic Electric Co., Yankee Nuclear Power Station, Technical Information and Final Hazards Summary Report, USAEC Report YAEC-167(Vols. I and II), Oct. 2, 1959.

Section IX

OPERATING EXPERIENCE

EBWR

Reference 1 is a collection of selected reports of tests conducted on the reactor and plant equipment comprising the EBWR since the facility was initially placed in operation. The tests reported are concerned with these general subjects: system components, reactor power, radiation and flux, control and control rods, physics, reactor dynamics, fuel, and water chemistry and corrosion. The following paragraphs contain abridged accounts of some of these reports. In the interests of brevity, only the objectives and conclusions reached are presented, in most cases, although many of the reports also contain descriptions of the procedures followed, the methods used, and some discussion of the test results.

Water Losses from EBWR (Report No. 14A)

The objective of this test was to determine the quantity and location of water losses in the plant in order to evaluate changes that must be made prior to heavy-water operation. Three possible types of leakage were considered:

1. External leakage from valves, magnetrols, equipment, etc.
2. Losses from the air-ejector discharge gases in the form of dissociated water (hydrogen and oxygen) and moisture rejected from the system with the gases.
3. Inleakage contamination.

The following conclusions were reached:

1. For this plant the present average total light-water leakage from valves, etc., is approximately 20 lb per day.
2. Approximately 63 lb of equivalent water weight per day is discharged from the air ejector to the stack in the form of dissociated hydrogen and oxygen at the 20-Mw power level. In addition to the dissociated gas discharged from the ejector, approximately 5 lb of water per day in the form of contained moisture is discharged with the gases.
3. The light-water leakage into the system is estimated to be 1.2 lb per day.

The report states that substantial reductions in these losses can be effected by changes in, and to, valves and by the installation and operation of a recombiner and an air-ejector gas dryer. The capitalized cost of the expected annual D_2O losses, after these modifications are made, is estimated to be as follows:

External equipment leakage	$34,100
Gas dissociation loss	27,300
Air-ejector moisutre loss	100
Unaccountable losses	6,800
Total	$68,300

The above total is based on a D_2O charge of $28 per pound and a capitalization factor of 12 per cent. On the basis of an 80 per cent load factor and a net electrical generating capacity of 5000 kw, these losses are estimated to contribute 0.187 mill/kw-hr to the cost of the electrical energy generated.

Turbine Inspection (Reports Nos. 36, 53, and 53A)

The objective of the inspection was to determine the level of radioactive contamination in the turbine and the major contributors to this contamination. As a result of this inspection, it was concluded that only minor contamination of the turbine had occurred. Moreover, only a negligible amount of the fission products present in the steam was observed to have "plated out" in the turbine and piping.

The activity levels at various locations within the steam piping and turbine after 2839 hr of

turbine operations (155×10^6 lb of steam throughput) were as follows:

Location	Activity level, mr/hr
No. 1 high-pressure steam seal	2.0
First row of blades	0.2
Blades in all succeeding rows	0.2 or less
Admission valve stems	3.0
Nozzle inlets	5.0
Inlet side of trip-throttle valve	2.0

The long-lived products causing these activities were estimated to be 92 per cent Co^{58}, 8 per cent Ba^{140}-La^{140}, and traces of Co^{60}, Cr^{51}, and Fe^{59}.

EBWR Power Run with Zero Bypass

(Reports Nos. 23, 23A, and 23B)

EBWR is designed to operate using steam bypass as a means of pressure- and power-level control. The objective of these experiments was to determine the feasibility of operating with zero or fixed steam bypass and achieving pressure- and power-level control by control-rod movement only.

Three modes of control were attempted. In mode 1 the operator was instructed to remove the center rod at the rate of 0.5 in./sec for 1 sec every 5 sec in response to a power-demand signal. Rod motion was begun when reactor pressure reached 540 psi. The center rod was reinserted when the pressure reached 560 psi at the same rate and interval of operation used for its removal. The steam bypass valve was closed during this experiment.

Control mode 2 consisted of adjusting the center control rod in or out in response to generator load changes of 200 kw/min. The operator used a Brush recorder to observe the rate at which reactor pressure changed, and the operator manipulated the rod as required to maintain the desired pressure within ±10 psi. The steam bypass valve was also closed for this test.

In mode 3 the steam bypass flow was set at 10 per cent, and the generator load was increased at the rate of 200 kw/min. The operator was instructed to maintain the 10 per cent steam bypass by moving the center rod 0.1 in. every 5 sec as required by bypass valve changes.

The results of these experiments were as follows:

1. Under control mode 1, reactor neutron flux and pressure varied sinusoidally with a frequency of 0.0056 cps, and reactor flux exhibited a peak-to-peak variation of 40 per cent with a phase angle of 72°.

2. The operator was able to maintain reactor pressure within the desired band under mode 2 and was similarly able to hold the 10 per cent steam bypass position in mode 3.

These experiments were repeated using an on-off relay amplifier to accomplish rod motion in response to a pressure error. The results were essentially the same as those obtained using human operator actuation.

Results of First Annual Inspection of EBWR

(Report No. 25B)

The objective of this inspection was to determine the effect of past operations upon the reactor fuel. The reactor was shut down on Dec. 24, 1957, after one year of operation; it had produced 3060 Mwd of thermal energy. The core loading employed during this period is shown in Fig. IX-1. The average banked control-rod position for this loading was 30 in. However, during the first 1000 Mwd of operation, the four boron–stainless steel rods were banked at 48 in., and the remaining five hafnium rods were banked at 28 in.

Both visual and radiation examinations of core components were conducted. Other than excessive scaling of the fuel plates, the visual inspection disclosed no abnormal conditions. However, it should be noted that the mechanical arrangement of the fuel is such as to preclude any definitive results without extensive destructive disassembly.

The radiation examinations were made by exposing an 0.8*N* $FeSO_4$ solution to the gamma radiation emanating from the fuel assemblies. The irradiation of this solution with gamma energy converts ferrous ions to ferric ions at a rate proportional to the activity level. A comparison of the preirradiation and postirradiation ratios of these ions yields a measure of the activity level to which the solution was exposed.

The irradiations were carried out in the reactor vessel on each fuel assembly in the northwest quadrant of the core. The method used consisted in first raising the assembly to be examined to a point 6 ft below the top of the vessel. An aluminum tube containing a series

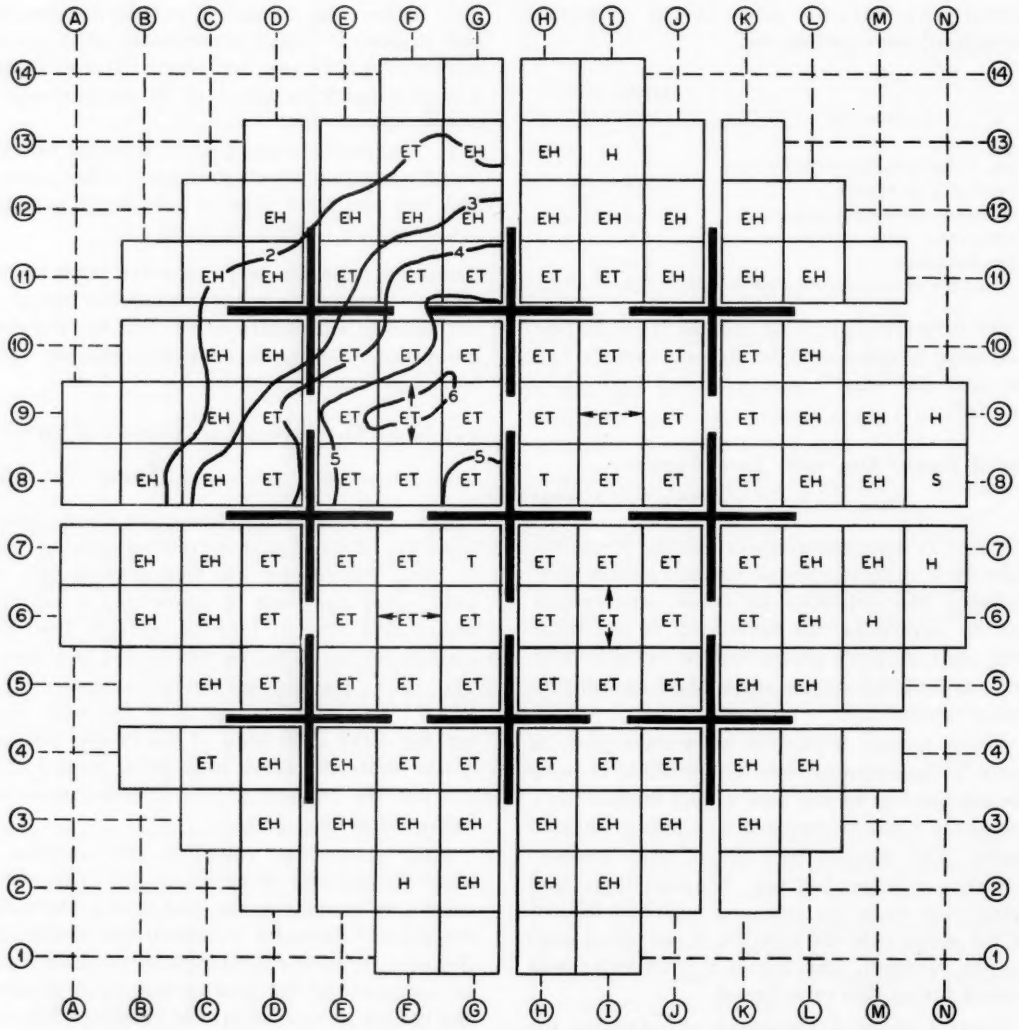

Fig. IX-1 Core loading No. 46, EBWR.[1] H, natural thick plates. T, natural thin plates. EH, enriched thick plates. ET, enriched thin plates.

of 2½-in.-long solution-filled plastic capsules, sufficient to extend the full length of a fuel plate, was then positioned adjacent to the assembly for a fixed period of time. Following exposure, the solutions were analyzed, and the results were interpreted in terms of the axial power distribution associated with that particular assembly. The distribution is, of course, an effective one, affected by the entire past operating history of the assembly.

In Fig. IX-1 the radial power distribution for the quadrant examined has been superimposed, in the form of lines of constant power density, on the core loading diagram. A similar presentation of the axial distribution is given in Fig. IX-2. The shift of the power peak away from the center of the reactor, radially, is probably caused by the flux-depressing effect of the two natural-enrichment assemblies located in two of the four central fuel positions. It may indicate, also, that the center control rod, on the average, was inserted farther than the other rods.

The axial asymmetry of the power distribution can be attributed to the relatively lower re-

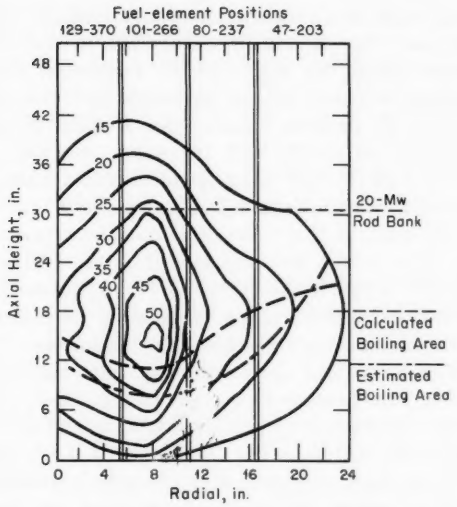

Fig. IX-2 Flux distribution in northwest vertical plane.[1]

activity of the upper portion of the reactor, due to the higher steam-void fraction, and to the partial insertion of control rods.

Determination of Thermal-Neutron Flux in EBWR by Cobalt Activation (Report No. 71)

Two natural-enrichment assemblies (of the thick-plate type) were equipped with cobalt wires and were irradiated in the outer edges of the EBWR core to determine the neutron flux in these regions. The assemblies were installed in positions 27-255 and 27-43, which are diametrically opposed positions in the next-to-last ring of core fuel positions.

The cobalt wires were strung between a pair of fuel plates in each assembly. Cadmium-covered wire was used in position 27-255, and bare wire was used in position 27-43. The thermal-neutron curve shown in Fig. IX-3 was derived by correcting the total neutron-activation curve for those activations caused by neutron energies above 0.5 ev. The plot of positions as a function of height are considered accurate to 0.2 in. The maximum thermal-neutron flux of $3.8 \pm 0.3 \times 10^{12}$ neutrons/(cm^2)(sec) occurred at a point 19 in. above the bottom of the assembly.

EBWR Operation at 62 Mw (Report No. 54B)

The objective of this experiment was to determine the safe operating limit of the reactor

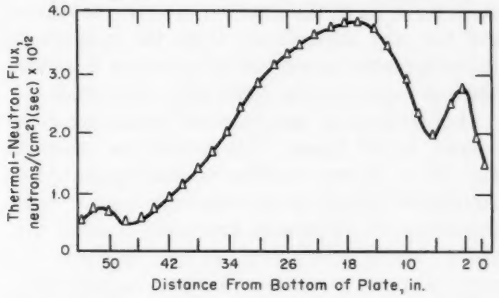

Fig. IX-3 Thermal-neutron flux.[1] Positions: 27-255 and 27-43.

from a stability standpoint. The reactor performed stably at a steady power output of 61.7 Mw(t), and it is believed that higher power levels could have been attained. However, feed-water pump capacity precluded further power increases during this experiment.

The report[1] presents a table of operating data taken during the high-power run. The readings are within the normal ranges except for somewhat higher radiation levels. This was to be expected since plant activity levels are usually power dependent.

Stability Analysis of the 60-Mw Run (Report No. 54C)

The data taken during the 60-Mw(t) power experiment were analyzed for any significant changes in operating stability with power (other than those to be expected because of the in-

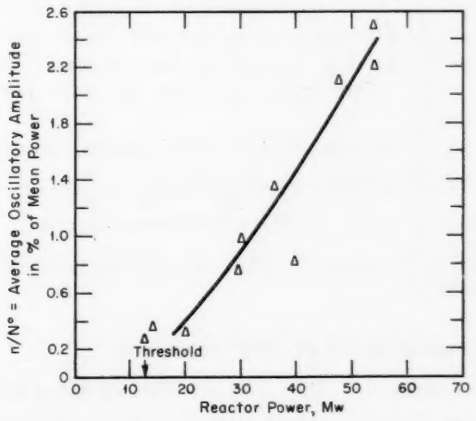

Fig. IX-4 Spontaneous EBWR oscillations as a function of power.[1]

creasing gain of the power-reactivity feedback) and for any departures from the operational characteristics predicted by previous transfer-function experiments. None were observed.

The buildup of spontaneous oscillations appeared to be linear with power as shown in Fig. IX-4. Abrupt changes or discontinuities in oscillation frequency or amplitude did not occur. Moreover, the resonant frequency change with power, which was predicted by low-power rod oscillation (transfer function) experiments, agreed quite well with the observed frequency changes, as can be seen in Fig. IX-5. The conservatism of the transfer-function predictions relative to the actual performance of the reactor was also noteworthy.

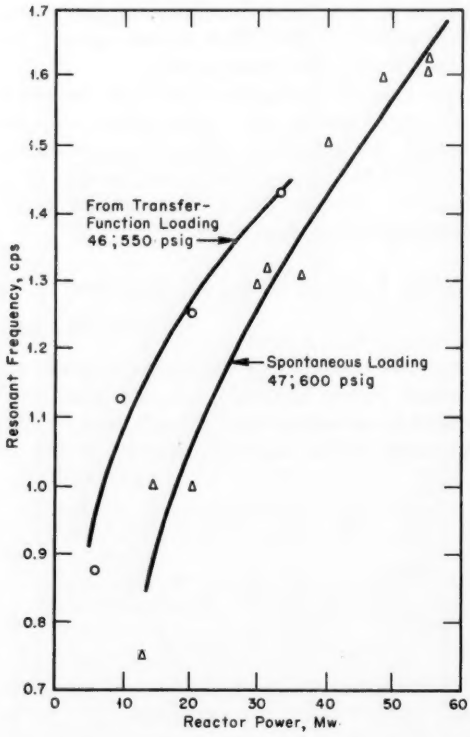

Fig. IX-5 Effect of power on resonant frequency (EBWR).[1]

Demonstrations of UTB Voidmeter

(Report No. 72A)

The purpose of this experiment was to determine the void distribution in various fuel-assembly positions at the 42.7-Mw power level. The voids are measured by comparing the epithermal flux to the thermal flux at various points along the length of the assembly. This method is based on the principle that the decrease in neutron moderation caused by the presence of voids will increase the ratio of epithermal-to-thermal neutron flux in a manner that can be related to the void content.

The neutron flux was determined by irradiating bare cobalt wires in four different fuel positions at 42.7 Mw(t) for 5.88 hr. Cadmium ratios were obtained by irradiating cadmium-covered wires in three assembly positions.

The axial flux distribution at four different radial fuel positions is given in Fig. IX-6. The voids calculated for points 24, 32.3, and 42 in. above the bottom of the fuel were 8.3, 19.5, and 33.5 per cent, respectively. The total reactivity held in voids during the irradiation run was measured as 3.38 per cent.

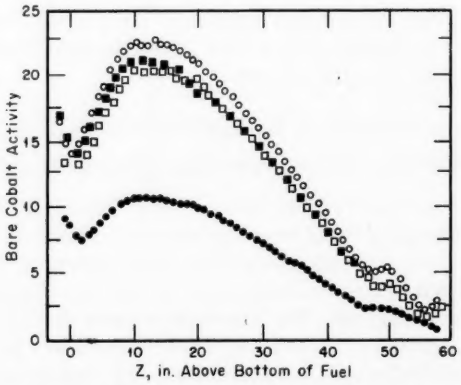

Fig. IX-6 Flux distributions in EBWR at 42.7 Mw and all control rods out.[1] ○, location 1, ET at $r = 8.5$ cm. ■, location 2, ET at $r = 22.9$ cm. □, location 3, ET at $r = 37.3$ cm. ●, location 4, EH at $r = 54.4$ cm.

Recirculation Flow-Rate Tests

(Report No. 39A)

The goal of this experiment was to determine the rate at which water was recirculated through the loop formed by the internal downcomer and the reactor core. The recirculation flow rate is computed using the relation

$$W_C = W_F \frac{(T_R - T_{FW})\,\bar{C}_F}{\Delta T_1\,\bar{C}_C} = \frac{\text{const.}}{\Delta T_1}$$

where

W_C = recirculation flow rate
W_F = feed-water flow rate
T_R = saturation temperature in reactor
T_{FW} = feed-water temperature
$\overline{C}_F$ = average specific heat over range (T_F – T_R)
$\overline{C}_C$ = average specific heat over range T_1
ΔT_1 = subcooling at reactor core inlet (T_R – T_{inlet})

All the variables necessary for a solution for W_C are known except ΔT_1. This subcooling was measured using 12 thermocouples installed in the reactor as follows:

2 below fuel element 27-255
2 below fuel element 27-43
2 below dummy element 0-173
1 below dummy element 0-278
1 below dummy element 0-67
1 below dummy element 0-384
1 center dummy element 0-384
1 top dummy element 0-384
1 steam zone

In order to average the core inlet temperature, eight of the nine thermocouples located in the lower end of the core were wired in parallel.

The results of this experiment are shown in Fig. IX-7. Data from the first recirculation rate experiments are also included in the figure for purposes of comparison.

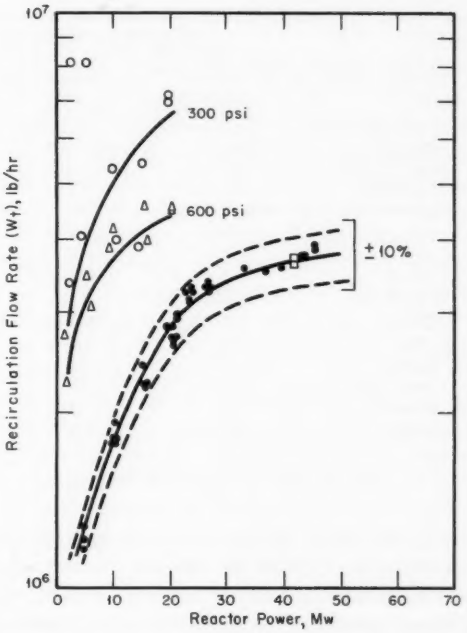

Fig. IX-7 Recirculation flow rate versus power (EBWR).[1] Δ, Bernsen's data at 600 psi. ○, Bernsen's data at 300 psi. ●, current data. □, equilibrium at 42.4 Mw.

Deposits on the Steam Side of the Condenser and Steam Dryer (Report No. 30)

During July 1957 the steam sides of both the condenser and steam dryer were inspected for radioactive contamination. At the time of the inspection, the reactor had produced 1370 Mwd of thermal energy, about half of which was generated during an effectively continuous power run.

Activity levels in the steam dryer measured 5 to 6 mr/hr, and those of the condenser measured 1 to 2 mr/hr in the hot well area and 0.1 to 0.2 mr/hr above the condenser tube banks. No evidence of erosion was observed. It should be noted that the activities reported resulted from long-lived contaminants only, since the reactor had been out of operation for a period of time prior to the inspection. Presumably, the contributions of the short-lived products would have yielded higher activity levels; however, the low levels resulting from the long-lived products indicate that radioactive contamination will pose no serious problem to the maintenance of this equipment.

The constituents of the corrosion-product deposits collected from the condenser and steam dryer and the locations from which they were taken are shown in Table IX-1. It is significant to note that the composition of the corrosion product differs markedly from that of the fuel assemblies. The report suggests that this fact may indicate that the deposit was not carried over from the reactor by reactor steam.

Reactor Steam Purity by Radioactive Sodium Tracer (Report No. 37)

This test concerns the use of sodium as a radioactive tracer to determine the amount of moisture carried over to the turbine by reactor steam.

The tracer consisted of 36 g of sodium sulfate which was added directly to the reactor water and which was irradiated for 3 hr in the reactor core at a power level of 40 Mw(t) before sampling was begun. These data were used to determine two decontamination factors: (1) the ratio

Table IX-1 SPECTROGRAPHIC ANALYSES OF DEPOSITS FROM STEAM SIDE OF EBWR CONDENSER AND STEAM DRYER–EMERGENCY COOLER[1]

Constituent (reported as metal; present as oxide)	Condenser tube shield samples				Steam-dryer sample
	Dull light red-brown color		Burnished-brass appearance		Dark red-brown
	Single shield, %	Composite of four shields, %	Single shield, %	Composite of four shields, %	Second row of tubes (from top), %
Iron	VS*	VS	VS	VS	VS
Aluminum	1.5	3	2	2	3
Nickel	1.5	3	3	4	1
Chromium	0.02	0.15	0.02	0.2	1.5
Copper	0.1	0.3	0.1	0.2	0.1
Lead	1.5	1.5	2	3	0.1
Sodium	0.08	0.7	0.08	0.7	0.2
Potassium	0.05	0.15	0.03	0.2	0.04
Calcium	0.08	0.4	0.02	0.3	0.04
Boron	<0.1	0.2	<0.1	0.2	<0.1

*VS = very strong or major constituent.

of reactor water activity to steam activity before the dryer and (2) the ratio of reactor water activity to steam activity after the dryer. Both of these decontamination factors are presented as functions of reactor power in Fig. IX-8.

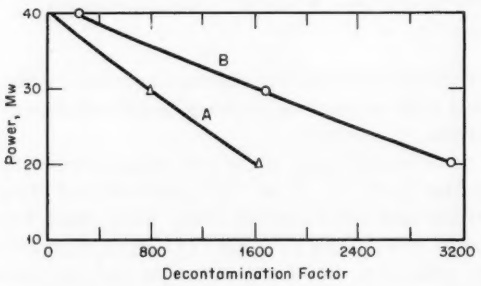

Fig. IX-8 Decontamination factor versus power (EBWR).[3] Curve *A*: Reactor water activity/steam activity before dryer. Curve *B*: Reactor water activity/steam activity after dryer. All activities in counts per minute per cubic centimeter of liquid.

The significant drop in both decontamination factors at the 40-Mw power level should be noted. The report does not explain this effect. However, subsequent information[2] indicates that foaming occurred to a considerable degree within the reactor vessel at these higher power levels. Since foam would not be expected to separate readily from the steam, the effect of foaming could be quite similar to submergence of the steam outlet nozzles. If this is the case, the high steam moisture content observed at the 40-Mw power level may be simply explained as an effect of reactor water level rather than of power.

In addition to the reports summarized in the foregoing paragraphs, the reference[1] also contains reports of the following tests:

Test report No.	Title
38	EBWR Pressure-Vessel Gasket Closure
58	Examination of the Kanigen Plating in the EBWR Main Steam Line
74A	Containment-Vessel Air Temperature
78C	Building Shell Pressure Leak Rate Test
101A	Turbine Seal Leak Tests
103	Volume of Water in the Reactor
8	Power Output Versus Galvanometer Reading
11	Decay Heating and Power Calibration Tests
7	Plant Radiation Levels
25, 25A	EBWR Flux Plots
34	Prediction of N^{16} Gamma Activity
34A	Distribution of N^{16} in EBWR
35	Flux Distribution in Tangential Instrument Tube
47	Neutron Survey Beneath EBWR
49	Gamma-Flux Determination of EBWR Core
49A	Measurement of Gamma Flux in EBWR
56	Radioactive Crud Cleanup in Nozzles Below EBWR
102,102A, and 102B	Relative Effectiveness of Sb-Be Source and Core-Induced Neutrons
2	Graphs of Rod Position Versus Time of Operation
9, 9B	Control-Rod Positions and Power Calibration
31, 42D, and 77	Control-Rod Data
41C	EBWR Void Reactivity Versus Power
42, 42B, and 42C	Reactivity Changes and Irradiation Effects

Test report No.	Title
100C	Effect of U^{235} Containing Stainless-Steel Followers on EBWR Reactivity and Control-Rod Worth
26	Some Kinetics Experiments in EBWR
41, 41A, and 41B	Reactor Transfer Function Measurements
43A	Analysis of EBWR Control-Rod Ejection Experiment
39	Preliminary Determination of Recirculation Rates in EBWR
39B	EBWR Recirculation Rate
39E	Further Recirculation Flow Rate Tests
39G	Measurement of Inlet Subcooling for the Determination of Recirculation Flow Rates
62, 62A, and 62B	Water-Level Measurements in the Reactor Vessel
51	Evaluation of the Fuel Transfer Coffin
55	First Defect Test in EBWR
64	Fuel-Transfer Radiation Survey
75	Probe of Fuel Channels with a 0.050-In. Clearance Gage
13A	Water Technology of EBWR During Initial Operation
15	Ion-Exchange Column No. 1 Resin Removal
22	Water Decomposition as a Function of Reactor Power
22A	Water Decomposition at Varying Reactor Powers and Pressures
29	Deposits from a Fuel Element and Dummy Fuel Elements
29A	Scale on Fuel Elements in EBWR
29B	Test for Scale Removal from Fuel Assembly H-18
29C	Postirradiation Heating of Fuel Element H-18
29D	Visual Inspection of Fuel Assemblies During Core Loading
66	Effect of H_2 Addition to Reactor Feed Water on Radiolytic Decomposition
73A	Measurement of Suspended and Dissolved Solids in EBWR Water
79	Corrosion of EBWR Steam Line Samples
104	Radiochemical Analysis of Samples from the EBWR Shock Shield

Two areas of major interest in water reactor technology are water chemistry and corrosion-product deposition. This is particularly true in the case of direct-cycle boiling-water reactors, such as the EBWR, wherein steam produced in the radiation environment of the core circulates through the various systems of the plant either as primary steam or as condensate. Entrained in the steam are dissociation products and radionuclides, which may preferentially contribute to system corrosion, wear, and radioactivity. The severity of these phenomena, their causes, and their effects on plant operation have been the subject of a considerable investigative effort during the past EBWR operational testing program. Reference 3 is a summary of the results of these investigations.

Previous operational experience with water reactors had demonstrated the occurrence of radiolytic decomposition of water in the presence of ionizing radiation. Further information was obtained from the BORAX series of experiments which indicated that the rate of decomposition increased when irradiation was accompanied by boiling of the coolant and moderator water. These same experiments also showed the oxygen content of steam generated in the core of a reactor to be higher than that observed in conventional steam plants.

One of the major effects of high oxygen content in steam is increased corrosion of metallic surfaces in contact with the steam. In view of the problems attendant to high corrosion rates in nuclear systems, an accurate determination of the oxygen content of the steam and the assessment of its effects on the corrosion of the various boiling-water reactor systems became a subject of increasing interest in the EBWR program.

The first water analysis was conducted on Dec. 23, 1956, shortly after the reactor was initially placed in operation at rated power. Additional analyses were conducted, periodically, through Feb. 20, 1957. The results of these analyses are given in Table IX-2. The average concentration was found to be 55.1 cm^3 of gas per liter of condensed steam (uncorrected for H_2 and O_2 dissolved in the condensate) containing 30.7 per cent O_2, 66.4 per cent H_2, and the rest inert gas.

The tests of Dec. 29, 1956, are of particular significance to plants contemplating the use of boric acid solutions for supplementary control. At the time this analysis was made, the reactor water contained 0.748 g of boric acid per liter. The decomposition products measured 53 cm^3 of total gas per liter, indicating that the boric acid had little or no effect upon the net decomposition rate.

The effects of both pressure and power level on dissociation were also investigated. The rate of oxygen production was found to decrease with increased pressure and to increase, linearly, with power. Both the power and pressure effects are shown in Fig. IX-9. Data obtained from the BORAX-IV experiments are included for purposes of comparison.

Previous experiments involving hydrogen additions, conducted on both pressurized- and

Table IX-2 EBWR WATER-DECOMPOSITION DATA[3]

Date of sample analysis	Time	Power level, Mw	Reactor water quality			Gas yield, cm^3/liter[a]	Condensed-steam gas analysis			Air-ejector gas flow, cfm[b]	Air-ejector gas analysis		
			pH	Conductivity: Determined, ohms/cm^3	Conductivity: Recorded, μmhos		O_2, %	H_2, %	Inert gas, %		O_2, %	H_2, %	Inert gas, %
12-23-56[c]	0115	20	7.0	180,000		50	22.7	47.0	30.3[d]		25.2	32.8	42.0
12-23-56[e]	2015	20	7.0	180,000		69	20.4	44.5	35.1[d]		22.6	27.2(?)	50.2
12-29-56[f]	2210	20	5.2	90,000		53	30.2	55.9	13.9		29.4	56.1	16.1
1-11-57[g]	1630	20	5.0(?)	410,000		47.5	29.7	68.6	1.7				
1-30-57	1715	20	7.05	900,000		66	31.0	63.4	5.6		30.4	53.9	15.7
2-11-57	1917	20	7.0	760,000		52.5	30.0	66.2	3.8		28.2	47.3	24.5
2-11-57	2330	20	7.0	600,000		46	29.2	62.4	8.4		28.9	44.6	26.5
2-12-57	1300	20	7.15	640,000		45.7	29.3	69.2	1.5				
2-12-57	2020	20	7.2		0.8	47.8	30.2	67.3	2.5		29.5	48.0	22.5
2-13-57	1030	20	7.1		0.9	58.5	31.6	66.6	1.8				
2-13-57	1920	20	7.08		0.9	55	30.0	66.0	4.0		29.9	47.5	22.6
2-14-57	1200	20	7.1		1.0	57.8	31.1	66.5	1.8		29.9	49.7	20.4
2-14-57	2110	20	7.02		1.0	63.3	32.5	67.5	0.0	1.2	29.7	51.8	18.5
2-18-57	1115	20	7.3		0.8	59.8	31.7	67.0	<1.3	1.0	30.5	56.0	13.5
2-20-57	1000	20	6.9		0.9	58.0	31.7	66.2	2.0	0.92	30.9	56.1	13.0
Average of samples of 1-11-57 through 2-20-57:						55.1	30.7	66.4	2.9		29.7	50.5	19.7

[a]Not corrected for gases dissolved in the condensed steam.
[b]Not corrected for gas density; values reported are for air at 80°F in cubic feet per minute.
[c]This sample was steam bypassed to the condenser.
[d]Values are high owing to transfer of sample or actual nitrogen in system.
[e]This sample was steam going to the turbine.
[f]Boric acid in the reactor water was 0.748 g/liter for this sample.
[g]Only 8.3 ppm boric acid was in the reactor water for this sample.

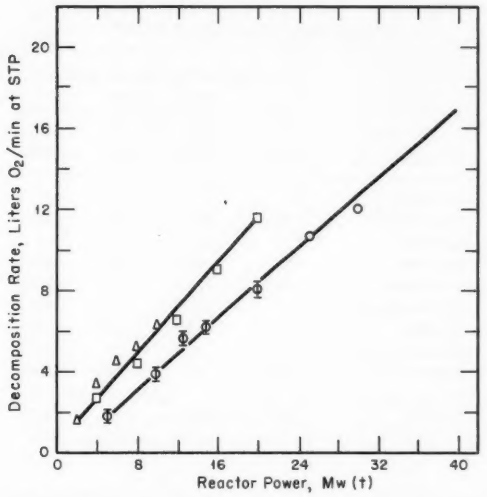

Fig. IX-9 Reactor power versus decomposition rate.[3] ○, EBWR: 600 psig, 488°F. □, EBWR: 300 psig, 420°F. △, BORAX-IV: 300 psig, 420°F. Water conditions, *p*H 7. Specific resistance 10^6 ohm-cm.

boiling-water reactors, have shown beneficial effects on dissociation rates. The effects of hydrogen gas additions on the EBWR are shown in Fig. IX-10. Additions of hydrazine, ammonia,

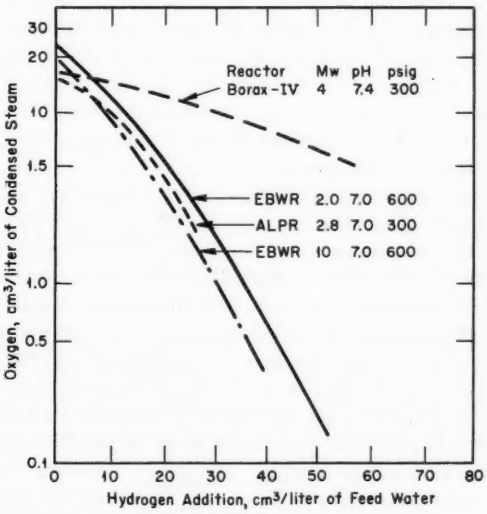

Fig. IX-10 Effect of H_2 addition on water decomposition.[3]

and nitrogen were of little or no benefit and, in some cases, increased the rate of dissociation. An interesting sidelight to these hydrogen gas addition experiments is the contrasting effect of such additions on the recombination of dissociated oxygen and the concentration of N^{16} in steam. For example, the addition of 40 cm^3 of H_2 per liter of EBWR feed water has resulted in a factor-of-20 reduction in the oxygen content of the steam and as much as a fourfold increase in plant N^{16} activity levels.

In an effort to determine the corrosive effects of the high oxygen content (28 ppm oxygen) on the reactor steam and condensate systems, extensive examinations have been made on the equipment and piping comprising these systems. In the main, only negligible corrosion of conventional system materials has been observed. Moreover, these corrosion products have had little or no effect on reactor maintenance and operation. Only the Kanigen nickel plating of the steam system surfaces, which, ironically, was included as a protection against the corrosion of these surfaces, has presented any difficulty. Examination of the plating has shown cracking, flaking, and erosion, particularly in regions of high steam velocity. The report also mentions the possibility that the nickel has contributed to the extensive corrosion-product depositions observed on the fuel plate surfaces.

Further attempts were made to ascertain the corrosive effect of the oxygenated steam on common structural materials by the installation of samples of various such materials in the steam system. The results of these exposures are shown in Fig. IX-11. The data shown do not

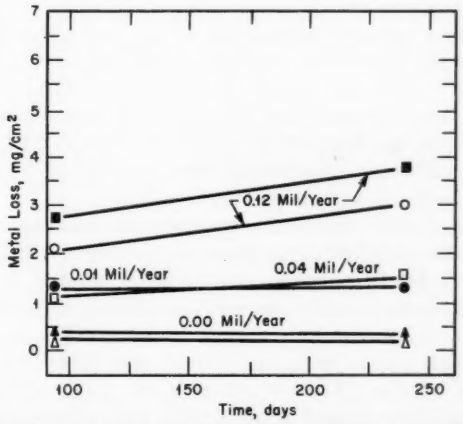

Fig. IX-11 Summary of EBWR steam-line corrosion rates.[3] (1 mil ≈ 20 mg/cm^2). ○, ASTM A-113 structural steel. □, AISI 4140 steel. △, type 403 stainless steel. ●, 1% Cr–0.5% Mo steel. ■, low-carbon steel. ▲, 13% Cr stainless steel (nonhardening).

cover the last month of operation, during which accelerated corrosion and pitting of the low-alloy samples were observed. The report postulates that the change in characteristics may have been caused by the addition of oxygen to the reactor water and/or the submersion of the samples in reactor water for approximately five weeks, both of which occurred immediately preceding the last month of operation.

The radioactive nuclide N^{16} is produced in the core as a result of the fast-neutron interaction with oxygen and is the major contributor to system radioactivity. Approximately 90 per cent of the N^{16} produced is of the anionic species (NO_2^-, NO_3^-) and remains in the water. The remaining 10 per cent is of the cationic (NH_4^+) and neutral (NO, NO_2) species, and the ratio of cationic to neutral species is about 7 to 1. Only these latter two species were observed in the steam. At 20 Mw(t), the total concentration of N^{16} in the steam is less than 1 per cent of the total N^{16} produced

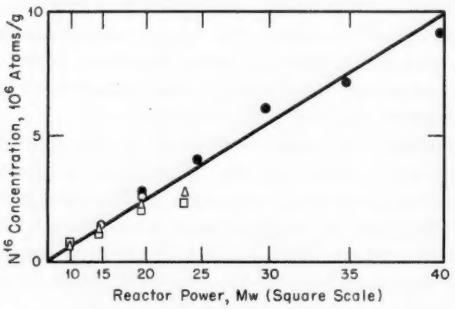

Fig. IX-12 N^{16} concentration in steam 92 in. above fuel at various operating powers and pressures.[3] ●, 600 psi. △, 500 psi. □, 400 psi. ○, 300 psi.

in the reactor. The variation of N^{16} concentration in the steam with power is shown in Fig. IX-12. Some plant activity levels resulting from N^{16} activity are shown in Table IX-3.

A second source of plant radioactivity is found in the radioactive nuclides carried as insoluble particles by primary reactor water, steam, and condensate. This source has proven to be of minor consequence, mainly because of the high steam decontamination factor associated with the boiling process and because the natural-convection design of the EBWR, with an internal downcomer, restricts essentially all the primary water to the reactor vessel proper. Measurements indicate that only about 0.1 per cent of the particulate matter contained in the primary

Table IX-3 EQUIPMENT SURFACE ACTIVITY[3] ATTRIBUTED PRIMARILY TO N^{16}

Location	Activity, mr/hr, for the indicated reactor power			
	10 Mw(t)	20 Mw(t)	40 Mw(t)	61.7 Mw(t)
Air ejector after cooler	90	400	4000	7000
Condenser hot well	10	40	240	580
Steam dryer	80	150	600	720
Turbine exhaust casing	2	4	14	20
Feed-water filters	8	10	50	100
Plant air exhaust	6	12	40	120

water is entrained in the steam and transported through the plant steam and condensate piping. A typical analysis of insolubles in these fluids is shown in Table IX-4.

The contribution to plant activity levels by steam-borne contaminants other than N^{16} is shown in Table IX-5. In contrast, regions containing liquid primary reactor water yield substantially higher readings. Activity levels as high as 50 and 65 r/hr were observed at the lower reactor vessel-head recirculation nozzles and the control-rod-drive-shaft bushings, respectively. It should be noted that these locations are particularly effective in collecting particulate matter. However, the difference in particle concentrations between the steam and water, as exemplified by the resultant activity levels, is significant.

In general, this situation holds true for the vessel internals as well as the external systems. Analyses made of deposits taken from the steam side of the vessel disclosed the predominant element to be iron, with lesser, but significant, amounts of nickel, calcium, and aluminum present. These deposits yielded activities ranging from 75 mr/hr at the top of the vessel to 1 r/hr at a point 6 in. above the top of the core structure. This last location is normally submerged during reactor operation. Washing the smooth surfaces in the steam dome regions with wet rags reduced these levels by 50 to 80 per cent. A similar cleaning treatment of the perforated shock shield was only about 10 per cent effective.

Although all reactor plants may be expected to exhibit some increase in system radioactivity

Table IX-4 SPECTROGRAPHIC ANALYSES OF INSOLUBLES CAUGHT ON MILLIPORE FILTERS[3]

[Values Are in Micrograms per Liter (Parts per Billion); Factor-of-2 Accuracy]

Element	Month and day (1957)	Reactor water			Feed water		Steam	
		S_5*	After prefilter S_6	After ion exchanger S_7	Before filter S_3	After filter S_4	Before dryer S_1	After dryer S_2
Al	6-18	20	16	7.1	1.2	0.3	0.2	1.6
Ca	6-18	0.6	0.3	0.4	0.4	0.1	0.1	0.5
Cu	6-18	1.2	1.1	0.8	0.4	0.1	T†	0.8
Fe	6-18	60	55	20	61	0.9	1.5	9.8
Mn	6-18	0.3	0.3	0.1	0.1	T†	T†	0.6
Na	6-18	0.1	0.6	0.2	0.1	0.1	T†	0.2
Ni	6-18	25	35	10	0.1	0.1	1.6	0.2
Pb	6-18	0.4	0.1	0.3	0.2	0.1	T†	9.8

*Sampling points S_1 through S_7 are shown on Fig. 1 of reference 3. Sampling point S_5 is between the cooler and the prefilter in the ion-exchange loop.

†Trace (<0.1 μg/liter).

Table IX-5 EBWR BUILDING ACTIVITY SURVEY[3]
(March 25, 1960)

	Hard radiation, mr/hr	Distance away, in.
4th Level (Main Floor)		
Background:		
Immediately inside airlock	0.08	
Between turbine and reactor	0.2	
Near storage well	0.17	
Main steam header	0.17	1
Main steam chest	0.11	1
Exhaust hood (max.)	0.14	1
3rd Level (Condenser Floor)		
Background:		
At east stairs	0.5	
At west stairs	0.09	
Opposite air ejectors	0.3	
Steam dryer and emergency cooler	1.3	1
Main steam line from dryer (top)	0.4	1
Relief steam line from dryer (bottom)	0.3	1
Feed-water filter No. 1	1.5	1
Feed-water filter No. 2	9	1
Air ejector after cooler	0.3	1
Air ejector between coolers	0.3	1
Desuperheater (max.)	0.4	1
2nd Level (Pump Floor)		
Line from purification system on reactor face	0.5	1
Startup heater	16	1
Shield cooling manifold	0.4	1
Rod cooling water line under manifold	6	1
Air-ejector discharge line	0.2	1
Air-ejector flowmeter	0.2	1
Twin strainer	0.25	1
Feed-water pump No. 1	0.18	1
Feed-water pump No. 2	7	2
Feed-water pump filter No. 1	7	2
Feed-water pump filter No. 2	7	1
Background:		
Between feed-water pump and face of reactor	0.3	
East stairwell	0.7	
1st Level (Basement)		
Retention tank No. 1	22	2
Retention tank No. 2	20	2
Background:		
West stairwell	2	
East stairwell	0.9	
Prefilter No. 1	18	2
Prefilter No. 2	5	1
Ion exchanger No. 1	21	2
Ion exchanger No. 2	17	2
After filter No. 1	32	2
Regenerative cooler No. 1:		
Left end	100	2
Right end	15	2
Secondary cooler No. 1:		
Left end	310	2
Right end	180	2
Regenerative cooler No. 2:		
Left end	130	2
Right end	20	2
Secondary cooler No. 2:		
Left end	240	2
Right end	100	2

with plant lifetime, the amount of deposition occurring in the EBWR core and on the wetted surfaces of the reactor vessel has been greater than expected. Specifically, extensive corrosion-product depositions, accumulating to form scale as much as 0.008 in. in thickness, have been observed on the heat-transfer surfaces of the fuel plates. The principal effect of this scaling is a reduction in the over-all heat-transfer characteristics of the fuel elements. Moreover, the thick, strongly activated scale has a tendency to flake off and to collect in the control-rod-drive seals and bushings, in the recirculation nozzles, and in other stagnant regions of the pressure vessel, and to result in increased deposits and concentrations of activity in these areas.

A number of reasons may be postulated to explain the type of scaling encountered, the quantity present, and its location. First, in keeping with the experimental role of the EBWR, a number of developmental materials were incorporated in the reactor core and primary systems. Principally, these were the aluminum-nickel alloy used in the dummy fuel assemblies and the Kanigen nickel plating of the steam system. Both of these materials, but particularly the dummy fuel assemblies, have exhibited abnormally high corrosion rates.

Second, one of the better methods for the removal of suspended or entrained solids from water is evaporation. Normally, the residue tends to collect upon the evaporating surface as a scale. This is especially true if the evaporation process is not particularly violent.

Table IX-6 ANALYSIS AND CALCULATED COMPOSITION OF EBWR FUEL-ELEMENT SCALE[3]

Element	Analysis, wt.%	Assumed compound	X-ray identification	Calculated, wt.%
Al	36.3	$Al_2O_3 \cdot H_2O$	Boehmite	80.6
Ni	10.6	NiO	Not identified	12.6
Fe	3.9	Fe_3O_4	Not identified	5.1
Si	0.8	SiO_2	Not identified	1.6
			Total	99.9

A chemical analysis of the scale, shown in Table IX-6, indicates the composition to be about 80 per cent boehmite (α-$Al_2O_3 \cdot H_2O$), with small amounts of nickel, iron, and silica. This is quite similar to the composition of the dummy-assembly corrosion product. As a result of this similarity of corrosion-product composition, and the rate of corrosion exhibited by the dummy assemblies, the report[3] concludes that much of the scaling is caused by the corrosion of the dummy assemblies. Furthermore, since all the conditions conducive to fuel-plate scaling exist, to some degree, in a boiling-water reactor, the observed location of the scale may be a result of these natural processes. This viewpoint is further substantiated by the apparent relation between scale buildup and maximum heat flux or burnup as shown in Fig. IX-13.

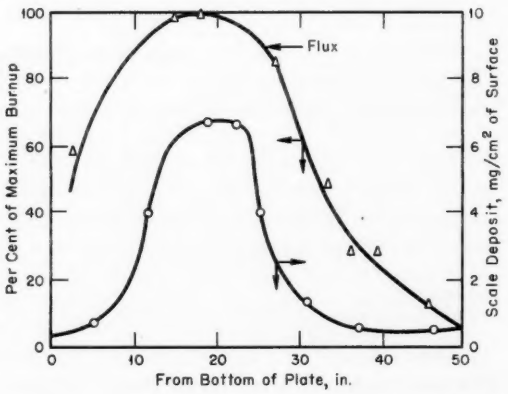

Fig. IX-13 Relation between scale buildup and burnup after operation for about one year.[3] ○, scale buildup. ▲, burnup analysis. Δ, gamma scan small sections.

It seems probable that the severity of the EBWR scaling deposits is a result of the relatively high corrosion rate of the developmental materials used in nonessential applications rather than the result of inherent features of the reactor type.

The effects of these corrosion-product accumulations during past reactor operations have been minor and have been limited to the control-rod drives and to the area immediately beneath the reactor in which the drives are mounted. The primary concern, in this regard, is with the relatively high (500 mr/hr) radiation levels immediately below the ceiling of the control-rod-drive room. The projected operation at 100 Mw(t) presents, operationally speaking, the more serious problem of fuel-element overheating and fuel alloy growth because of the thermal resistance of the scale.

The initial approach to this problem was to determine the thermal conductivity of the scale so that heat-transfer calculations might be performed for the purpose of predicting fuel temperatures. The apparatus used consisted of two copper bars fitted with thermocouples and enclosed within an insulation-filled box. The scale specimen was clamped between the ends of the bars, and a controlled heat flow through the bars and the specimen was obtained by electrically heating the top end of the top bar and by cooling the lower end of the lower bar.

The heat transfer through the scale was measured by comparing the temperature differences along the bars and through the scale specimen. The thermal conductivity determined by this method was 0.44 ± 0.09 Btu/(hr)(ft)(°F). The report contains a detailed description of the apparatus and the procedures used and of the calculational methods employed in making this determination.

By using the measured thermal conductivity of the scale, the fuel-plate centerline temperatures were calculated as functions of scale thickness and reactor power. The 100-Mw(t) power case was calculated for scale thicknesses ranging between 0.002 in. on one plate heat-transfer surface to 0.008 in. on both heat-transfer surfaces. The calculated maximum temperatures corresponding to these two conditions were 864 and 1692°F, respectively. The calculated maximum temperature for the more likely case of 0.004 in. in scale thickness on both surfaces was 1229°F. The report concludes that, on the basis of a 900°F threshold for fuel growth, some permanent fuel-plate distortion is to be expected during operation at the projected increased power level.

In the light of this conclusion, removal of the fuel-plate scale assumes increasing importance. To this end, a number of approaches, both chemical and mechanical, were attempted. The chemical processes consisted mainly of acid-solution baths or slurry treatments and were generally unsuccessful. Chemical treatment capable of removing the scale also removed the Zircaloy-2 cladding with equal facility, thereby rendering the plate unfit for further service.

Attempts to remove the scale by chipping or flaking, either mechanically or thermally, were equally unsuccessful. The thermal approach employed, which was based on weakening the scale-to-plate bond by driving off the water of hydration of the boehmite, was interesting in concept and moderately successful in operation. However, the temperatures required to produce the desired effect (600 to 700°C) resulted in sufficient differential thermal expansion between the fuel plates and the fuel-assembly side plates to cause permanent distortion of the side plates. The mechanical interference between adjacent assemblies and permanent core structure, resulting from this distortion, precluded the reinstallation of these assemblies in the core. The report[3] describes, in detail, the methods and apparatus employed in these experiments and the results of the work.

Leak Testing of Gas-Cooled Reactors

A recent article[4] on leak tests performed on British gas-cooled reactors presents interesting data concerning the adequacies of soap tests and pressure-loss tests for determining leakage rates. Originally, when the Calder Hall plants were designed, construction according to the best steam-plant practices was considered to give satisfactory leakage rates. The first plant, when completed according to these practices, was found to have a leakage rate of about 2 tons of CO_2 per day. By the use of very simple soap tests and by the measurement of internal pressure loss, this leakage rate has been reduced to 600 lb per day for the sixth reactor.

The Calder Hall reactor circuit consists of four primary loops, each complete with its own blower and heat exchanger, connected to one reactor vessel. The volume of this system has been calculated to be 108,000 cu ft.

Two methods were used to locate and establish leakage rates. The leak location was accomplished by a soap test. At room temperature a mixture of 5 parts water and 1 part liquid soap, and at higher temperatures a mixture of 1 part liquid soap and 20 parts glycerine, was painted on the suspected surface after the system was pressurized with air. Leakage was indicated by bubble formation in the soap-mixture coating.

With an internal pressure of 100 psi, leaks of less than 0.01 lb/day were located by experienced personnel using the soap-water mixture. The soap-glycerine mixture is somewhat less sensitive than the soap-water mixture. This test was accompanied by a loss-of-pressure test

Table IX-7 MEASURED LEAKAGE RATES FOR REACTORS OF THE CALDER HALL TYPE[4]

	Leakage, lb/day				
	Calder reactor			Chapelcross reactor	
	2	3	4	1	2
Total air leakage indicated by loss of pressure	2130	885	740	1000	600
Loss by oil sampling	23	17	17	17	17
Measured individual leaks	1240	115	316	270	335
Leakage indicated by pressure-loss tests on individual items	*	175	52	33	36
Air loss not located	867	578	355	680	212
Equivalent to hole diameter (coefficient of discharge 0.7), in.	0.069	0.056	0.044	0.060	0.034

*No tests.

Table IX-8 BREAKDOWN OF LEAKAGE AMONG VARIOUS SOURCES[4]

	Leakage, lb/day				
	Calder reactor			Chapelcross reactor	
	2	3	4	1	2
Relief valve seats	573	40	132	1	16
Other valve seats	468	14	12	43	20
Valve glands	129	48	119	156	231
Flanges, welds, and similar joints	54	13	53	21	47
Others	16			49	21
Total	1240	115	316	270	335

to establish that all major leaks were located since only the most likely leakage points were inspected.

The loss-of-pressure test was accomplished by pressurizing a portion of the system, isolating it, and measuring the decrease of pressure with time. Since the sensitivity of this test varies inversely as the volume of the system checked, the circuits were divided into smaller units by inserting blanking flanges.

An infrared gas analyzer was used to check the heat exchangers. This test consisted of pressurizing the unit with CO_2 and probing the surface with a tube connected to the infrared gas analyzer. The limit of sensitivity was found to be about the same for this test as for the soap test.

During the final check, individual leak rates were measured by various techniques and were compared to the calculated value from the pressure-loss test. Tests on reactor 2 showed that individually measured leaks accounted for 1263 lb/day as compared to a total calculated leakage rate of 2130 lb/day.

Tables IX-7 and IX-8 show the results of tests on five reactors.* Table IX-7 shows the diameter of the single hole which would result in the same total leakage for each reactor.

It is to be noted that the unaccounted loss is always an appreciable portion of the total loss. From additional testing performed on individual circuits, it was concluded that this leakage was due to "seepage" through valve glands, flange joints, etc., which were below the sensitivity of the soap test.

References

1. V. M. Kolba (Comp.), EBWR Test Reports, USAEC Report ANL-6229, Argonne National Laboratory, November 1960.
2. J. M. Harrer et al., Performance Evaluation of Direct Cycle Boiling Water Nuclear Power Plants Based on Recent EBWR and BORAX Data, *Proceedings of the Second United Nations International Conference on the Peaceful Uses of Atomic Energy, Geneva, 1958*, Vol. 9, p. 264, United Nations, New York, 1958.
3. C. R. Breden et al., Water Chemistry and Fuel Element Scale in EBWR, USAEC Report ANL-6136, Argonne National Laboratory, November 1960.
4. J. K. Smith and J. Cheetham, Leak Tests on Calder Type Reactors, *J. Brit. Nuclear Energy Conf.*, 6(1): 62–69 (January 1961).

*Tables IX-7 and IX-8 are reprinted here by permission from the *Journal of the British Nuclear Energy Conference*.[4]

Section X

NUCLEAR SUPERHEAT PROGRAM

In June 1959 the AEC initiated a program to conduct sufficient engineering and development work to determine the most feasible and economical methods of producing nuclear superheated steam from a boiling-water reactor. The following contractors are conducting the various major projects indicated:

Argonne National Laboratory:
- BORAX-V
- In-pile test in EBWR

Atomics International:
- Zirconium hydride moderated integral boiling-superheating reactor

Combustion Engineering, Inc., and General Nuclear Engineering Corporation:
- General research and development
- BONUS Project

General Electric Company's Atomic Power Equipment Department (APED):
- General research and development

Northern States Power Company and Allis-Chalmers Manufacturing Company:
- Pathfinder Project

The progress of these projects has been reported in the progress reports listed in the references at the end of this section. The reactor designs will not be discussed inasmuch as the BONUS, BORAX-V, and Pathfinder projects were previously reviewed, respectively, in the September 1960 issue of *Power Reactor Technology*, Vol. 3, No. 4; the December 1960 issue, Vol. 4, No. 1; and the June 1959 issue, Vol. 2, No. 3.

The use of superheated steam for the generation of electricity in conventional power plants has been common for over 50 years, and its advantages in the turbine system are well known. The generation of superheated steam in a water-cooled reactor involves certain problems and complications whose effects must be balanced against these advantages.

The nuclear superheat program encompasses the superheating of steam by direct passage through the reactor. The reactor may be either a separate steam-cooled reactor (separate superheat reactor) or a reactor that serves the functions of both steam generation and superheating (integral superheat reactor). In both reactor types the obvious problems of providing fuel elements adequate for the high-temperature steam atmosphere exist; and in addition there may be problems, such as the accumulation of deposits on fuel elements, which are related to the process of heating steam, and problems such as turbine contamination, which are connected with the direct-cycle operation. If the reactor is water moderated, there are the additional problems of insulating the high-temperature superheating elements from the liquid moderator and of avoiding the possibility of dangerous reactivity changes caused by the flooding of the superheating elements by liquid water. The problem of effective steam-water separation is also important, since the entrainment of liquid water in the steam fed to the superheating elements is likely to aggravate the problem of deposition. In the integral superheating reactors, the problem of maintaining the proper division of power generation between the boiling regions of the reactor and the superheating regions makes additional demands on the reactor physics design and on the control-element installation.

The work of each of the several nuclear superheat contractors is reviewed in the following sections.

General Electric APED[1–10]

The GE APED program is divided into a number of task areas. The fifth quarterly progress report lists the following:

Task A, Conceptual Design Studies and Program Evaluation
Task B, Fuel Technology
Task C, Material Development
Task D, Experimental Physics
Task E, Corrosion and Coolant Chemistry
Task F, Heat Transfer
Task G, Mechanical Development
Task H, Superheat Advance Demonstration Experiment (SADE)
Task I, Mixed Spectrum Superheater Study (MSS)

The conceptual design studies have centered about both separate and integral superheating reactors. Table X-1 is a summary of the characteristics of a separate superheat reactor (SHR) to be utilized with a boiling-water reactor (BWR) in a plant producing 300 Mw(e). The superheater reactor utilizes a square core configuration employing 52 boxes of 7×7 annular fuel elements. Flow is single pass, with the steam entering the top of the elements from a plenum and progressing to bottom plenums, where it is piped out of the reactor. The individual fuel elements are annular in shape, with steam flowing both in the hole and between the exterior of the fuel element and a stainless-steel liner that defines an annular steam flow passage. The water moderator is insulated from the steel liner by means of a Zircaloy process tube coaxial with the liner and so arranged that a small volume of stagnant steam is trapped between the two. Although resonant (vibrational) compaction is given in the table as the "fuel form," it is stated that pelletizing, combined with swaging or high-temperature isostatic pressing, is being considered for fuel fabrication. Control is achieved by square, box-shaped control rods which "enclose" fuel cells when the rods, or boxes, are raised into the core. To measure power distribution within the core, provisions are made to monitor outlet steam temperatures from the fuel cells and also to monitor neutron flux by means of axial-traversing miniature ionization chambers.

The GE Test Reactor (GETR) is being used to determine whether differential expansion between the oxide fuel and the stainless-steel cladding will produce permanent deformation of the cladding and limit the element lifetime. Annular fuel pellets clad with aluminum or stainless steel have been irradiated in the GETR, yielding heat fluxes from 160,000 to 585,000 Btu/(hr)(sq ft). The effects of varying the diametral and axial clearances between fuel and cladding are being studied. It has been determined that plastic strain cycling of the outer cladding does occur. After plastically deforming the outer cladding, the UO_2, upon cooling, shrinks; a ratcheting effect is present because the shrinkage is less than the expansion. Axial growth has also been noted. Whether these dimensional changes will seriously affect the life of the element has not yet been determined. Other programs have been established to investigate the suitability of zirconium as a process tube material and to produce an insulated (with Al_2O_3) process tube. Another investigation is concerned with the behavior of compacted-powder fuel elements when defects are present in the cladding.

The critical experiment program is concerned entirely with the separate superheater reactor. In general, it consists of critical size and reactivity determinations at different water-to-fuel ratios and with the steam channels both flooded and voided. Measurements are to be made of flux distributions in a single cell as well as over-all. Both triangular and square lattices are to be studied.

An electrically heated superheat corrosion test loop has been constructed to study the behavior of materials in a superheated-steam environment. The apparatus exposes samples of materials to controlled superheat conditions as listed in Table X-2. A somewhat unusual feature of the test loop is an electrolytic decomposition element installed in the subcooled water portion of the loop to generate O_2 and H_2; these gases are, of course, normally present in the operation of a boiling-water reactor. Few data have been reported since the apparatus was but recently put into operation.

Several experimental heat-transfer investigations have been undertaken. The once-through boiling experiment is designed to study the regime between bulk boiling and film boiling, wherein a decrease in the film coefficient is experienced. The purpose behind the experiments is to investigate a "once-through" reactor design in which subcooled water is converted to superheated steam within the individual fuel elements. The basic piece of

Table X-1 SUMMARY OF SEPARATE SUPERHEAT REACTOR DATA[10]

Thermal Power	
Thermal power (to steam), Mw(t)	199.4
Thermal power (to moderator), Mw(t)	15.0
Total thermal power	214.4
Steam Conditions	
Exit steam condition	980 psia, 900°F
Inlet steam condition, psia	1055
BWR steam flow, lb/hr	2,561,000
SHR moderator steam flow, lb/hr	56,000
Total steam flow, lb/hr	2,617,000
Reactor Description	
Reactor vessel:	
Inside diameter, ft	8.33
Inside height, ft	43.43
Wall thickness (base), in.	3¾
Material	¼-in. stainless-steel-clad
Design pressure, psig	1310
Design temp., °F	650
Reactor core:	
Active equivalent diameter, ft	5.83
Active height, ft	7.5
Active core volume, cu ft	201.0
Total uranium loading, kg	10,720
Initial enrichment, %	3.50
Final enrichment, %	1.65
Structural material	Type 304 stainless steel
Neutron moderator	Light water
Moderator-to-fuel ratio	2.60
Reflector:	
Material	Light water
Axial thickness, ft	8
Radial thickness on equivalent diameter, in.	15
Fuel elements:	
Fuel material	UO_2
Fuel-element geometry (annular), in.	0.260 ID, 0.692 OD
Cladding material	Type 304 stainless steel
Fuel meat thickness, in.	0.216
Cladding thickness, in.	0.012
Fuel form	Resonant compacted
Gap filler material	Helium
Fuel assemblies:	
Total number	52
No. of elements per assembly	49
Cross-section assembly, in.	8.65
Process-tube material	Zircaloy-2
Process-tube dimensions, in.	0.932 OD by 0.025 wall
Process-tube insulation	0.008-in. type 304 stainless-steel liner and stagnant steam
Process-tube spacing, in.	1.18
End fitting material	Zircaloy and type 304 stainless steel
Reactor control:	
Method of control	Control-rod movement
Absorber material	Boron steel
No. of control elements	24
Cross-sectional dimensions, sq in.	8.65 by 8.65
Effective length, ft	7.17
Type of drive	Hydraulic locking piston
Performance Data	
Reactor coolant	Steam
Reactor coolant outlet temp., °F	900
Reactor coolant inlet temp., °F	553.5
Steam inlet pressure, psia	1055
Steam outlet pressure, psia	980
Steam coolant flow, lb/hr	2,617,000
Av. core coolant flow, ft/sec (entrance)	89.5
Av. core coolant flow, ft/sec (exit)	167
Max. fuel temp. (125% power), °F	3800
Max. cladding temp., (100% power), °F	1250
Max. core heat flux (125% power), Btu/(hr)(sq ft)	525,000
Av. core heat flux, Btu/(hr)(sq ft)	148,000
Av. core power density, kw/cu ft	1070
Peak-to-average power ratio:	
Axial	1.40
Radial	1.25
Local	1.30
Overpower	1.25
Inside cladding surface/av. cladding surface	1.25
Total	3.54
Av. specific power, kw/kg	20
Fuel management	Fuel batch (20%)
Average fuel burnup, Mwd/metric ton of U	19,800
Peak-to-average burnup ratio	1.77

Table X-2 SUPERHEAT CORROSION-TEST-LOOP OPERATING CONDITIONS[1]

Inlet steam temp., °F	546
Inlet steam pressure, psig	1000
Moisture content, %	0.8
Steam flow, lb/hr	500
Inlet velocity (heater section), ft/sec	86
Outlet velocity (heater section), ft/sec	185
Outlet pressure (heater section), psig	910
Outlet temp. (heater section), °F	1050
Heat flux, Btu/(hr)(sq ft)	175,000

apparatus being used in the study is an electrically heated test section in which a high-quality steam-water mixture can be studied in the transition and film boiling regimes. Another investigation involves the determination of convective heat-transfer coefficients. These experiments will extend the McAdams-Addoms-Kennel and the Heineman correlations (reviewed in the March 1960 issue of *Power Reactor Technology*, Vol. 4, No. 2) to flow and temperature conditions more representative of those found in steam-cooled reactors. Another experiment, concerned with shutdown cooling of superheater elements, is discussed in the heat-transfer section of this issue of *Power Reactor Technology*.

Mechanical development has concentrated on the development of steam-water separators, and steam dryers, or demisters. Also, flow tests on prototype fuel bundles are being done, as well as tests with various methods of holding the elements in the core grid. This latter item is important, since an underwater seal is needed that will ensure a negligible amount of leakage of the moderator water into the superheated-steam regions. The seal must be such that it can operate successfully for the requisite number of fuel-element changes and, probably, remotely.

The SADE loop is a facility incorporated in the Vallecitos Boiling-Water Reactor (VBWR). It has been used to demonstrate the use of superheated steam as a reactor coolant and to provide data on fuel performance. Two experimental steam-cooled elements have been irradiated[4] in SADE, assemblies SH-1 and SH-2. Both elements were made of annular UO_2 pellets of 2.3 per cent enrichment, with a nominal outside diameter of 1.15 in. and a nominal inside diameter of 0.75 in. The pellets were approximately 0.75 in. in length, and the active length of the test element (including two ZrO_2 end, and one center, spacer pellets) was slightly over 3 ft. The inner cladding was fabricated of type 347 stainless steel, whereas the outer cladding was type 304. The element was placed in an uninsulated process tube that defined an annular flow channel for the steam; flow was two-pass: down the annular steam passage and up the center hole. The difference between SH-1 and SH-2 was in the incorporation of a bellows in the outer cladding of the SH-2 element to accommodate differential expansion between the inner and outer claddings. Saturated steam was taken from the VBWR main steam line to cool the element, and an air cooling system was provided to cool the test element during VBWR startup and shutdown. Instrumentation was provided to measure pressure, temperatures, and flow rates. The in-pile loop was inserted in a single channel in the core, replacing a conventional VBWR element, and was piped through a refueling port in the pressure vessel.

The first assembly irradiated was SH-2; the test period was from May 1, 1959, to June 30, 1959. The maximum steam temperature obtained was 825°F (1000 psi), corresponding to approximately 280° of superheat. The integrated maximum fuel exposure was about 550 Mwd/ton. On May 8 the VBWR scrammed due to loss of a-c power; the gasoline-powered auxiliary air compressor failed to operate to provide emergency cooling air flow to the SADE loop, and the test element was forced to cool by radiation of heat to the process tube; it was estimated that the maximum cladding temperature of SH-2 was 1500°F at a position on the inner cladding which presumably corresponded to the region of the axial power peak. Subsequently a rise in the activity level of the stack monitor was noted that was comparable to the stack activity observed previously when purposely defected fuel elements had been tested. The reactor was brought to power, and the loop was operated for six additional weeks with indications that activity was escaping from the test element. After termination of the irradiation of SH-2, the SH-1 element was installed and tested from July 31, 1959, until the VBWR was shut down for modification on Sept. 23, 1959. No indications of cladding failure were present throughout the irradiation of SH-1. Other information about the two test elements is given in Table X-3.

Postirradiation examination revealed that the bellows in SH-2 had experienced a defect in the

Table X-3 INFORMATION ON SH-1 AND SH-2 SADE TEST ELEMENTS[1]

Active fuel length, in.	36 (approx.)
Outer cladding OD, in.	1.25
Inner cladding OD, in.	0.75
Instrument tube OD, in.	0.373
Outer cladding thickness, in.	0.049
Inner cladding thickness, in.	0.035
Pellet OD, in.	1.145 ± 0.003
Pellet ID, in.	0.757 ± 0.003
Cladding material	Type 347 stainless steel
Fuel enrichment, % U^{235}	2.3
UO_2 density, % of theoretical	95
Fuel loading, kg	3
Power output, kw	46
Steam pressure, psi	1000
Steam flow, lb/hr	670
Inlet steam temp., °F	545
Outlet steam temp., °F	825
Max. cladding temp. (first pass), °F	1040
Max. cladding temp. (second pass), °F	1070
Max. heat flux (first pass), Btu/(hr)(sq ft)	192,000
Max. heat flux (second pass), Btu/(hr)(sq ft)	200,000
Max. fuel temp., °F	2080
UO_2 conductivity, Btu/(hr)(ft)(°F)	1.1

form of a crack. Although this had allowed steam to enter the element, and gaseous fission products to escape, the UO_2 was found to be in "good condition"; the fission-gas release rate from the cracked bellows was estimated to be 200 μc/sec. In addition, hairline cracks were found in the type 347 cladding on the fuel side of the tube. Some of these cracks extended more than halfway through the cladding, about 15 mils, and the cracks were randomly spaced around the periphery of the cladding. The reference states that there is, at present, "no explanation" for the occurrence of the cracks other than the possibility that they may have been present initially. The first-steam-pass cladding of SH-2 exhibited a loose, dark corrosion film on the fuel cladding, whereas the second pass surface was bright, with no apparent corrosion film. The three ZrO_2 spacers, which were located at either end and in the middle of the UO_2 pellet stack, were found to have powdered to the extent that the fuel had shifted one pellet length.

Postirradiation examination of SH-1 revealed a black corrosion film on the first-pass heat-transfer surface, whereas the second-pass surface was "bright." Heavy deposits of corrosion products were found in a region where the superheated steam exited the test element, about 5 ft from the bottom of the stack of pellets. These deposits had low activity and were suspected to come from the corrosion of silver parts of the loop. Table X-4 presents the dimensional surveys of two test elements.

From the reactor design data presented in Table X-1, it is evident that the SH-1 and SH-2 tests were conducted under conditions that yielded lower heat flux and lower maximum UO_2 temperature (and burnup) than will be encountered under the reference-design conditions. The results are, nevertheless, useful. A number of other fuel-element concepts, described in reference 11, are being developed for test in the SADE loop.

The MSS is an integral boiler-superheater power reactor. The steam is superheated in an inner, unmoderated (fast) region, and water is boiled in an outer, moderated (thermal) region. The two regions would be separated by "buffer" zones, and steam would flow through steam separators before being piped into the fast superheater. Some of the characteristics of the preliminary design are given in reference 12.

Table X-4 DIMENSIONAL SURVEYS OF TEST ELEMENTS[4]

	SH-2 (bellows type)		SH-1 (no bellows)	
	Preirradiation	Postirradiation	Preirradiation	Postirradiation
Outside diameter, in.	1.250 ± 0.001	1.250 ± 0.002	1.250 ± 0.001	1.250 ± 0.003
Inside diameter, in.	0.677	0.677–0.671	0.677–0.674	0.673–0.665
Warpage in 40-in. fuel length:				
0°		0.016*	0.017	0.015
90°		0.005	0.026	0.010
180°		0.010	0.018	0.006
270°		0.004	0.013	0.004
Length of fuel section, in.			40.609 ± 0.020	40.611 ± 0.010

*Resulted from clamping element during removal of hardware section.

Combustion Engineering–General Nuclear Engineering Corp.[13–20]

The CE-GNEC studies are concerned with the following broad categories of design and development:

1. Development of reference-design criteria for a large boiler-superheater reactor that produces steam at 1050°F and 1200 psig. (The objective of this portion of the work is to establish design criteria based on technology proven and developed under this contract and other Commission-sponsored efforts.)
2. Performance of theoretical and experimental (critical experiments) studies on the peculiar nuclear problems inherent in a boiler-superheater reactor.
3. Development of steam-water separators to accomplish the required degree of separation of steam from water within the reactor pressure vessel before the steam enters the superheater fuel elements.
4. Development of final design criteria for a large boiler-superheater reactor based on results of research and development work performed by all contractors involved in the current AEC nuclear superheat development program.
5. Performance of development work on certain specific problems pertaining to the 17.3-Mw(e) Boiling Nuclear Superheater (BONUS) plant being designed for the AEC by General Nuclear Engineering Corporation.

The reference-design report for the integral boiler-superheater reactor (NUSU) has been issued.[19] The design is based on a fuel element that boils water and superheats steam simultaneously. The element is composed of two annular cylinders of clad UO_2 arranged coaxially. Steam flows in a single pass from the bottom to the top of the reactor, flowing both in the annulus between the cylinders and in the hole at the center of the inner cylinder. The reasons for the simultaneous boiling and superheating are twofold. If boiling is not allowed on the external surface of superheater fuel elements, it is necessary to place a thermal barrier between each of these elements and the surrounding water moderator. This barrier is usually in the form of a stagnant-steam space, bounded on both sides by stainless steel. This parasitic stainless steel has a substantial adverse effect on neutron economy. The insulating gap itself also makes the dissipation of shutdown heat difficult and increases the leakage of neutrons.

A summary of the preliminary reference-design details is given in Table X-5. The reactor is composed of two distinct zones. The inner zone, in the shape of a right circular cylinder, is composed of the boiler-superheater fuel elements just described. Surrounding this is an annular section in which only boiling is accomplished; this section is fueled with stainless-steel-clad rods of UO_2. The necessity for this "pure boiler" section is dictated by thermal considerations; the boiler-superheater zone splits its power approximately equally between boiling and superheating, and since about twice as much power is needed for boiling as for superheating, the additional boiler power must come from the pure boiler section.

The inside diameter of the pressure vessel, 13.9 ft, is dictated by the consideration of limiting the steam velocity in the upper part of the pressure vessel to 1 ft/sec, to ensure good gravitational separation of the moisture. If the development of mechanical steam-water separators were successful, this diameter could probably be reduced to between 11 and 12 ft.

The combination of the annular boiler with the central boiling-superheating zone produces a relatively flat radial power distribution in the boiler-superheater region. Of particular interest in an integral reactor such as this is the change in division of power between the zones as lifetime proceeds. A maximum change in the power-split ratio (power in pure boiler to power in boiler-superheater) of +5.7 per cent at an average burnup of 3000 Mwd per ton of uranium is reported, decreasing to +3.2 per cent at the end of core lifetime (average burnup of 10,600 Mwd per ton of uranium). Although the calculations are preliminary, they are indicative of the stability of the power-sharing process in this type of boiler-superheater reactor.

The use of fuel elements having contact with boiling water on their outside surfaces and with superheated steam on their inside surfaces is accompanied with the following characteristic problem: the fraction of heat transferred to the water increases as the total power output decreases (assuming no steam- or water-temperature changes). Thus, if the reactor is designed to give some outlet steam temperature at full power, and the power in both zones, and

Table X-5 SUMMARY OF NUSU PRELIMINARY REFERENCE DESIGN[19]

General

Reactor type	Thermal neutron, heterogeneous, H_2O moderated
Reactor heat-transfer system	Integral boiler-superheater within pressurized vessel
Location of boiler-superheater region	Central
Location of boiler region	Peripheral
Reactor coolant	Water and steam (H_2O), forced circulation
Reactor fuel	Uranium dioxide (UO_2), slightly enriched
Plant steam cycle	Direct with superheat
Gross electric output, Mw(e)	200
Gross heat output, Mw(t)	518
Thermal power to boiling, Mw(t)	352
Thermal power to superheating, Mw(t)	166
Gross cycle efficiency, %	38.6
Total reactor steam flow, lb/hr	1,610,000
Total reactor water flow:	
lb/hr	23,800,000
gal/min	67,500
Reactor nominal operating pressure, psia	1270
Saturated-steam temp., °F	573
Superheated steam:	
Temp., °F	1050
Pressure, psig	1200
Feed-water temp., °F	450
No. of feed-water heaters	5
Av. steam voids in reactor core water, vol.%	17.38
Core diameter, ft	8.51
Core height, ft	9
Av. core power density, kw(t)/liter	36.4

Reactor Core

	Core region	
	Boiler	Boiler-superheater
Size and geometry of active region	8.51-ft OD; annulus 0.948 ft thick by 9 ft high	6.62 (diam.) by 9 ft (height)
Power transferred to coolant:		
Mw(t)	198	320
Btu/hr	6.72×10^8	10.94×10^8
Saturated steam produced, lb/hr	0.903×10^6	0.707×10^6
Total fuel-cladding heat-transfer surface, sq ft	6806	5240 (superheater) 4100 (boiler)
No. of fuel elements	6690	1159
Av. heat flux, Btu/(hr)(sq ft)	99,200	107,000 (superheater) 130,000 (boiler)
Max. heat flux, with rod followers, Btu/(hr)(sq ft)	374,000	340,000 (superheater) 310,000 (boiler)
Water saturation temp., °F	573	573
Coolant exit temp., °F	573	573 (water) 1060 (steam)

Table X-5 (Continued)

	Core region	
	Boiler	Boiler-superheater
Total water flow to coolant channels:		
lb/hr	13.4×10^6	10.4×10^6
gal/min	38,000	29,500
Av. steam-volume fraction at exit of coolant channels	0.50	0.50
Length of boiling, ft	7.4	7.4
Av. void in coolant water, %	20.6	20.6
Ratio, coolant H_2O to total H_2O	0.85	0.85
Max. fuel-cladding surface temperature with hot-channel factors, °F	655	1250
Water entrance velocity, ft/sec	10.5	6.0
Boiling-side pressure drop, psi	4.7	1.0
Superheating-side pressure drop, psi		51.6
Structural metal within active core	Type 304 stainless steel	Type 347 stainless steel and Inconel X
No. of fuel cells in core cage	30 (hexagonal) and 30 (rhombic)	61 (hexagonal)
No. of fuel assemblies per core cage cell	4	1
Fuel Assembly		
No. of fuel elements	6690	1159
Type of fuel element	Rod	Double annular
Boiler fuel-element dimensions:		
Cladding outside diameter, in.	0.445	
Cladding wall thickness, in.	0.020	
Fuel outside diameter, in.	0.400	
Boiler-superheater fuel-element dimensions (outer fueled annulus):		
Outer cladding OD, in.		1.500
Outer cladding thickness, in.		0.032
Outer cladding material		Type 347 stainless steel
Inner cladding OD, in.		1.000
Inner cladding thickness, in.		0.034
Inner cladding material		Inconel X
Fuel OD, in.		1.426
Fuel thickness, in.		0.209
Inner fueled annulus:		
Outer cladding OD, in.		0.750
Outer cladding thickness, in.		0.018
Outer cladding material		Type 347 stainless steel
Inner cladding OD, in.		0.269
Inner cladding thickness, in.		0.016
Inner cladding material		Type 347 stainless steel
Fuel OD, in.		0.705
Fuel thickness, in.		0.216
Steam coolant cross-section dimensions:		
Annulus thickness, in.		0.091
Hole diameter, in.		0.237
Ratio, volume of UO_2 to volume of cladding	4.7	3.7
Fuel-element pitch spacing, in.	0.620	1.915

Table X-5 (Continued)

Control Rods

No. of control rods	84
Shape	Y
Blade span, center line to blade tip, in.	4.625
Material	2% natural boron in stainless steel
Thickness, in.	0.25
Length of poison section, ft	$8\frac{5}{6}$
Length of follower, ft	$8\frac{1}{6}$
Control-rod channel thickness, in.	0.625
Control-rod drives	Vertical, bottom mounted, rack and pinion

Pressure Vessel

Vessel shape	Cylindrical, hemiellipsoidal bottom head, spherical top head
Vessel wall composition, base metal	Carbon steel, ASTM A302 Grade B
Vessel internal wall cladding	Stainless steel, AISI type 304
Vessel inside diameter, ft	13.896
Vessel over-all height, ft	50
Vessel wall thickness, base metal, in.	7.5
Vessel cladding thickness, in.	0.25
Operating pressure, psig	1300
Operating temp., °F	580
Internal thermal shield	Stainless-steel cylinder, AISI type 304
Internal thermal shield thickness, in.	3
Forced-circulation inlets	Two, $16\frac{1}{8}$-in. ID Two, $14\frac{3}{8}$-in. ID
Forced-circulation outlets	Three, $16\frac{1}{8}$-in. ID Three, $14\frac{3}{8}$-in. ID
Superheated-steam outlet	One, 24-in. ID

Nuclear Characteristics

	Core region	
	Boiler	Boiler-superheater
Fuel elements	Rod	Double-annular
Fuel cell	168-rod cluster	19-element cluster
H_2O-to-UO_2 volume ratio	2.00	1.80
Volume fraction steam channel void		0.07
Av. void fraction, %	17.4	17.4
Av. power density, kw/liter	36.7	36.2
Av. specific power, Mw/ton of U	14.0	13.6
Core life, 80% load factor, years	2.68	2.68
Av. fuel burnup, Mwd/ton of U	10,950	10,637

Table X-5 (Continued)

	Core region	
	Boiler	Boiler-superheater
Initial power split (no control rods), % of total	43.8	56.2
Power split, end-of-life (no control rods), % of total	43.0	57.0
Initial max./av. radial power ratio	1.23	1.03
Initial max./av. axial power ratio	1.90	1.75
Control-rod channel peaking factor	1.32	1.32
Distortion factor*	1.27	1.27
Over-all peaking factor	3.77	2.93
Initial enrichment, % U^{235}	4.7	2.3
Initial conversion ratio	0.444	0.625
Initial power-split ratio, R†	0.7804	
Power-split ratio, at end-of-life	0.7555	
Initial reactivity, hot operating, no poison	1.1041	
Initial reactivity, with burnable poison	1.0240	
Cold clean reactivity, no poison	1.2539	
Reactivity change (Δk):		
Temperature, cold to hot	−0.0780	
Operating void	−0.0364	
Xenon and samarium	−0.0354	
Burnup and operating allowance	−0.1041	
Combined strength of control blades, Δk	0.2188	
Shutdown margin, initial cold clean voided, Δk	−0.0607	
Reactivity in burnable poison, initial (Δk), hot	8.0%	
Reactivity in burnable poison (Δk), cold	9.58%	
Reactivity change on flooding (Δk), hot	−1.00%	
Reactivity change on flooding (Δk), cold	−0.97%	

	Reactivity, $\Delta k/k$	Power split, ΔR†
Coefficients of reactivity and power split:		
Temperature, hot operating	-3.13×10^{-4}/°F	−0.00140/°F
Temperature, cold	-0.212×10^{-4}/°F	
Void, hot operating	-18.99×10^{-4}/% void	−0.0106/% void
Void, cold clean	-12.84×10^{-4}/% void	
Doppler	-1.51×10^{-5}/°F	
Void in boiler region	-14.11×10^{-4}/% void	−0.0245/% void
Void in superheater region	-7.49×10^{-4}/% void	+0.0102/% void

*Distortion factor represents an allowance for control-blade distortion, for burnable poison mismatch, and for shifts in radial maximum-to-average power ratios with fuel burnup.

†R is defined as the ratio of power in the boiler region to power in the superheater region.

the steam flow, are reduced proportionately, then the outlet steam temperature will decrease. There are several possible methods of compensating this effect, including adjustment of feed-water temperature, preferential insertion of control rods in the pure boiling zone, and adjustment of the recirculation ratio.

The reference-design report also discusses alternate fuel-element designs, among them a "heat exchanger" type, consisting of a number of small superheater tubes passing longitudinally through a massive cylinder of jacketed UO_2. Boiling takes place at the outside of the cylindrical element.

The nuclear physics criticality work has been directed toward the BONUS reactor with rod type fuel and toward experimentation with double-annular fuel elements. Double-annular elements have been fabricated for the critical experiments by vibratory compaction. Measurements taken have included criticaltiy and power-distribution data and temperature and flooding coefficients.

The Combustion Engineering corrosion-erosion studies on cladding material are being done in a device called the "steam-purity test loop." This is an electrically heated section operating at the conditions shown in Table X-6.

Table X-6 TEST-SECTION DESIGN PARAMETERS[20]

Inlet pressure, psig	1350
Pressure drop, psi	35
Steam temp., °F:	
Inlet	582
Outlet	1060
Wall temp., (max.), °F	1250
Heat flux (av.), Btu/(hr)(sq ft)	140,000
Mass flow, lb/hr	220
Mass velocity, lb/(hr)(sq ft)	717,500
Velocity, ft/sec:	
Inlet	63
Outlet	125
Reynolds number (av.)	224,000
Internal diameter, in.	0.237
Tube wall thickness, in.	0.040
Tube material	Type 347 stainless steel, ASTM grain, size No. 10
Tube length, in.	108
Ratio of length to diameter	457

Table X-7 TEST-SECTION DATA[20]

(Steam Temperatures After 413 Hr of Operation: Inlet, 582°F Saturated; Outlet, 1060°F)

Coupon* identification	Temp., °F	Corrosion product weight, mg/dm²	Metal† corroded, mg/dm²	Penetration, mils	Penetration‡ per year, mils
1T	730	34.1	23.8	0.012	0.26
2B	760	34.6	24.2	0.012	0.26
3B	820	36.7	25.6	0.013	0.27
4T	880	64.1	44.8	0.022	0.48
5B	920	103.0	72.0	0.035	0.77
6B	970	180.8	126.4	0.062	1.35
7T	1070	286.3	200.2	0.098	
8T	1130	272.6	190.7	0.093	
9B	1150	246.6	172.4	0.085	
10B	1200	294.7	206.1	0.101	
11T	1220	312.8	218.7	0.107	

*T and B refer to the top half and bottom half of the test section, respectively.

†Based on corrosion product being Fe_2O_3.

‡Linear extrapolation. Penetrations have not been tabulated beyond coupon 6B due to the possibility of high erosion at the higher temperature conditions.

The results reported to date represent 413 hr of operation on the first test section and are given in Table X-7. The coupons were cut from the test section at more or less uniform intervals along its length. Although the corrosion rates shown are high, the behavior is typical; corrosion rates are often high at the beginning of a test, decreasing to much lower values as the test proceeds.* The importance of long-time dynamic corrosion tests of various potential cladding materials is great, however, since turbine-condenser contamination could well define the success of the steam-cooled reactor concept.

Steam-water separations are being performed[21] in a device shown in Fig. X-1. The drawing applies to a setup for gravity separation tests with a particular discharge-nozzle design, but it is possible to adapt the apparatus for tests of mechanical separators. Tests are being conducted to evaluate the effect of the submergence of the steam-water nozzle, the effect of the circulation ratio and steam release rate, and pressure.

The various CE-GNEC quarterly progress reports also describe progress related to various research and development tasks being done

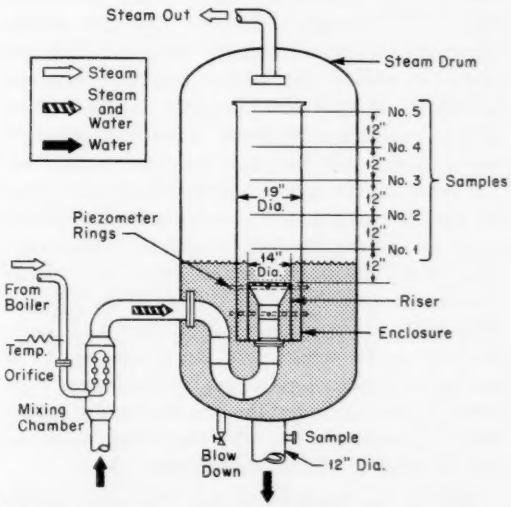

Fig. X-1 High-pressure steam-water gravity separation tests.[21]

for the BONUS reactor. Reference 22 reports on an experiment designed to "flood" an electrically heated BONUS superheater mockup. The experiment was designed to measure this flooding time for various assumed accidental superheat piping ruptures; these data, together with the flooding coefficient of reactivity, would permit the calculation of the reactivity effect

*Data for static and low-velocity steam corrosion of type 347 stainless steel are reported in the following documents: H. A. Pray and W. K. Boyd, Corrosion of Stainless Steels in Supercritical Water, USAEC Report BMI-901, Battelle Memorial Institute, 1954; *Trans. ASME*, 79: 308 (1957).

of such an accident. The results indicate that flooding of the hot superheater tubes can occur only slowly.

Another BONUS report (reference 23) describes tests performed on two alternate control system concepts—a metallic-tape-driven vertical-moving control-rod-drive system and a radial displacement control-element drive system, utilizing swinging arms to support absorber elements or fuel elements that can be moved radially by a drive arm.

Allis-Chalmers[24–54]

Much of the research and development done by Allis-Chalmers under the superheat program is aimed at solving problems peculiar to the Pathfinder integral boiler-superheater reactor, but some programs of more general interest are also under way.

A steam corrosion-erosion loop is being operated by Allis-Chalmers to study the effect of saturated steam (600 psig, 489°F) on stainless steel. Saturated steam flows downward over three sample stations. The top station contains three concentric tubes of different stainless steels; the middle section contains a specimen of type 316 stainless steel; and the bottom contains a duplicate of the middle specimen, except that the steel has been irradiated. The nonradioactive specimens will be examined by weight changes and electrolytic film stripping, and fiberglass filters located downstream will trap eroded material from the active sample for counting. Comparison of the counting data with an experimentally determined calibration curve would give the gross weight of corrosion product collected by the filter. Provisions are made for the introduction of moisture and oxygen in the saturated steam to simulate various in-pile environments.

One of the changes in the reference design for Pathfinder has been the substitution of Zircaloy-2 for aluminum for the boiler fuel-element cladding material. The concept of axially varying metal-to-water ratio has been retained, however, in that the fuel-rod diameter is reduced in the upper half of the boiler core. Fabrication of the high-enrichment prototype superheater fuel elements, of UO_2–stainless steel cermet, is continuing, and work has been initiated on the development of a low-enrichment superheater element for the third Pathfinder core (1963). These elements would be stainless-steel-clad UO_2 rods, and the basic cell would be a seven-pin cluster of the rods. Both pelletizing and swage-compaction are being studied as possible fabrication techniques.

The superheater control-rod design has been modified also. Instead of the cruciform control rods operating in the water moderator as discussed in the earlier reports, the superheater control will be accomplished by tubular control rods. These rods will operate in a steam environment, and 13 rods will be ganged to form a single cruciform bundle. The rods are contained in double-wall process tubes similar to the fuel-element process tubes.

The steam-separation methods have been discussed in recent ACNP progress reports. In the Pathfinder reactor the steam separators are located in the downcomer and serve the purpose of removing entrained steam from the recirculating water by centrifugal force. Steam dryers are also incorporated in the reactor in the upper portion of the steam dome above the core. These are mesh type devices, inclined 15° from the horizontal, and are expected to provide steam of at least 99.9 per cent quality. Before selecting the mesh type dryers, two types of centrifugal dryers were tested, but they did not make as efficient use of the available reactor cross-sectional area as did the mesh. Gravitational separation was also studied; Fig. X-2 shows the effect of the steam release rate on the entrained moisture and indicates the "break point" for various pressures and mass rates. If a reactor is designed to operate below the break point, very little mechanical separation is necessary.

Argonne National Laboratory[55–57]

Argonne National Laboratory is conducting an extensive series of tests on the gravity separation of steam and water. These will be accomplished on three different experimental facilities:

1. Within the EBWR.
2. On an atmospheric air-water loop.
3. On a 2000-psi test loop.

The EBWR is being equipped with a number of probes to measure carryunder (steam entrainment in the downcomer), vapor holdup above the riser, riser voids, carryover (entrainment), and interface height. The air-water loop is

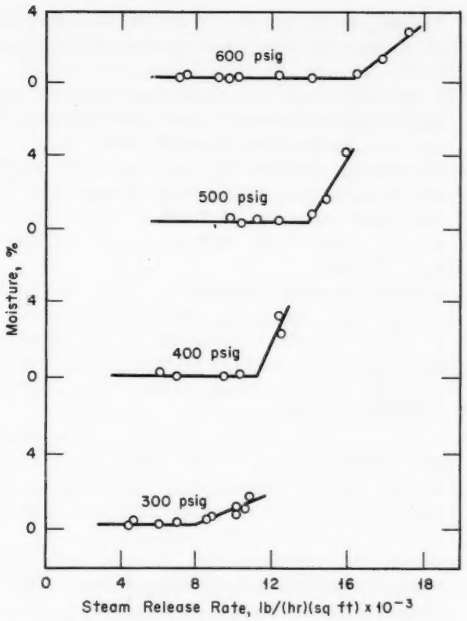

Fig. X-2 Moisture entrained 33 in. above interface in a 19-in.-diameter test section.[54]

designed to obtain data on riser gas fraction and downcomer gas fraction. The high-pressure test loop is designed to operate at pressures between 600 and 2000 psi, with steam-dome vapor velocities of 0.25 to 4 ft/sec and with disengagement heights from 10 to 30 in. Preliminary data have been obtained from the atmospheric loop with the remaining facilities scheduled for operation by mid-1961.

Much of the development work is being carried out in support of BORAX-V. For example, the natural-circulation performance, burnout, and stability of BORAX-V have been studied in an electrically heated test section designed to mock up the boiler core as closely as possible, but containing only two parallel, heated rods in the test section. (BORAX-V has 49 rods per boiler assembly.) Seals are also being studied since BORAX-V requires a seal between the bottom of the superheater fuel elements and the interpass plenum.

At the third nuclear superheat meeting,[58] ANL presented a design for an integral, coupled fast-thermal boiler-superheater reactor having a breeding ratio of 1.4. This concept is similar in some respects to the General Electric mixed-spectrum integral reactor, but it was designed specifically for breeding, and no boiling is done in the core. The core consists of an internal fast superheater region surrounded by a thermal pressurized-water region; the two are separated by a radial buffer zone. Above and below both fast and thermal regions are axial fuel blankets, and a radial blanket surrounds the thermal core. The reactor produces most of its power in the fast, steam-cooled core to attain a high breeding ratio. Some of the superheated steam is used to generate saturated steam by mixing with feed water in a vessel outside the reactor.

Atomics International

Atomics International studied the use of zirconium hydride as a solid moderator for an integral boiler-superheater reactor. The reference design consisted of a centrally located superheater composed of 45 moderator logs of zirconium hydride. Each log contained 16 fuel bundles composed of seven rods of stainless-steel-clad UO_2 per bundle. A Zircaloy-2-clad boiler surrounded the superheater region. The study indicated that the capital cost of the moderator logs added about $3,330,000 to the cost of a similar water-moderated process-tube integral reactor and that no economic incentive exists for the concept.

References

1. R. T. Pennington, Nuclear Superheat Project, First Quarterly Progress Report, July to September 1959, USAEC Report GEAP-3290, General Electric Co., Atomic Power Equipment Dept., Dec. 1, 1959.
2. E. Janssen, Superheat Process Tube Heat Transfer Tests, Nuclear Superheat Project, USAEC Report GEAP-3319, General Electric Co., Atomic Power Equipment Dept., Jan, 5, 1960.
3. General Electric Co., Atomic Power Equipment Dept., Nuclear Superheat Project, Second Quarterly Progress Report, October to December 1959, USAEC Report GEAP-3371, September 1960.
4. E. A. Lees et al., Nuclear Superheat Project, Fabrication, Irradiation, and Evaluation of Superheat Fuel Element SH-1 and SH-2, USAEC Report GEAP-3387, General Electric Co., Atomic Power Equipment Dept., Apr. 7, 1960.
5. General Electric Co., Atomic Power Equipment Dept., Final Report, COO, Steam Separation Program, February to March 1960, USAEC Report GEAP-3389, 1960.
6. R. T. Pennington, Nuclear Superheat Project,

Third Quarterly Progress Report, January to March 1960, USAEC Report GEAP-3468, General Electric Co., Atomic Power Equipment Dept., July 1, 1960.
7. R. T. Pennington, Nuclear Superheat Project, Fourth Quarterly Progress Report, April to June 1960, USAEC Report GEAP-3538, General Electric Co., Atomic Power Equipment Dept., 1960.
8. J. I. Riesland, Nuclear Superheat Project, Interim Report on Steam Dryer Development, USAEC Report GEAP-3563, General Electric Co., Atomic Power Equipment Dept., 1961.
9. H. D. Ongman and A. G. Steamer, Interim Report, Results of Air-Water and Steam-Water Tests on Primary Steam Separators, USAEC Report GEAP-3564, General Electric Co., Atomic Power Equipment Dept., Oct. 7, 1960.
10. General Electric Co., Atomic Power Equipment Dept., Nuclear Superheat Project, Fifth Quarterly Progress Report, July to September 1960, USAEC Report GEAP-3581, 1960.
11. Chicago Operations Office, Nuclear Superheat Meeting No. 1, September 21 to 23, 1959, USAEC Report TID-7595, Nov. 3, 1959.
12. Chicago Operations Office, Nuclear Superheat Meeting No. 2, April 7 and 8, 1960, USAEC Report TID-7596, June 30, 1960.
13. Combustion Engineering, Inc., and General Nuclear Engineering Corp., Nuclear Superheat Development Program, First Quarterly Progress Report for July to September 1959, USAEC Report GNEC-118, 1960.
14. Combustion Engineering, Inc., and General Nuclear Engineering Corp., Nuclear Superheat Development Program, Second Quarterly Progress Report for October to December 1959, USAEC Report GNEC-125, 1960.
15. Combustion Engineering, Inc., and General Nuclear Engineering Corp., Nuclear Superheat Development Program, Third Quarterly Progress Report for January to March 1960, USAEC Report GNEC-131, September 1960.
16. R. W. Deutsch, Method for Analyzing Low-Enrichment Light-Water Cores, Supplementary Study Related to BONUS and Large Nuclear Superheat Programs, USAEC Report GNEC-133, General Nuclear Engineering Corp., Oct. 5, 1960.
17. Combustion Engineering, Inc., and General Nuclear Engineering Corp., Nuclear Superheat Development Program, Fourth Quarterly Progress Report, April to June 1960, USAEC Report GNEC-138, November 1960.
18. Combustion Engineering, Inc., and General Nuclear Engineering Corp., Nuclear Superheat Development Program, Fifth Quarterly Progress Report, July to September 1960, USAEC Report GNEC-149, 1960.
19. Combustion Engineering, Inc., and General Nuclear Engineering Corp., A 200-Mw(e) Boiler-Superheater Reactor Preliminary Design, Preliminary Reference Design for the AEC Program on Nuclear Superheat Development, USAEC Report GNEC-136, Oct. 25, 1960.
20. V. C. Hall, Jr., et al., NUSU Steam Purity Tests, USAEC Report CEND-117, Combustion Engineering, Inc., Nuclear Div., January 1961.
21. Combustion Engineering, Inc., and General Nuclear Engineering Corp., Nuclear Superheat Development Program, Monthly Technical Report No. 21, March 1961, USAEC Report GNEC-170, Apr. 10, 1961.
22. General Nuclear Engineering Corp., Water Injection Test Simulating Moderator Flooding of BONUS Superheater Assembly, Terminal Report Under Activity No. 50-00-00, Heat-Transfer Tests Simulating Loss of Coolant, USAEC Report GNEC-156, Feb. 15, 1961.
23. General Nuclear Engineering Corp., Tape Drive and Radial Drive Control Systems, Terminal Report Under Activity No. 70-00-00, Control Development, USAEC Report GNEC-155, Feb. 27, 1961.
24. Martin Co., Nuclear Div., Coated Particle Investigation, Final Summary Report, Vol. 1, USAEC Report MND-AC-1755-1, April 1959.
25. Allis-Chalmers Mfg. Co., Pathfinder Atomic Power Plant, Technical Progress Report for April 1, 1958 to June 30, 1958, USAEC Report AECU-3782, June 30, 1958.
26. Allis-Chalmers Mfg. Co., 1957. (Unpublished)
27. Allis-Chalmers Mfg. Co., Pathfinder Atomic Power Plant, Technical Progress Report for August 1957 to March 1958, USAEC Report AECU-3683, Mar. 31, 1958.
28. Allis-Chalmers Mfg. Co., 1959. (Unpublished)
29. Allis-Chalmers Mfg. Co., Nuclear Superheater for a Controlled Recirculation Boiling Reactor, USAEC Report AECU-3704, May 9, 1958.
30. Allis-Chalmers Mfg. Co., Allis-Chalmers Critical Facility, Preliminary Safeguards Report, USAEC Report ACNP-5809, 1958 (superseded by ACNP-5910).
31. Allis-Chalmers Mfg. Co., Pathfinder Atomic Power Plant, Technical Progress Report for April 1958 to June 1958, USAEC Report AECU-3782, June 30, 1958.
32. Allis-Chalmers Mfg. Co., Pathfinder Atomic Power Plant, Technical Progress Report for July 1958 to September 1958, USAEC Report AECU-3910, Oct. 15, 1958.
33. Allis-Chalmers Mfg. Co., Pathfinder Atomic Power Plant, Technical Progress Report for October 1958 to December 1958, USAEC Report ACNP-5904, Mar. 1, 1959.
34. Allis-Chalmers Mfg. Co., Pathfinder Atomic Power Plant, Safeguards Report, USAEC Report ACNP-5905, Mar. 10, 1959.
35. Allis-Chalmers Mfg. Co., 1960. (Unpublished)
36. Allis-Chalmers Mfg. Co. (Unpublished)
37. Allis-Chalmers Mfg. Co., Pathfinder Atomic

Power Plant, Technical Progress Report for January 1959 to March 1959, USAEC Report ACNP-5909, May 1, 1959.

38. Allis-Chalmers Mfg. Co., Allis-Chalmers Critical Facility, Final Safeguards Report, USAEC Report ACNP-5910, May 1, 1959.
39. R. Corcoran et al., Pathfinder Atomic Power Plant, Radiation Shielding Study, USAEC Report ACNP-5912, Allis-Chalmers Mfg. Co., June 22, 1959.
40. Allis-Chalmers Mfg. Co., Pathfinder Atomic Power Plant, Technical Progress Report for April 1959 to June 1959, USAEC Report ACNP-5915, Aug. 15, 1959.
41. M. Armando et al., Pathfinder Atomic Power Plant, Study of Liquid and Solid Waste Disposal Requirements, USAEC Report ACNP-5916, Allis-Chalmers Mfg. Co., July 20, 1959.
42. Allis-Chalmers Mfg. Co., Pathfinder Atomic Power Plant, Final Feasibility Report, Boiling Water Reactor with Internal Superheater, USAEC Report ACNP-5917, Aug. 31, 1959.
43. A. Jacobs and R. H. Vollmer, Pathfinder Atomic Power Plant, Measurements of Nuclear Parameters of Boiler and Superheater Lattices, USAEC Report ACNP-5918, Pennsylvania State University and Allis-Chalmers Mfg. Co., Aug. 31, 1959.
44. J. Wilson and R. Styles, Pathfinder Atomic Power Plant, Final Report, Coolant Distribution Tests, USAEC Report ACNP-5920, Allis-Chalmers Mfg. Co., Nov. 15, 1959.
45. J. Wilson and M. McDermott, Pathfinder Atomic Power Plant, Final Report, Moisture De-Entrainment Tests in Two- and Four-Inch Diameter Test Sections, USAEC Report ACNP-5921, Allis-Chalmers Mfg. Co., Nov. 15, 1959.
46. R. G. Michel, Pathfinder Atomic Power Plant, Final Report, Conceptual Design Study of CRBR Quick-Operating Pressure Vessel Closure and Self-Energizing Seal Tests, USAEC Report ACNP-5922, Allis-Chalmers Mfg. Co., Oct. 15, 1959.
47. Allis-Chalmers Mfg. Co., Pathfinder Atomic Power Plant, Technical Progress Report, July 1959 to September 1959, USAEC Report ACNP-5924, Nov. 15, 1959.
48. Allis-Chalmers Mfg. Co., Pathfinder Atomic Power Plant, Technical Progress Report, October 1959 to December 1959, USAEC Report ACNP-6001, Mar. 15, 1960.
49. Allis-Chalmers Mfg. Co., Pathfinder Atomic Power Plant, Coated Particle Investigation, Final Summary Report, USAEC Report ACNP-6002, Mar. 30, 1960. (See also reference 24.)
50. J. T. Stone et al., Pathfinder Atomic Power Plant, Interim Progress Report of Reactor System Dynamic Analysis with Pathfinder Transient Simulator, USAEC Report ACNP-6005, Allis-Chalmers Mfg. Co., Mar. 15, 1960.
51. Allis-Chalmers Mfg. Co., Pathfinder Atomic Power Plant, Technical Progress Report, January 1960 to March 1960, USAEC Report ACNP-6006, June 15, 1960.
52. Allis-Chalmers Mfg. Co., Pathfinder Atomic Power Plant, Technical Progress Report, April 1960 to June 1960, USAEC Report ACNP-6007, Oct. 15, 1960.
53. E. E. Mason and W. M. Chmielewski, Pathfinder Atomic Power Plant, IBM-704 Program for Reactor Containment, Pressure Suppression Analysis, USAEC Report ACNP-6008, Allis-Chalmers Mfg. Co., July 15, 1960.
54. Allis-Chalmers Mfg. Co., Pathfinder Atomic Power Plant, Technical Progress Report, July 1960 to September 1960, USAEC Report ACNP-6012, Jan. 5, 1961.
55. E. S. Nowak and R. J. Grosh, An Investigation of Certain Thermodynamic and Transport Properties of Water and Water Vapor in the Critical Region, USAEC Report ANL-6064, Purdue Research Foundation, October 1958.
56. Argonne National Laboratory, Preliminary Design and Hazards Report, Boiling Reactor Experiment V (BORAX-V), USAEC Report ANL-6120, February 1960.
57. J. B. Heineman, An Experimental Investigation of Heat Transfer to Superheated Steam in Round and Rectangular Channels, USAEC Report ANL-6213, Argonne National Laboratory, September 1960.
58. A. Mravca, Nuclear Superheat Meeting No. 3, October 13 and 14, 1960, USAEC Report TID-7609, Nov. 10, 1960.

Section XI

CORE FOR A MARINE BOILING-WATER REACTOR

Reference 1 is a design summary report on the core of the direct-cycle boiling-water reactor studied by General Electric[2] for tanker propulsion. The reactor is of interest because of its unusual core design and because the application of a natural-circulation boiling-water reactor to ship propulsion involves some questions as to reactor stability. With regard to the latter point, reference 1 states that a study of the effects of ship's motion has been in progress at General Electric since the spring of 1958 and that, in April 1959, a more comprehensive study of the problem was undertaken for the AEC. The work was scheduled to continue into 1961. The reference states also that results of the investigations are incorporated into the design of the core. The report does not, however, discuss any general results of the investigation, which would be of considerable interest to all designers of boiling-water reactors. Reference 3 does present some of the analytical and analogue work done as part of the study, based on a model in which the reactor is represented by two parallel reactors coupled hydraulically and by the neutron flux.

The reactor in this design study provides 30,000 SHP for a tanker of 40,000 dead-weight tons. It produces 78 Mw(t), which yields 275,000 lb of 1000-psi steam per hour. It employs internal natural circulation with light water as the moderator coolant. Steam separation occurs above the free surface in the pressure vessel, and steam passes through a drying assembly in the pressure vessel and then directly to the turbines.

The basic core structure consists of an egg-crate structure fabricated of Zircaloy sheets (0.109 in. thick) supported by a stainless-steel bottom-support grid. The structure is fabricated by fitting the Zircaloy sheets into longitudinally slotted Zircaloy corner posts at each corner of the 10.25-in.-square egg-crate cells (Fig. XI-1). Each of the cells contains two fuel assemblies, each of which has the shape of a rectangle with two of the corners chopped off

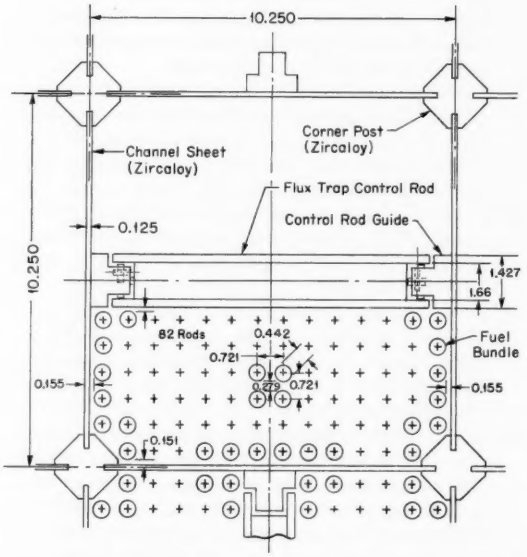

Fig. XI-1 Cell of the boiling-water core for a tanker.[1] Dimensions are in inches.

to make room for the corner posts of the egg-crate structure. The fuel assemblies are of the open (unshrouded) type, each containing 82 stainless-steel-clad UO_2 rods of 0.442 in. outside diameter and 64 in. length. The rods are arranged in a 6×14 array with two corner rods removed. When two assemblies are installed in one of the egg-crate cells, a slot approximately $1\frac{1}{2}$ in. wide is left between the two. The control rod moves in this slot, guided by channel sections attached to the egg-crate

structure which make internal contact, through rollers, with the control-rod structure. The total core consists of 21 of the egg-crate cells arranged in a 5×5 array with the corners removed and of four half cells, one in each of the vacant corner locations. Above the core, a mating egg crate fabricated of stainless steel forms chimneys to promote the natural circulation of the coolant. Each of the 21 control rods consists of a box section of boron steel with a 1-in.-thick interior water space. Extension of the side plates beyond the sides of the box forms 1-in.-thick channels on the narrow sides of the rod. These channels fit over the roller-equipped guides attached to opposite walls of the egg-crate cell (Fig. XI-1). The boron-steel-water segment of the rod is 58 in. long, and its upper end is attached to a "follower" of the same cross section, consisting of a Zircaloy box section packed with sintered aluminum oxide blocks. When the water-filled poison section is withdrawn downward from the core, the space between fuel elements is filled with the Zircaloy–aluminum oxide follower.

The effectiveness of the water-filled control rod is well known, and it has been used in the past, notably in the MTR and in the APPR type reactors. In those applications the follower consisted of a fueled section. The inert follower used in the tanker reactor appears to be simpler, although it does leave some absorber in the reactor core after the highly absorbing section has been withdrawn. This is probably not very important in a stainless-steel core.

The analysis of the reactor core performance indicates a very favorable local power peaking factor: the calculation on the nominal design gives a local factor of 1.01, and increasing the tolerances to give an additional 100-mil water gap results in a calculated local factor of 1.14. As in all H_2O-moderated reactor designs, the local peaking is a very sensitive function of the clearances and tolerances around fuel assemblies and control rods, and the accuracy of predicting the local peaking factor depends on an accurate evaluation of these mechanical characteristics.

References

1. J. R. Birle, Summary Design Report. The Flux-Trap Core for a Marine Boiling Water Reactor in the T-7 Tanker, USAEC Report GEAP-3476, General Electric Co., Atomic Power Equipment Dept., July 15, 1960.
2. General Electric Co., Atomic Power Equipment Dept., Nuclear Powered Tanker Design and Economic Analysis, Direct Cycle Boiling Water Reactor, USAEC Report GEAP-3294, Dec. 15, 1959.
3. J. M. Case, Neutron and Parallel Flow Channel Coupling Effects on the T-7 Flux Trap Reactor, USAEC Report GEAP-3508, General Electric Co., Atomic Power Equipment Dept., Aug. 15, 1960.

Section XII

SODIUM GRAPHITE REACTORS

A number of reports have been published during the past year which summarize the results of design studies on sodium graphite reactors and which may point the direction for the future development of that reactor type.

Reference 1 is a study of the physics and thermal characteristics of three different sodium graphite reactor concepts and of the relation of these characteristics to the relative costs of power from reactors of the three different types. The differences in concept have to do with the method of separating the coolant sodium from the graphite moderator. The methods considered are (1) canning of individual blocks of the graphite moderator, (2) a calandria arrangement wherein the coolant is contained within the calandria tubes, and (3) a thimble arrangement wherein the fuel resides in thimbles which enter the graphite region from the top and wherein the coolant, entering and leaving from the top, makes a double pass within the thimble.

The active portion of the fuel element is the same for all three concepts. Each element consists of two coaxial tubes, each made up of a stack of uranium oxide rings jacketed inside and outside with stainless steel. The larger of the two fuel annuli is apparently about $2\frac{1}{2}$ in. in outside diameter. Coolant flows over all four jacket surfaces of the complete element. The study was made for a reactor of 100 Mw(e) net output, with a sodium inlet temperature of 630°F and an outlet temperature of 1000°F.

The canned-moderator concept employs hexagonal graphite blocks of full reactor length, individually canned in 16-mil, type 304 stainless steel. The corners of the hexagonal blocks are scalloped in such a way that a circular coolant-flow channel is left open at the corners where three of the close-packed hexagonal blocks meet. Zircaloy-2 process tubes are installed in these channels. The double-annular fuel elements, of full core length, are installed in the process tubes, and cooling is maintained by flow of sodium over all surfaces in parallel.

In the calandria design the steel calandria tubes, which constitute the process tubes, are arranged on a hexagonal lattice and pass through central holes in the hexagonal graphite moderator blocks. The holes in the graphite blocks are lined with thin-walled zirconium tubes so that any possible sodium leakage from the process tube will be segregated from the graphite and will flow to a sump at the bottom of the calandria tank, whence it can be pumped out. A shroud arrangement at the top of the core is used to protect the graphite from any sodium that might enter from the top. The process tubes are fixed at the bottom of the tank and are provided with bellows at the top to allow for thermal expansion.

In the thimble design the thimbles penetrate through central holes in hexagonal graphite blocks; at the top of the structure the thimbles penetrate flat circular inlet and outlet tanks, the outlet tank being arranged above the inlet tank. The thimbles are permanently fixed in the inlet and outlet tanks, and the double-annular fuel elements simply hang in the thimbles. The coolant enters the annular space between the outside fuel tube and the wall of the thimble, flows downward through this space, and, at the bottom, enters the annulus between the two fuel tubes and the central hole of the inner fuel tube, flowing in parallel through these two passages. Because the outer jacket of the larger fuel tube is cooled by cool inlet sodium, whereas the inner jacket is cooled by the heated sodium in its second pass, it is considered necessary to provide a bellows in the fuel cladding to allow for differential thermal expansion.

The differences in thermal performance of the three designs, for a given lattice spacing, led to some differences in reactor size to produce the required power output. These differences resulted in capital cost differences; however, the capital cost differences were relatively small. The differences in amount of absorber material associated with each process tube led to differences in neutron economy and consequent differences in fuel costs. The fuel cost differences were substantial: for a fixed reactor diameter of 14.5 ft with lattice spacing adjusted to give the same power output for all reactors, the fuel cost was approximately 0.22 mill/kw-hr lower for the thimble design than for the canned-moderator design and was approximately 0.75 mill/kw-hr lower for the calandria design than for the canned-moderator design. The differences in total power cost were nearly the same.

Since the economic performance of the calandria design was best, the calandria was judged to be the most attractive of the three concepts studied. A summary of the advantages and disadvantages of the three concepts is quoted[1] below:

CANNED-MODERATOR CONCEPT

Advantages. Individual containment of small sections of the moderator facilitates installation and replacement, if necessary, of the moderator. To avoid complication of removing the loading face shield for moderator removal, it is necessary to provide for rotation of the shield. Rotatability adds considerably to the cost of the top shield.

Only a relatively small portion of the graphite moderator is saturated with sodium in case of cladding failure.

Feasibility of the design has been proven by construction and operation of the SRE.

Disadvantages. Graphite-cladding introduces neutron poisons into core and decreases neutron economy.

Probability of failure of moderator containment is highest because of large surface area exposed to sodium, and relative thinness of canning material. Because of the geometry of moderator cans, stress relief (such as through use of a bellows) is difficult. Thermal gradients and transients can lead to buckling and cracking of cladding material.

Variation of lattice spacing in a core is difficult.

THIMBLE CONCEPT

Advantages. Cladding and structural material in core region is minimized, improving neutron economy and reducing fuel costs.

Small sodium leaks into moderator region can be tolerated.

Variation of lattice spacing in the core is feasible.

Disadvantages. Double-plenum tanks in which process tubes are installed present fabrication and installation problems.

Natural convection cooling of the fuel elements is difficult to achieve. Removal of decay heat would be more difficult in case of loss of coolant pumping.

A major rupture of thimble or plenum tank would necessitate replacement of the entire core. This would be a major undertaking, requiring the removal of both coolant plenums.

Provision for differential thermal expansion of fuel element cladding is necessary because of difference in coolant temperature on inner and outer surfaces.

Pressure drop through core is considerably increased by double pass of coolant. Pumping power is therefore increased. Power density in fuel may be limited by core pressure drop, and freedom is restricted in selection of fuel element geometry.

Graphite temperatures are high since the only means for heat removal is by conduction to the thimble. This leads to impairment of neutron economy, since neutron yield from U^{235} and Pu^{239} decreases with temperature.

CALANDRIA CONCEPT

Advantages. Structural and cladding material in core is minimized—highest neutron economy—lowest fuel-cycle costs.

Small sodium leaks into moderator region can be tolerated.

Variation of lattice spacing in core is feasible.

Disadvantages. A major rupture in calandria tube or moderator containment vessel would require replacement of calandria. This would necessitate removal of loading face shield and a rather heavy and bulky calandria.

Provision for differential thermal expansion of each calandria tube is required.

Graphite temperature is high, reducing the potential gains in neutron economy.

References 2 and 3 are design and power cost studies for large sodium graphite plants of "current" and "advanced" technologies. In reference 4 the power cost estimates are made in accordance with the methods specified for the AEC Ten-Year Reactor Program study.

The "current technology" design employs the canned-graphite concept and uranium-molybdenum alloy fuel. The graphite moderator elements are hexagonal in cross section, 22.35 in. across flats. Each hexagonal element contains an axial hole for a process tube, and each

face of the hexagon contains a longitudinal semicircular channel which, in conjunction with the similar channel on the adjacent moderator element, forms another process tube. Four process tubes are thus associated with each modeator element. The elements are 19 ft high, and each is made up of three graphite logs stacked vertically and keyed together with cylindrical graphite plugs. Each moderator element is canned in a 0.016-in.-thick stainless-steel skin, which is welded to ½-in.-thick top and bottom heads.

The full-core-length fuel assemblies are clusters of 61 fuel rods. The fuel rods consist of uranium–10 wt.% molybdenum alloy rods, 0.330 in. in diameter, jacketed in stainless steel, with a sodium bond. The rods are approximately 17 ft long, with the lower 15 ft containing the fuel slugs and the remaining 2 ft providing space for expansion and fission gases.

The reactor core with its surrounding graphite reflector forms a right cylinder, 19½ ft in diameter and 19 ft high. The reactor is controlled by 18 shim-safety rods which operate in thimbles in process channels and which are cooled by sodium convection.

The reactor vessel is fabricated of stainless steel. Sodium enters the bottom of the vessel, flows upward through the core, and forms a pool 14 ft deep above the top of the core. It leaves the vessel through pipes which have their nozzles above the core level and flows to the four sets of intermediate heat exchangers, which are located in separate cells.

A two-region core loading is used; fuel in the inner region is enriched to 3.5 at.%, and fuel in the outer region is enriched to 4.0 at.%. The average fuel exposure attainable with this loading is about 13,000 Mwd per metric ton of uranium, and the initial conversion ratio is 0.47.

The station utilizes a 300-Mw(e), cross-compound, three-cyclinder, double-flow, reheat, condensing turbine-generator unit. It is rated at 300 Mw(e) at 3½ in. Hg backpressure, and its capability is 320 Mw(e) at 1½ in. Hg backpressure. Seven extraction openings are utilized, six for feed-water heat and one for the turbine drives on the boiler feed pumps.

The reactor coolant system employs four primary heat-transfer loops, each with its own 18,000 gal/min vertical centrifugal pump, four sets of intermediate heat exchangers (two each), and four secondary loops, each serving a steam generator and a superheater. Steam is generated at 1250 psi and 850°F and is reheated to 850°F at a pressure of 230 psia.

The "advanced technology" design utilizes the calandria concept and a "submerged" primary system reminiscent of the EBR-II arrangement. The graphite moderator is in the form of graphite logs, 9.91 in. across flats and 16 ft long. Each log is penetrated, on its axis, by one of the calandria tubes. The entire calandria vessel, 16.5 ft in diameter by 19 ft high, is submerged in sodium in the reactor vessel (Fig. XII-1) and serves as a single "can" for the total moderator assembly. The graphite is protected against small leaks in the calandria tubes by a system of baffles and by a set of drain tubes that are made of zirconium. These drain tubes surround the stainless-steel (type 304) calandria tubes to form a double-wall construction with a drain between the walls. The fuel elements are installed in the calandria tubes. The intermediate heat exchangers, of which there are three, are also submerged in the sodium in the reactor vessel and are made in the form of curved segments which fit against the vessel wall. The primary sodium flow takes place entirely within the reactor vessel by means of nine electromagnetic pumps; the pumps utilize the wall of the vessel to form one side of the narrow slot which constitutes the pump throat. The magnetic circuit of the pump passes through the reactor vessel wall, utilizing laminated silicon-steel core segments both inside and outside the wall, with the coil structure mounted outside the wall. The pumps operate on three-phase, 220-volt, 15-cycle current.

The reactor vessel is surrounded by a containment vessel that is intended to hold any sodium that may leak from the primary system. The containment vessel is of such a size that the sodium level would remain above the reactor core in case of a large leak.

The sodium in the primary system is blanketed with nitrogen gas. However, helium is used within the calandria vessel because of its superior heat-transfer characteristics.

The full-length fuel elements are clusters of 19 fuel rods. Each rod consists of 0.50-in.-diameter UC slugs sheathed in stainless-steel jackets. The jackets are 0.520 in. in inside diameter, and they have 0.010-in.-thick walls. The fuel rods are about 14 ft long, with the lower 12 ft containing the fuel slugs and the remaining 2 ft providing space for fission-gas

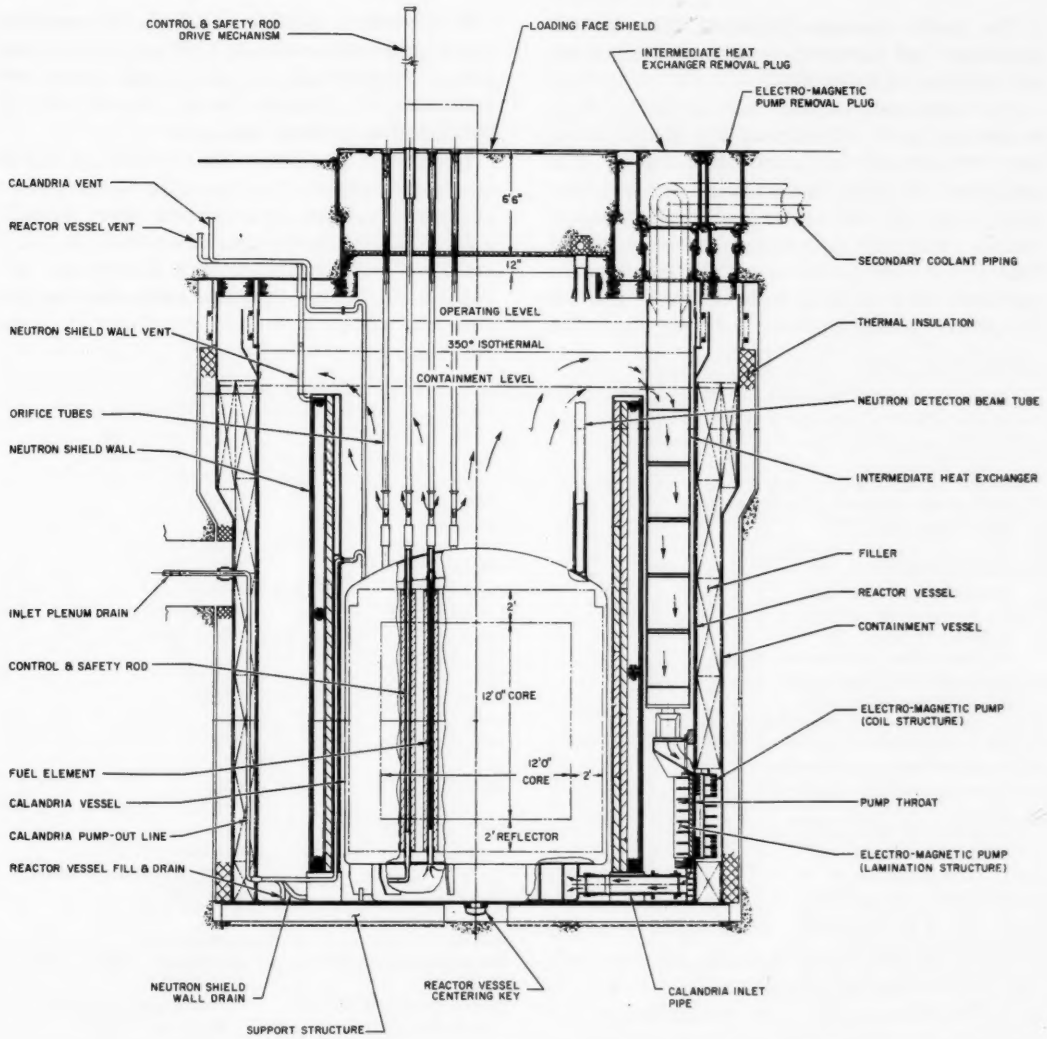

Fig. XII-1 General arrangement of the Advanced Sodium Graphite Reactor.[3]

release. A sodium bond is used between the slugs and jackets. The assemblies are hung, by hanger rods, from shield plugs in the loading face shield (Fig. XII-1). The reference states that no full-scale fuel elements of UC have yet been tested but that UC elements will be inserted in the SRE in the near future. Also, the second core for the Hallam Nuclear Power Facility is expected to be fabricated of UC. Uranium carbide fuels were reviewed in the December 1960 issue of *Power Reactor Technology*, Vol. 4, No. 1, pp. 45 to 52.

Eighteen control rods are used, driven from above. They operate in the calandria tubes and are cooled by natural convection of the sodium.

The secondary sodium system is divided into three parallel loops, each serving one steam generator, and each utilizing a single variable-speed electromagnetic pump of the helical rotor type. Steam is generated at 2450 psig and 1050° F and is reheated to 1000° F and 504 psig. Steam generator construction is of the once-through monotube type, with steam and water on the tube side and sodium on the shell side.

The main characteristics of the current-technology and advanced-technology designs are summarized in Table XII-1.

The estimated capital cost of the current-technology plant of nominal 300-Mw(e) rating was $57,313,000, or about $186/kw(e). With estimates of 3.22 mills/kw-hr for the fuel cycle, 0.68 mill/kw-hr for operation and maintenance, and 0.23 mill/kw-hr for insurance, a total power cost estimate of 7.86 mills/kw-hr resulted. The capital cost estimate for the 256-Mw(e) advanced-technology plant was $59,426,000, or $232/kw(e). Fuel and operating costs were estimated at 1.67 and 0.39 mills/kw-hr, respectively, to give a total power cost estimate of 6.70 mills/kw-hr. Escalation was not included in either estimate.

Reference 5 reports the results of a fuel burnup calculation for the advanced-technology reactor. Uniform enrichments from 2.50 to 3.25 at.% U^{235} in the uranium carbide fuel elements were investigated by a four-group calculation (CANDLE code). A batch-loading fuel program was used, with excess reactivity com-

Table XII-1 CHARACTERISTICS OF SODIUM GRAPHITE REACTOR DESIGNS[2,3]

	Current technology	Advanced technology
Main steam pressure, psig at throttle	1235	2400
Main steam temp., °F	850	1050
Reheat steam pressure, psig	215	504
Reheat steam temp., °F	850	1000
Throttle steam flow, lb/hr	2.465×10^6	1.835×10^6
No. of feed-water heaters	6 + evaporator	7 + evaporator
Feed-water temp., °F	445	540
Condenser backpressure, in. Hg abs.	$1\frac{1}{2}$	$1\frac{1}{2}$
Gross electrical power, Mw	320	270
Net electrical power, Mw	307.6	255.9
Gross turbine-cycle heat rate, Btu/kw-hr	8780	7550
Net turbine-cycle heat rate, Btu/kw-hr	8780	7750
Steam-raising plant efficiency, %	98.5	98.5
Net plant heat rate, Btu/kw-hr	9280	8090
Reactor:		
Reactor thermal power, Mw	835	606
Reactor coolant	Sodium	Sodium
Coolant temp., °F	625°F inlet, 945°F outlet	650°F inlet, 1200°F outlet
Coolant flow, lb/hr	29.3×10^6	12.6×10^6
No. of primary loops	4	3
Secondary coolant	Sodium	Sodium
Coolant temp., °F	585°F inlet, 905°F outlet	600°F inlet, 1150°F outlet
Coolant flow, lb/hr	29.3×10^6	12.6×10^6
Fuel	61-rod cluster of U–10 wt.% Mo alloy slugs, 0.33 in. in diam., clad in S.S. with Na bond	19-rod cluster of ½-in.-diam. by 1-in. UC pellets in S.S. tubes with Na bond
No. of fuel elements	214	151
No. of control-safety rods	18	18
Initial enrichment, at.% U^{235}	3.5 inner region, 4.0 outer region	2.7
Initial excess reactivity with equilibrium Xe and Sm poison		0.127
Initial conversion ratio	0.47	0.505
Av. fuel burnup, Mwd/metric ton of U	13,000	17,100
Uranium in core, kg	50,600 kg of U 56,200 kg of U-Mo alloy	16,200
Active core size	$15\frac{1}{2}$ ft in. diam. by 15 ft high	12 ft in. diam. by 12 ft high
Peak-to-average power ratio	2.0	2.87
Specific power (av. for new core), kw/kg of U^{235}	420	1400
Max. fuel temp., °F	1050	2250
Av. heat flux, Btu/(hr)(sq ft)	150,000	425,000
Max. heat flux, Btu/(hr)(sq ft)	300,000	1.24×10^6
Av. thermal-neutron flux in fuel, neutrons/(cm^2)(sec)		8×10^{13}

pensated by control rods. The rods were approximated in the calculation by uniformly distributed absorber. The calculations cover the period from initial startup to removal of the first batch of fuel; the batch may consist of all or part of the total fuel.

The results of the calculations are of general interest, inasmuch as they illustrate a number of the characteristics of batch-loaded reactors. The changes in spatial distribution of power, since continuing operation reduces preferentially the reactivity of the highest power regions, are particularly interesting. Figures XII-2 and XII-3 illustrate this effect, the former showing the change in radial peak-to-average power density with exposure and the latter showing the change in peak-to-average fuel exposure. Table XII-2 lists the average exposure attained, up to the time that all excess reactivity has been used up, with each initial enrichment, as well as the initial conversion ratio for each enrichment. All initial compositions except enrichment were held fixed, and the decrease in initial conversion ratio as enrichment is increased reflects the increasing effectiveness of the U^{235} in competing with U^{238} for the neutrons.

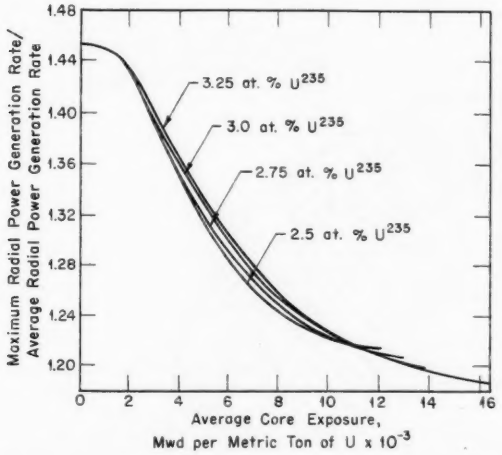

Fig. XII-2 Variation of ratio of maximum radial power generation rate to average radial power generation rate with burnup for the Advanced Sodium Graphite Reactor.[5]

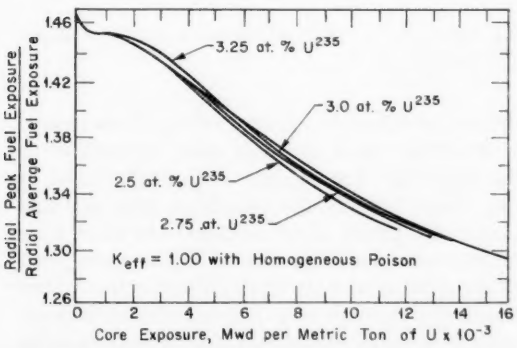

Fig. XII-3 Variation of ratio of radial peak fuel exposure to radial average fuel exposure with burnup for the Advanced Sodium Graphite Reactor.[5]

Table XII-2 VARIATION OF ATTAINABLE AVERAGE FUEL EXPOSURE AND INITIAL CONVERSION RATIO WITH INITIAL ENRICHMENT FOR 255-Mw(e) ADVANCED SODIUM GRAPHITE REACTOR[5]

Enrichment, at.% U^{235}	Initial conversion ratio	Av. exposure when k_{eff} = 1.0, Mwd/metric ton of U
2.50	0.516	9,000
2.75	0.495	11,250
3.00	0.479	13,400
3.25	0.463	16,000

A General Electric design for a 200-Mw(e) sodium graphite reactor is described in reference 6. The reactor core consists of a set of 37 modules — each containing a coolant thimble, a large fuel assembly, and the moderator associated with one fuel assembly — suspended in a concrete shield pit. The pit also contains a graphite reflector which surrounds the group of fuel-moderator modules. Each module is of full core length and is coaxial with a stainless-steel coolant thimble containing the fuel and coaxial counterflow coolant passages. The thimble is surrounded by a cylinder of graphite in a Zircaloy can (Fig. XII-4). The Zircaloy can is insulated from the contained graphite, which is cooled primarily by conduction to the fuel thimble, but the Zircaloy can has additional graphite attached to its outside, cooled by nitrogen flow in an annular passage between the can and the outer graphite. The outer graphite extends the cross section of the module to a square shape, 28.72 by 28.72 in., so that the modules can be close-packed (on 30-in. centers) to form a core having the shape of a jagged-edged octagon. Cruciform control rods operate in slots at the corners of the modules and are also cooled by flowing nitrogen. With this arrangement, the sodium coolant is contained within the fuel thimble; if a leak should occur in any thimble, the Zircaloy can acts as a

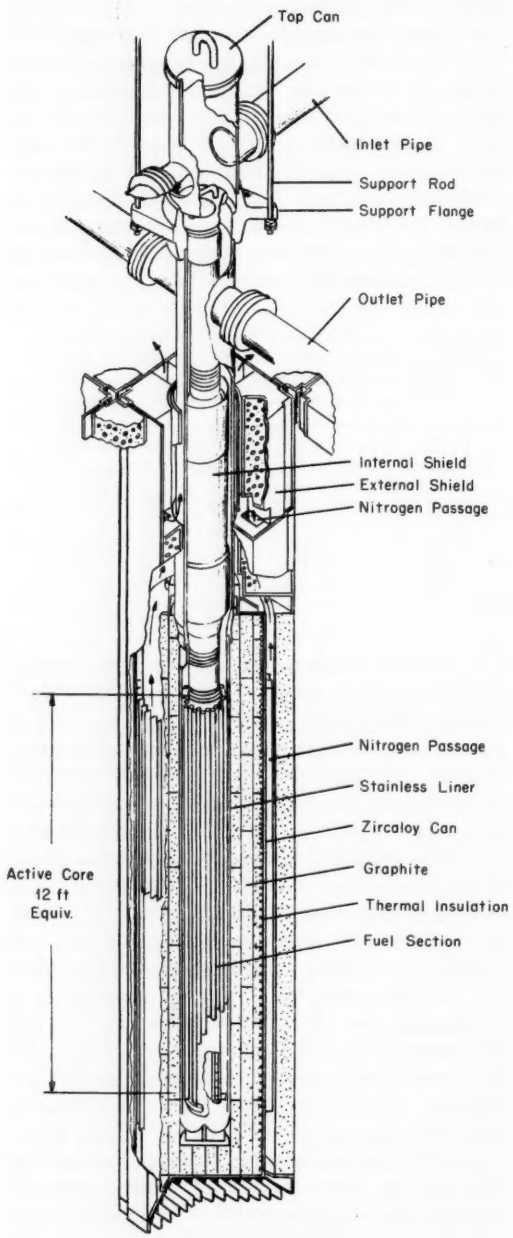

Fig. XII-4 Module unit for the Sodium Modular Reactor.[6]

second barrier to confine the sodium within the cylindrical section of the single module.

Each module is suspended by hanger rods that connect at a support flange on the coolant thimble, as shown in Fig. XII-4. This maintains a nearly constant position for the inlet and outlet coolant-pipe flanges and allows thermal expansion downward as necessary. Refueling is accomplished by (1) removing the central tube, which defines the inlet pass of the coolant and which has the fuel rods attached to its outside, (2) submerging the assembly in an oil-filled pit, where the spent fuel is removed and where fresh fuel may be installed, and (3) reinstalling the assembly in the coolant thimble. Transfer of the assembly between the reactor and the pit is accomplished by a monorail and crane, in the shielded reactor room, without the use of a coffin. A cross section of the inner tube assembly in the core region is shown in Fig. XII-5. The inlet (downward) coolant pass is

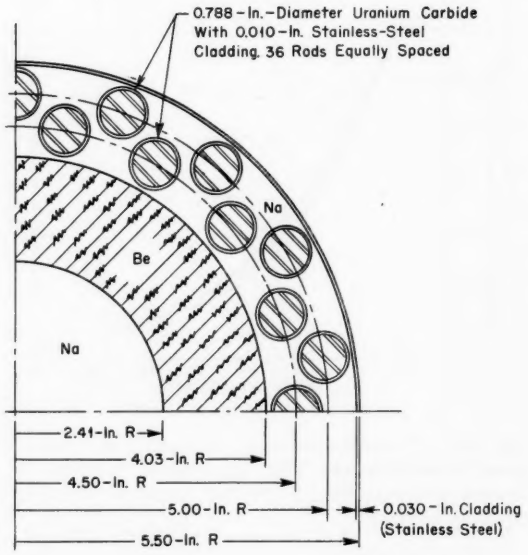

Fig. XII-5 Cross section of coolant thimble, Sodium Modular Reactor.[6]

defined by a hollow cylinder of beryllium canned in stainless steel (the can does not appear in the drawing). The 36 fuel rods are located in two rings outside the beryllium tube and are cooled by upflow of the sodium. The outer ring of stainless steel shown in the figure is the wall of the coolant thimble itself. The function of the beryllium cylinder is to provide sufficient moderation to give a reasonably flat thermal-neutron flux across the ring of fuel rods.

The fuel elements are rods of uranium monocarbide jacketed with stainless steel. As is

Table XII-3 CHARACTERISTICS OF SODIUM MODULAR REACTOR[6]

Reactor Materials (Total Amounts in Core)	
Moderator:	
AGOT graphite, lb	176,000
Beryllium, lb	14,000
Fuel cladding (type 347 stainless steel), lb	7580
Module-unit walls (Zircaloy-2), lb	25,500
Main coolant (sodium), lb	5010
Moderator coolant (nitrogen), lb	85
Fuel (uranium monocarbide), lb	44,000
Core Physical Arrangements	
Core effective dimensions (without reflector)	18.3 ft in diam. by 12 ft long
Module diameter (containing fuel and sodium), in.	11
Module unit size (containing module and moderator), in.	28.72
No. of modules per reactor	37
Array	Square spacing on 30-in. centers; rows of 3, 5, 7, 7, 7, 5, and 3 modules
Module-liner wall thickness (steel), in.	0.030
Module-unit wall thickness (Zircaloy-2), in.	0.100
Core Heat-Transfer Data	
Total power peaking factor	3.0 : 1
Radial power peaking factor	1.23 : 1
Max. power per module removed by sodium, kw(t)	18,000
Av. power per module removed by sodium, kw(t)	14,650
Inlet and outlet sodium temp., °F	800 and 1050
Max. sodium flow per module, lb/hr	81.6×10^4
Total heat removed by nitrogen, kw(t)	16,560
Fuel-element surface area per module, sq ft	91.3
Max. heat flux, Btu/(hr)(sq ft)	1,644,000
Av. heat flux, Btu/(hr)(sq ft)	548,000
Sodium velocity, ft/sec	26.2
Hydraulic diameter, ft	0.0915
Heat-transfer coefficient, Btu/(hr)(sq ft)(°F)	11,650
Max. central temp., °F	3290
Max. cladding temp., °F	1113
Pressure drop through fuel, psi	20.2
Total reactor pressure drop, psi	56.5
Primary Sodium System	
Reactor inlet temp., °F	800
Reactor outlet temp., °F	1050
Primary sodium flow, lb/hr	6,330,000
Primary pumps:	
Number	4
Pump capacity at 800°F, gal/min	15,000
Head at full flow, psi	75
Intermediate heat exchanger:	
No. of units	8
Area per unit, sq ft	2700
Secondary Sodium System	
Temperature at intermediate heat exchanger:	
Inlet, °F	680
Outlet, °F	1000
No. of loops	4
Flow per loop, lb/hr	4,730,000
No. of pumps	4
Pump capacity at 680°F, gal/min	12,000
Head at full flow, psi	55
No. of boilers	8
Area per unit, sq ft	1960
Shell design pressure, psig	200
No. of superheaters	4
Area per unit, sq ft	2000
Shell design pressure, psig	200
No. of steam reheaters	4
Area per unit, sq ft	1913
Shell design pressure, psig	200
Turbine Electric System	
Steam conditions at turbine throttle:	
Pressure, psig	1450
Temp., °F	900
Flow, lb/hr	1,630,000
Reheat steam conditions:	
Pressure, psig	300
Temp., °F	900
Flow, lb/hr	1,400,000
Condenser pressure, in. Hg	3.5
Generator rating, kw	218,952
Sodium pump power, kw	4573
Nitrogen compressor power, kw	3020
Other plant auxiliaries, kw	8417
Net plant output, kw	202,942
Net plant heat rate, Btu/kw-hr	9399
*Fuel Cycle with 5-Batch Reloading**	
Graphite-to-fuel volume ratio	30 : 1
Av. fuel irradiation, Mwd(t)	10,000
Days between reloading	77
Initial atom fraction of U^{235}	0.0285
Final atom fraction of U^{235}	0.0180
Atom fraction of U^{235} burned	0.0105
Atom fraction of discharged Pu	0.0044
Av. conversion ratio	0.508
Fuel costs, mills/kw-hr	2.33

*Calculations are for the case of no steel cladding on beryllium. Inclusion of 10-mil cladding increases required initial atom fraction of U^{235} to 0.0291.

evident from Fig. XII-5, the elements are relatively thick, and a single average assembly produces 14.7 Mw of thermal power, or about 400 kw per fuel rod. The calculated central temperature of the fuel slugs is 3290°F. A design was also considered in which highly enriched steel–UO_2 plates were used outside the beryllium cylinder, and rod type elements of depleted uranium carbide were used inside the cylinder, in the initial sodium pass. This arrangement did not appear to have economic advantages.

Outside the reactor proper, the remainder of the plant is more or less conventional, using a primary and a secondary coolant system with intermediate heat exchangers and producing steam at 900°F and 1465 psi, with reheat to 900°F at 350 psi.

With a fuel program utilizing five-batch radial reloading, a feed enrichment of 2.85 at.% U^{235} is required for an average fuel exposure of 10,000 Mwd/ton. The estimated fuel cost at this exposure is 2.33 mills/kw-hr. Extension of the average exposure to 20,000 Mwd/ton is estimated to reduce the fuel cost to 1.98 mills/kw-hr. The estimated construction cost for a 200-Mw(e) plant (exclusive of land and interest on construction) is $62 million. The total power cost for the case of 10,000 Mwd/ton fuel exposure is estimated at 9.6 mills/kw-hr. The reference states that in a larger, 400 Mw(e), plant considerable benefits on fuel cost would be obtained from the lower neutron leakage.

The main characteristics of the plant are summarized in Table XII-3.

An interesting feature of the recommended research and development program, directed toward the development of a large reactor, is the proposal to construct a prototype reactor consisting of a single module, with thermal output in the 18- to 25-Mw range.

References

1. G. L. Reed, Evaluation of Calandria, Thimble, and Canned-Moderator Concepts for Sodium Graphite Reactors, USAEC Report NAA-SR-3573, Atomics International, June 10, 1960.
2. J. Renard et al., 300,000-KWE SGR Nuclear Power Plant of Current Technology, USAEC Report NAA-SR-4873, Atomics International, Aug. 1, 1960.
3. J. R. Churchill and J. Renard, An Advanced Sodium Graphite Reactor Nuclear Power Plant, USAEC Report NAA-SR-3829, Atomics International, Mar. 15, 1960.
4. Sargent & Lundy, Power Cost Normalization Studies, Civilian Power Reactor Program, USAEC Report SL-1674, Sept. 1, 1959.
5. A. L. Aronson, Fuel Burnup Studies for a 255 Mw(e) Advanced Sodium Graphite Reactor, USAEC Report NAA-SR-4529, Atomics International, June 15, 1960.
6. J. F. Cage, Jr., et al., Design Study, Sodium Modular Reactor, USAEC Report GEAP-3334, General Electric Co., Atomic Power Equipment Dept., Jan. 15, 1960.

LEGAL NOTICE

This document was prepared under the sponsorship of the U. S. Atomic Energy Commission. Neither the United States, nor the Commission, nor any person acting on behalf of the Commission:

A. Makes any warranty or representation, expressed or implied, with respect to the accuracy, completeness, or usefulness of the information contained in this report, or that the use of any information, apparatus, method, or process disclosed in this report may not infringe privately owned rights; or

B. Assumes any liabilities with respect to the use of, or for damages resulting from the use of any information, apparatus, method, or process disclosed in this report.

As used in the above, "person acting on behalf of the Commission" includes any employee or contractor of the Commission, or employee of such contractor, to the extent that such employee or contractor of the Commission, or employee of such contractor prepares, disseminates, or provides access to, any information pursuant to his employment or contract with the Commission, or his employment with such contractor.

NUCLEAR SCIENCE ABSTRACTS

The U. S. Atomic Energy Commission, Office of Technical Information, publishes *Nuclear Science Abstracts (NSA)*, a semimonthly journal containing abstracts of the literature of nuclear science and engineering.

NSA covers (1) research reports of the U. S. Atomic Energy Commission and its contractors; (2) research reports of government agencies, universities, and industrial research organizations on a world-wide basis; and (3) translations, patents, books, and articles appearing in technical and scientific journals.

Complete indexes covering subject, author, source, and report number are included in each issue. These are cumulated quarterly, semiannually, and annually providing a detailed and convenient key to the literature.

Availability of *NSA*

SALE *NSA* is available on subscription from the Superintendent of Documents, U. S. Government Printing Office, Washington 25, D. C., at $18.00 per year for the semimonthly abstract issues and $15.00 per year for the four cumulated-index issues. Subscriptions are postpaid within the United States, Canada, Mexico, and all Central and South American countries, except Argentina, Brazil, British and French Guiana, Surinam, and British Honduras. Subscribers in these Central and South American countries, and in all other countries throughout the world, should remit $22.50 per year for subscriptions to semimonthly abstract issues and $17.50 per year for the four cumulated-index issues.

EXCHANGE *NSA* is also available on an exchange basis to universities, research institutions, industrial firms, and publishers of scientific information. Inquiries should be directed to the Office of Technical Information Extension, U. S. Atomic Energy Commission, P. O. Box 62, Oak Ridge, Tennessee.

TECHNICAL PROGRESS REVIEWS may be purchased from Superintendent of Documents, U. S. Government Printing Office, Washington 25, D. C. for $2.00 per year for each subscription or for $0.55 per issue. The use of the coupon below will facilitate the handling of your order.

POSTAGE AND REMITTANCE: Postpaid within the United States, Canada, Mexico, and all Central and South American countries except as hereinafter noted. Add $0.50 per year, or $0.15 per single issue, for postage to all other countries, including Argentina, Brazil, British and French Guiana, Surinam, and British Honduras. Payment should be by check, money order, or document coupons, and MUST accompany order. Remittances from foreign countries should be made by international money order, or draft on an American bank, payable to the Superintendent of Documents, or by UNESCO book coupons.

order form

SUPERINTENDENT OF DOCUMENTS
U. S. GOVERNMENT PRINTING OFFICE
WASHINGTON 25, D. C.

Enclosed:
document coupons ☐ check ☐ money order ☐

Charge to Superintendent of Documents No. _____

Please send a one-year subscription to

☐ REACTOR CORE MATERIALS
☐ POWER REACTOR TECHNOLOGY
☐ NUCLEAR SAFETY
☐ REACTOR FUEL PROCESSING

(Each subscription $2.00 a year; $0.55 per issue.)

SUPERINTENDENT OF DOCUMENTS
U. S. GOVERNMENT PRINTING OFFICE
WASHINGTON 25, D. C.

(Print clearly)

Name _____

Street _____

City _____ Zone ____ State _____